UNIVERSIDADE FEDERAL DE SANTA MARIA
CENTRO DE CIÊNCIAS NATURAIS E EXATAS
PROGRAMA DE PÓS-GRADUAÇÃO EM CIÊNCIAS BIOLÓGICAS:
BIOQUÍMICA TOXICOLÓGICA

Fernanda D'Avila da Silva

JM-20 COMO COMPOSTO MULTIALVO: AVALIAÇÃO DO POTENCIAL ANTIOXIDANTE, INIBIDOR DE COLINESTERASES E CITOTOXICIDADE

Santa Maria, RS
2020

Fernanda D'Avila da Silva

JM-20 COMO COMPOSTO MULTIALVO: AVALIAÇÃO DO POTENCIAL ANTIOXIDANTE, INIBIDOR DE COLINESTERASES E CITOTOXICIDADE

Tese de doutorado apresentada ao Programa de Pós- Graduação em Ciências Biológicas: Bioquímica Toxicológica da Universidade Federal de Santa Maria como requisito parcial para a obtenção do título de **Doutora em Ciências Biológicas: Bioquímica Toxicológica**

Orientador: Prof Dr. João Batista Teixeira da Rocha

Santa Maria, RS
2020

This study was financied in part by the Coordenação de Aperfeiçoamento de Pessoal de Nível Superior - Brasil (CAPES) – Finance Code 001

Silva, Fernanda D'Avila da
JM-20 como composto multialvo: avaliação do potencial antioxidante, inibidor de colinesterases e citotoxicidade / Fernanda D'Avila da Silva.- 2020.
81 p.; 30 cm

Orientador: João Batista Teixeira Rocha
Tese (doutorado) - Universidade Federal de Santa Maria, Centro de Ciências Naturais e Exatas, Programa de Pós-Graduação em Ciências Biológicas: Bioquímica Toxicológica, RS, 2020

1. JM-20 2. cholinesterases 3. antioxidante 4. toxicidade 5. docking I. Rocha, João Batista Teixeira II. Título.

Sistema de geração automática de ficha catalográfica da UFSM. Dados fornecidos pelo autor(a). Sob supervisão da Direção da Divisão de Processos Técnicos da Biblioteca Central. Bibliotecária responsável Paula Schoenfeldt Patta CRB 10/1728.

Declaro, FERNANDA D'AVILA DA SILVA, para os devidos fins e sob as penas da lei, que a pesquisa constante neste trabalho de conclusão de curso (Tese) foi por mim elaborada e que as informações necessárias objeto de consulta em literatura e outras fontes estão devidamente referenciadas. Declaro, ainda, que este trabalho ou parte dele não foi apresentado anteriormente para obtenção de qualquer outro grau acadêmico, estando ciente de que a inveracidade da presente declaração poderá resultar na anulação da titulação pela Universidade, entre outras consequências legais.

Fernanda D'Avila da Silva

JM-20 COMO COMPOSTO MULTIALVO: AVALIAÇÃO DO POTENCIAL ANTIOXIDANTE, INIBIDOR DE COLINESTERASES E CITOTOXICIDADE

Tese de doutorado apresentada ao Programa de Pós- Graduação em Ciências Biológicas: Bioquímica Toxicológica da Universidade Federal de Santa Maria como requisito parcial para a obtenção do título de **Doutora Ciências Biológicas: Bioquímica Toxicológica**

Aprovado em 29 de outubro de 2020:

João Batista Teixeira da Rocha, Dr (UFSM)
(Presidente/Orientador)

Thais Posser, Dra (Unipampa – São Gabriel)

Daiana Silva Ávila, Dra (Unipampa - Uruguaiana)

Roselei Fachinetto, Dra (UFSM)

Roselia Spanevello, Dra (UFPel)

Santa Maria, RS
2020

DEDICATÓRIA

A minha mãe e meus avós meus maiores incentivadores. Dedico também aos meus amigos e demais familiares que me apoiaram em todos os momentos.

AGRADECIMENTOS

A realização desse trabalho foi possível principalmente pela participação, incentivo e compreensão de várias pessoas. Agradeço a todos que de alguma maneira colaboraram para a conclusão desse estudo, em especial agradeço:

- A minha mãe Josselaine Medianeira D'Avila pelo carinho e força diária durante todo o processo, pois sempre acreditou na minha capacidade e tudo o que conquistei foi graças a ela.

- Aos meus avós Ivone Oliveira D'Avila e Luiz Carlos D'Avila pelo carinho, paciência e compreensão em todos os momentos.

- Aos amigos que compreenderam minhas ausências e sempre me incentivaram.

- Aos colegas de laboratório pelo companheirismo, parceria, experiências e momentos de descontração. Especialmente aos colegas e grandes amigos Bruna Candia Piccoli, Cláudia Sirlene de Oliveira e Pablo Andrei Nogara.

- Aos colegas e amigos de outras nacionalidades, especialmente o Goke, Blessing e Bright, que proporcionaram e compartilharam muitos aprendizados e experiências de vida.

- Ao Professor Dr. Daniel Mendes Pereira Ardisson de Araújo pela amizade, apoio e incentivo sempre.

- Ao Professor Dr. Denis Brook Rosemberg pela amizade, pareceria e ensinamentos.

- Ao meu orientador, Professor Dr. João Batista Teixeira da Rocha, pela oportunidade concedida, ensinamentos e orientações.

- Ao Professor Dr. Yanier Nuñez-Figueredo pela confiança, contribuições e orientações.

- Aos Professores do Programa de Pós-Graduação em Ciências Biológicas: Bioquímica Toxicológica por contribuírem de algum modo pela conquista desse título.

- As agencias financiadoras FAPERGS, CNPq e CAPES, pelo auxilio e bolsas de estudo, sem esse incentivo tudo ficaria muito mais difícil.

- A Universidade pública, gratuita e de qualidade pela oportunidade de desenvolver este estudo.

- E por fim, não menos importante, a Deus por iluminar meu caminho sempre.

Enfim, a todos aqueles que fazem parte da minha vida e que são essenciais para a minha evolução nessa jornada.

Gratidão!!!!

RESUMO

JM-20 COMO COMPOSTO MULTIALVO: AVALIAÇÃO DO POTENCIAL ANTIOXIDANTE, INIBIDOR DE COLINESTERASES E CITOTOXICIDADE

AUTOR: Fernanda D'Avila da Silva
ORIENTADOR: João Batista Teixeira da Rocha

Compostos multialvo tem despertado o interesse de muitos pesquisadores. Estas substâncias tem como principal característica a capacidade de agir através de diferentes mecanismos de ação, fato relevante em casos de patologias originadas por múltiplas causas. Neste contexto, em alguns casos de doenças neurodegenerativas pode ocorrer a perda neuronal em determinadas regiões cerebrais as quais contem neurônios colinérgicos, consequentemente causando comprometimento de funções cognitivas. O estresse oxidativo é caracterizado pelo desequilíbrio entre a produção das espécies reativas e as defesas antioxidantes e pode estar diretamente relacionado as causas ou consequências de patologias relacionadas ao SNC. Estudos anteriores mostraram que o JM-20, 1,5-benzodiazepina fundida a uma fração de di-hidropiridina, tem diferentes propriedades farmacológicas de interesse clínico. Neste sentido, o objetivo principal deste estudo foi avaliar o efeito do JM-20 na AChE e na BChE de diferentes fontes, identificar o tipo de inibição enzimática e compreender as interações entre o composto e as enzimas utilizando ferramentas *in sílico de docking molecular*. Além disso, verificar o efeito protetor no estresse oxidativo induzido por Fe^{2+} em leucócitos e determinar a atividade *scavenger* de radicais livres. Do mesmo modo, averiguar a possível citotoxicidade utilizando células sanguíneas humanas e predizer parâmetros ADMET utilizando ferramentas *in sílico* de *screening* virtual. A BChE utilizada foi purificada de *Equus ferus* e presente no plasma humano, enquanto que a AChE foi de *Electrophorus electricus*, eritrócitos totais e presente nas membranas isoladas de eritrócitos humanos (ghost). As enzimas foram pré-incubadas durante 30 minutos na presença de diferentes concentrações de JM-20 (1 nM - 200 μM). Para avaliar o tipo de inibição enzimática, foi realizado um estudo cinético variando a concentração do substrato (0,05 - 1,6 mM). O sangue humano foi obtido de voluntários saudáveis. Imediatamente após a coleta do sangue, os leucócitos ou eritrócitos foram isolados, lavados e tratados com diferentes concentrações de JM-20 e avaliados de acordo com cada teste específico. Os resultados demonstraram o potencial efeito inibitório na atividade da AChE. Estes efeitos foram observados em todas as enzimas testadas (IC_{50} = 123 nM ± 0,2 para *E. electricus*, 172 nM ± 0,2 para eritrócitos totais e 158 nM ± 0,1 para ghost). Além disso, sugerimos que o composto apresenta um tipo misto de inibição já que altera o K_m e V_{max} da AChE. O *docking molecular* demonstrou a existência de oito isômeros diferentes do JM-20 e os isômeros 4R interagem melhor com a *Hs*AChE. O resultado do TBARS aponta para um potente efeito antioxidante e efeito *scavenger* de radicais livres observados na fase lenta da reação. Entretanto, a exposição a todas as concentrações de JM-20 testadas (10-50 μM) causou um aumento significativo nos níveis de espécies reativas intracelulares (ER). Embora tenha sido observada diminuição da viabilidade celular e aumento da produção de ER, a exposição ao JM-20 (10-50 μM) não alterou o ciclo celular, assim como não causou hemólise. Análises de *screening* virtual do JM-20 demonstraram similar perfil ADMET a nifedipina. Assim, nossas descobertas apoiam o potencial uso clínico do JM-20, para o tratamento de patologias associadas ao SNC.

Palavras-chave: JM-20, cholinesterase, antioxidante, toxicidade, analise computacional

ABSTRACT

JM-20 AS MULTI-TARGET COMPOUND: EVALUATION OF ANTIOXIDANT POTENTIAL, CHOLINESTERASE INHIBITOR, AND CYTOTOXICITY

AUTHOR: Fernanda D'Avila da Silva
ADVISOR: João Batista Teixeira da Rocha

Multi-target compounds have aroused the interest of many researchers. The main characteristic of these substances is the ability to act through different mechanisms of action, a relevant fact in cases of pathologies caused by multiple causes. In this context, in some cases of neurodegenerative diseases, a neuronal loss may occur in certain brain regions that contain cholinergic neurons, consequently causing impairment of cognitive functions. Oxidative stress is characterized by the imbalance between the production of reactive species and antioxidant defenses and can be directly related to the causes or consequences of pathologies related to the CNS. Previous studies have shown that JM-20, 1,5-benzodiazepine fused to a dihydropyridine fraction, has different pharmacological properties of clinical interest. In this sense, the main objective of this study was to evaluate the effect of JM-20 on AChE and BChE from different sources, identify the type of enzyme inhibition and understand the interactions between the compound and the enzymes using silicon molecular docking tools. Besides, to verify the protective effect on oxidative stress induced by Fe^{2+} in leukocytes and to determine the scavenger activity of free radicals. Likewise, investigate possible cytotoxicity using human blood cells and predict ADMET parameters using in silico virtual screening tools. The BChE used was purified from *Equus ferus* and present in human plasma, while AChE was from *Electrophorus electricus*, total erythrocytes and present in membranes isolated from human erythrocytes (ghost). The enzymes were pre-incubated for 30 minutes in the presence of different concentrations of JM-20 (1 nM - 200 µM). To assess the type of enzyme inhibition, a kinetic study was performed varying the concentration of the substrate (0.05 - 1.6 mM). Human blood was obtained from healthy volunteers. Immediately after blood collection, the leukocytes or erythrocytes were isolated, washed, and treated with different concentrations of JM-20 and evaluated according to each specific test. The results demonstrated the potential inhibitory effect on AChE activity. These effects were observed in all enzymes tested (IC_{50} = 123 nM ± 0.2 for *E. electricus*, 172 nM ± 0.2 for total erythrocytes and 158 nM ± 0.1 for ghost). Besides, we suggest that the compound has a mixed type of inhibition as it changes the K_m and V_{max} of AChE. Molecular docking demonstrated the existence of eight different isomers of JM-20, and the 4R isomers interact better with *Hs*AChE. The TBARS result points to a potent antioxidant and scavenger effect of free radicals seen in the slow phase of the reaction. However, exposure to all tested JM-20 concentrations (10-50 µM) caused a significant increase in the levels of reactive intracellular species (RS). Although decreased cell viability and increased RS production have been observed, exposure to JM-20 (10-50 µM) did not alter the cell cycle, nor did it cause hemolysis. Analyzes of virtual screening of the JM-20 demonstrated a similar ADMET profile to nifedipine. Thus, our findings support the potential clinical use of JM-20, for the treatment of pathologies associated with the CNS.

Keywords: JM-20, cholinesterase, antioxidant, toxicity, computational analysis

SUMÁRIO

APRESENTAÇÃO

A tese apresentada está organizada de acordo com os seguintes tópicos: inicialmente é descrita uma introdução, com uma breve revisão sobre os temas abordados no trabalho, seguidos da justificativa e dos objetivos. Em seguida, o desenvolvimento na forma de um artigo publicado no periódico internacional "Biochimie" e um manuscrito que será submetido a um periódico igualmente internacional "Toxicology *in vitro*". As seções Introdução, Materiais e métodos, Resultados, Discussão, Conclusão e Referências bibliográficas encontram-se no artigo e manuscrito e representam a íntegra deste estudo. Finalmente, no item discussão são apresentados interpretações e comentários gerais sobre os trabalhos. As referências bibliográficas apresentadas no final da tese referem-se às citações que aparecem nos itens introdução e discussão.

1 INTRODUÇÃO

O interesse por compostos multialvo para o tratamento de diferentes patologias, principalmente as associadas ao sistema nervoso central (SNC), tem despertado o interesse de muitos pesquisadores (DIAS et al., 2015; MONTANARI, 1995; SAMEEM et al., 2017). Estas moléculas têm como característica principal a capacidade de agir em diferentes mecanismos, fato relevante em casos de patologias multicausais (DIAS et al., 2015; LU et al., 2012; SPILOVSKA et al., 2017).

Dessa forma, o JM-20 (3-etoxicarbonil-2-metil-4- (2-nitrofenil) 4,11- di-hidro-1H-pirido [2,3-b] [1,5] benzodiazepina) é um composto derivado do 1,5-benzodiazepínico que apresenta uma porção 1,4- dihidropiridina (Figura 1) (NUÑEZ-FIGUEREDO et al., 2013, 2014a, 2014b). A partir de sua estrutura podemos observar a similaridade com moléculas atualmente utilizadas na prática clínica, como por exemplo, o Diazepam® e a Nifedipina®. O primeiro é um benzodiazepínico com propriedades anticonvulsivantes, ansiolítica, sedativa e relaxante muscular (MANDELLI; TOGNONI; GARATTINI, 1978). O Diazepam® age através do aumento da atividade do ácido gama-aminobutírico (GABA), um neurotransmissor presente no SNC (MANDELLI; TOGNONI; GARATTINI, 1978). Enquanto que a Nifedipina® (Figura 1), uma di-hidropiridina, foi descrita pela primeira vez na literatura em 1972 juntamente com outras di-hidropiridinas e atua como bloqueador dos canais de cálcio (LEE et al., 2014). A Nifedipina® é indicada para o tratamento da angina e hipertensão (LEE et al., 2014; OMS, 2019). Neste contexto, estudos prévios com o JM-20 demonstraram a manutenção dos efeitos como ansiolítico, sedativo, anticonvulsivante (semelhante ao Diazepam®) e bloqueador dos canais de cálcio (equivalente a Nifedipina®), além de apresentar outras propriedades farmacológicos de interesse clinico resumidas na Tabela 1.

Figura 1 – Estrutura do JM-20, nifedipina e diazepam.

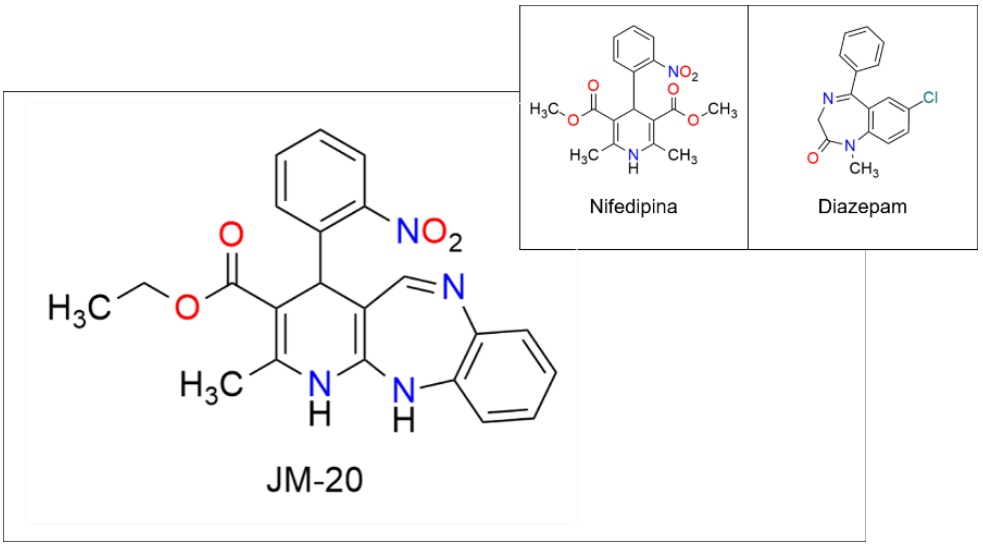

Estrutura molecular do composto JM-20 (3 – etoxicarbonil – 2 – metil – 4 - (2 - nitrofenil) – 4 – 11 – dihidro – 1 – H – pirido [2, 3 - b] [1, 5] benzodiazepino), nifedipina e diazepam. Fonte: o autor

O JM-20 (2, 4, 8 e 10 mg/Kg) manteve o perfil ansiolítico, semelhante aos derivados dos benzodiazepínicos como o Diazepam (Figura 1), avaliados no teste do campo aberto e do labirinto em cruz elevada em camundongos. Nestes testes comportamentais, os animais apresentaram um aumento no número de entradas e tempo gasto na parte central do aparato (teste de campo aberto) e nos braços abertos (labirinto em cruz elevada) após a administração oral das drogas (NUÑEZ-FIGUEREDO et al., 2013). O JM-20 foi capaz de reduzir o comportamento agressivo de camundongos socialmente isolados, possivelmente, pela modulação positiva dos receptores GABAérgicos (NUÑEZ-FIGUEREDO et al., 2013). Semelhante aos sedativos, o JM-20 também aumentou significativamente o período de sono em ratos (NUÑEZ-FIGUEREDO et al., 2013). Além disso, este composto conferiu proteção em modelo de convulsões induzidas por pentilenotetrazol em camundongos, aumentou o período de latência para o início da crise convulsiva e a porcentagem de sobrevivência destes animais (NUÑEZ-FIGUEREDO et al., 2013).

Adicionalmente, o JM-20 pode atuar como um agente neuroprotetor de múltiplos alvos, reduzindo a lesão excitotóxica neuronal e protegendo as mitocôndrias da toxicidade induzida por Ca^{2+}, preservando, desse modo, o balanço energético celular (NUÑEZ-FIGUEREDO et al., 2014a, 2014c, 2014b). O JM-20 também foi capaz de atenuar os efeitos da lesão isquêmica, possivelmente, através da modulação da neuroinflamação e da via de sinalização celular antiapoptótica (NUÑEZ-FIGUEREDO et al., 2015, 2016, 2018; RAMÍREZ-SÁNCHEZ et al., 2015). Recentemente, foi avaliado o efeito do JM-20 em modelo de doença de Parkinson induzida por rotenona *in vitro* e *in vivo* (FONSECA-

FONSECA et al., 2019a). Neste estudo foi possível observar, *in vitro*, o efeito protetor do composto ao diminuir a morte celular induzida pela rotenona. Nas análises *in vivo*, o JM-20 atenuou com sucesso as alterações comportamentais induzida pela rotenona em ratos (FONSECA-FONSECA et al., 2019a). O JM-20 aumentou a atividade de enzimas como a superóxido dismutase e a catalase, responsáveis pelo equilíbrio redox dos animais (FONSECA-FONSECA et al., 2019a). Além disso, o JM-20 teve efeito sobre a aquisição e consolidação de memória em ratos após o comprometimento cognitivo induzido por escolopamina (WONG-GUERRA et al., 2019). Estes fatos nos levam a considerar sua utilização como um composto promissor para uso terapêutico e incentiva o estudo dos efeitos do JM-20 em outras vias principalmente as associadas ao SNC.

Tabela 1. Efeitos do composto JM-20 descritos na literatura.

Efeito	Modelo	Referência
Ansiolítico	Camundongo	(NUÑEZ-FIGUEREDO et al., 2013b)
Redução do comportamento agressivo induzido por isolamento	Camundongo	(NUÑEZ-FIGUEREDO et al., 2013b)
Proteção em modelo de convulsões induzidas por PTZ	Camundongo	(NUÑEZ-FIGUEREDO et al., 2013b)
Sedativo	Camundongo	(NUÑEZ-FIGUEREDO et al., 2013b)
Neuroprotetor	Cultura celular de Feocromocitoma (PC-12) e mitocôndrias isoladas do fígado de ratos	(NUÑEZ-FIGUEREDO et al., 2014a)
	Mitocôndrias e sinaptossomas isolados do cérebro de ratos	(NUÑEZ-FIGUEREDO et al., 2014b)
Atenuou efeitos da lesão isquêmica	Cultura de fatias de hipocampo de ratos Ratos	(NUÑEZ-FIGUEREDO et al., 2014c)
	Vesículas sinápticas, sinaptossomas, partículas submitocondriais e culturas de células (astrócitos) de cérebro de ratos	(NUÑEZ-FIGUEREDO et al., 2015)
	Ratos	(NUÑEZ-FIGUEREDO et al., 2016)
	Cultura de fatias de hipocampo de ratos	(RAMÍREZ-SÁNCHEZ et al., 2015)
Proteção da memória após comprometimento induzido por escopolamina	Ratos	(WONG-GUERRA et al., 2019)
Proteção contra danos induzidos por rotenona	SHSY-5Y humano (ATCC® CRL-2266 ™) Ratos	(FONSECA-FONSECA et al., 2019b)

O SNC, sistema nervoso periférico (SNP) e a junção neuromuscular apresentam em comum o sistema colinérgico. (MCCORRY, 2007; PICCIOTTO; HIGLEY; MINEUR, 2013). Este sistema é constituído pelo neurotransmissor acetilcolina (ACh), seus receptores e as enzimas responsáveis pela sua síntese e degradação (MCCORRY, 2007). A ACh é sintetizada no neurônio pré-sináptico, a partir da colina (proveniente principalmente da recaptação de colina pelo transportador de colina (ChT) e da acetil-CoA (proveniente do piruvato), em uma reação catalisada pela enzima colina acetiltransferase (ChAT). Posteriormente, é transferida para vesículas e liberada na fenda sináptica onde irá atuar nos receptores muscarínicos ou nicotínicos iniciando a transmissão sináptica (Figura 2) (MCCORRY, 2007; PICCIOTTO; HIGLEY; MINEUR, 2013; POHANKA, 2014). A interrupção da neurotransmissão colinérgica se dá através da hidrólise da ACh em acetato e colina por enzimas colinesterases (ChE) (MCCORRY, 2007; PICCIOTTO; HIGLEY; MINEUR, 2013). Nos seres humanos, podem ser encontrados dois tipos de colinesterases: a butirilcolinesterase (BChE) e a acetilcolinesterase (AChE) (MCCORRY, 2007; PICCIOTTO; HIGLEY; MINEUR, 2013).

Figura 2 - Ação da acetilcolinesterase na fenda sináptica.

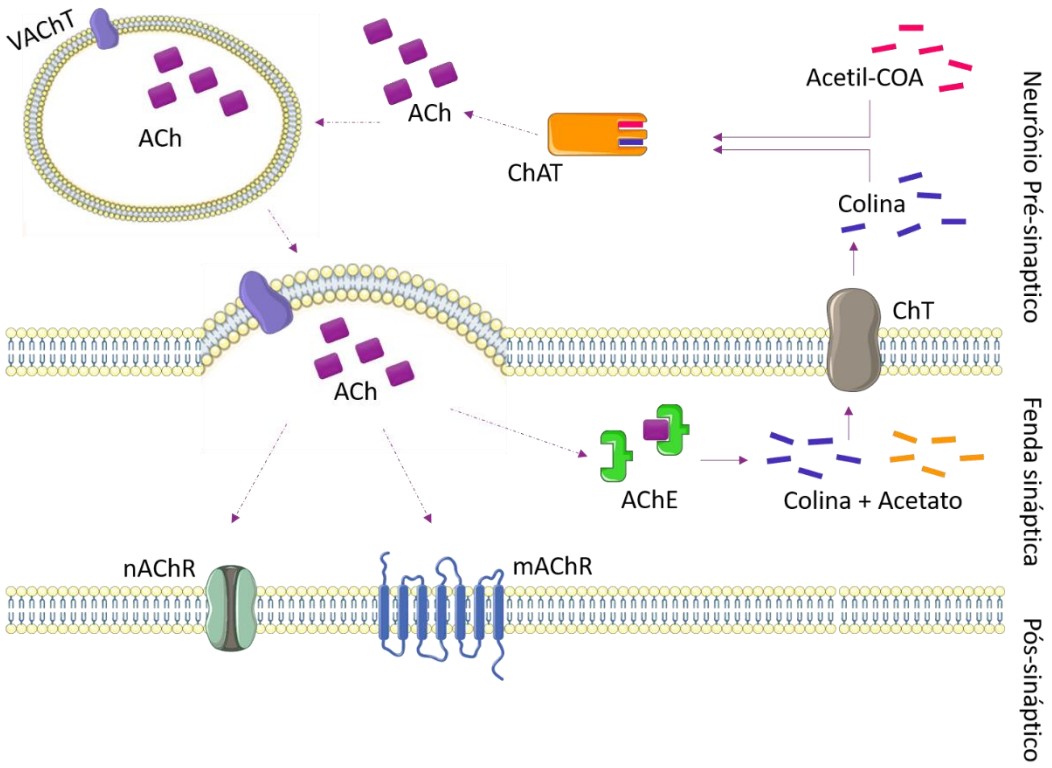

A ACh liberada na fenda sináptica pelos neurônios pré-sinápticos, através transportadores vesiculares de ACh (VAChT), pode interagir com os receptores nicotínicos (nAChR) ou muscarínicos (mAChR) presentes no neurônio pós-sinápticos. Ao término da neurotransmissão, a ACh é degradada em acetato e colina pela AChE ou BChE. A colina retorna ao neurônio pré-sináptico através do transportador de colina (ChT) e pode fazer parte da síntese de uma nova molécula de ACh pela ChAT. Fonte: o autor.

A AChE é uma hidrolase que apresenta alta eficiência catalítica (PETRONILHO; PINTO; VILLAR, 2011). Esta enzima possui um sitio ativo com diferentes subsítios (DA SILVA et al., 2018a; GRISARU et al., 1999). O subsítio esterático é onde encontra-se a tríade catalítica (serina, histidina e glutamato) diretamente responsável pela hidrolise da ACh (DA SILVA et al., 2018a; GRISARU et al., 1999; PETRONILHO; PINTO; VILLAR, 2011; SIEGEL et al., 2006). Também existe um subsítio aniônico (formado pelos resíduos de triptofano e glutamato), que interage com a parte catiônica da ACh (amina quaternária) e posiciona adequadamente o substrato para a hidrólise (DA SILVA et al., 2018a; GRISARU et al., 1999; PETRONILHO; PINTO; VILLAR, 2011; SIEGEL et al., 2006). Além disso, existe outra região denominada subsítio aniônico periférico, que influencia a conformação do subsítio catalítico, e pode estar envolvido na ação de alguns inibidores exógenos da enzima ou na inibição por excesso de substrato (DA SILVA et al., 2018a; GRISARU et al., 1999; PETRONILHO; PINTO; VILLAR, 2011; SIEGEL et al., 2006). Diferentes estudos tem demonstrado alterações na função da AChE relacionadas a sua inibição ou atividade acelerada (H. FERREIRA-VIEIRA et al., 2016; LÓPEZ; PASCUAL-VILLALOBOS, 2010; POHANKA, 2012; RICHENDRFER; CRETON, 2015; WOREK et al., 2000). Um exemplo bastante comum de inibição da AChE é a intoxicação por pesticidas organofosforados, essas substâncias tem a capacidade de se ligar a enzima e impedir que a mesma realize sua função de hidrolise da ACh consequentemente impedindo a interrupção da neurotransmissão colinérgica, causando reações como perda do controle muscular, convulsões e até mesmo a morte (DA SILVA et al., 2018b; JOHN; SHAIKE, 2015; OCHOA; RODRIGUEZ; ZULUAGA, 2016). Por outro lado, quando ocorre a redução na liberação da ACh ou um aumento na produção ou atividade da AChE, a transmissão colinérgica pode ser prejudicada gerando sintomas como perda de memória. (LANCTÔT; RAJARAM; HERRMANN, 2009; MEHTA; ADEM; SABBAGH, 2012; NOGARA et al., 2015; RACCHI et al., 2004; YAN et al., 2008). Assim sendo, novas opções terapêuticas para patologias neurológicas, as quais apresentam uma disfunção no sistema colinérgico, tem sido amplamente estudadas (COLOVIC et al., 2013; FALSAFI et al., 2012).

A descoberta da síntese de ACh fora do sistema nervoso (não-neuronal) adicionou mais funções a esta molécula que estava sendo considerada apenas um neurotransmissor (GWILT; DONNELLY; ROGERS, 2007; WESSLER et al., 2003; WESSLER; KIRKPATRICK, 2001, 2016, 2008). Primeiramente, foi sugerido que poderia haver ACh fora no sistema nervoso devido a presença de seus precursores nas células. A acetil-CoA, é o principal produto do catabolismo de carboidratos, proteínas e lipídios (WESSLER; KIRKPATRICK; RACK, 1998)

e a colina é proveniente da quebra intracelular de fosfolipídios ou da captação de colina extracelular por meio de transportador de colina (WESSLER et al., 2003; WESSLER; KIRKPATRICK, 2001, 2016, 2008; WESSLER; KIRKPATRICK; RACK, 1998). Uma vez que a acetil-CoA e a colina estão presentes na maioria das células, torna-se possível a síntese da ACh além do sistema nervoso (GWILT; DONNELLY; ROGERS, 2007; WESSLER et al., 2003; WESSLER; KIRKPATRICK, 2001, 2016, 2008). De fato, a expressão dos componentes do sistema colinérgico foi encontrada nas células epiteliais (pele, vias aéreas, intestino), nas células imunes (linfócitos) e nos eritrócitos (FUJII et al., 2017; SALDANHA, 2017; WESSLER; KIRKPATRICK, 2008). A ACh não-neuronal está envolvida na regulação de funções celulares básicas como proliferação, diferenciação, organização do citoesqueleto e liberação local de mediadores (óxido nítrico (ON)) e citocinas pró-inflamatórias, por exemplo) (WESSLER et al., 2003; WESSLER; KIRKPATRICK, 2016, 2008; WESSLER; KIRKPATRICK; RACK, 1998). Diferentemente da liberação de ACh através de vesículas pelos neurônios, o conhecimento sobre os mecanismos de liberação da ACh não-neuronal ainda é escasso (WESSLER; KIRKPATRICK, 2016). Entretanto, existem evidências que a ACh não-neuronal pode ser liberada imediatamente após sua síntese pela célula (WESSLER; KIRKPATRICK, 2001). Após a liberação a ACh pode interagir com receptores nicotínicos e muscarínicos da célula de origem ou de células vizinhas (WESSLER; KIRKPATRICK, 2001).

Outro mecanismo importante nos organismos aeróbios é o sistema antioxidante endógeno, o qual neutraliza as espécies reativas produzidas fisiologicamente (BIRBEN et al., 2012; RAHAL et al., 2014). Algumas dessas espécies reativas desempenham importantes papeis biológicos contra infecções, como mediadores da resposta inflamatória e, por este motivo, não são imediatamente neutralizadas (BIRBEN et al., 2012; RAHAL et al., 2014). Porém, quando há o desequilíbrio entre a produção de espécies reativas e a capacidade da célula de neutralizá-los, ocorre um o processo denominado estresse oxidativo (BIRBEN et al., 2012; RAHAL et al., 2014). O estresse oxidativo pode levar a dano aos lipídios, proteínas e ácidos nucleicos, devido à interação das espécies reativas com estas moléculas, induzindo necrose ou a apoptose (BIRBEN et al., 2012).

O alto consumo de oxigênio aliado ao baixo nível de antioxidantes e a alta concentração de ácidos graxos poli-insaturados resultam na grande susceptibilidade dos tecidos ao dano oxidativo (Figura 3) (ARUOMA, 1998; BIRBEN et al., 2012; FLOYD; HENSLEY, 2002). A interação entre as espécies reativas de oxigênio e de nitrogênio com os ácidos graxos insaturados das membranas celulares provocam um processo denominado peroxidação lipídica (BIRBEN et al., 2012; FLOYD; HENSLEY, 2002). Este processo está presente durante o

metabolismo celular normal e, em excesso nas doenças neurodegenerativas, é responsável pelo comprometimento celular, incluindo alteração na liberação de neurotransmissores. (ARUOMA, 1998; BIRBEN et al., 2012; FLOYD; HENSLEY, 2002; UTTARA et al., 2009). O estresse oxidativo em doenças neurodegenerativas se manifesta através da presença de proteínas oxidadas, de produtos de glicosilação avançada e da peroxidação lipídica (POHANKA, 2014). Consequentemente, há a formação de espécies tóxicas, tais como peróxidos, álcoois, aldeídos, carbonilas, cetonas e modificações no DNA nuclear e mitocondrial (BIRBEN et al., 2012; FLOYD; HENSLEY, 2002). Assim, a ingestão de antioxidantes exógenos pode colaborar no estado de equilíbrio (ARUOMA, 1998; BIRBEN et al., 2012).

Figura 3 - Esquema representativo do dano oxidativo.

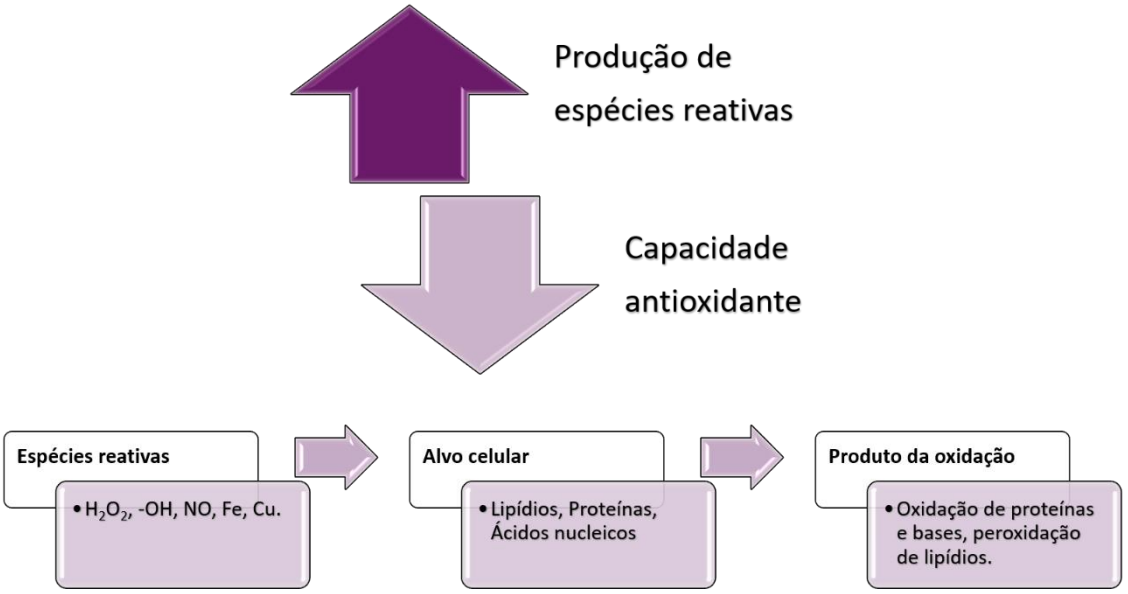

As espécies reativas descritas são produzidas e interagem com alvos celulares, formando produtos de oxidação responsáveis pelos danos no tecido. FONTE: o autor.

Para o estudo de doenças humanas, de moléculas terapêuticas potenciais e de toxicologia usa-se animais de experimentação, principalmente, modelos mamíferos de pequeno porte como camundongos e ratos. Entretanto, o uso de animais de experimentação para estudos toxicológicos de diferentes substâncias tem sido cada vez mais questionado (BHANUSHALI et al., 2015; JENNINGS, 2015; LIMONCIEL, 2014; ROBINSON, 2005). Têm-se preconizado a utilização de metodologias alternativas, as quais têm como principal objetivo a substituição, a redução no número de animais para este fim e quando necessário sua utilização o refinamento das técnicas empregadas (3Rs do inglês *replacement*, *reduction* e *refinement*) (BHANUSHALI et al., 2015; JENNINGS, 2015; LIMONCIEL, 2014;

ROBINSON, 2005) (Figura 4). Testes preliminares em células estão de acordo com a diretiva dos 3Rs, mas há a necessidade de que os testes *in vitro* sejam confiáveis e precisos para que as substâncias estudadas sejam adequadamente avaliadas antes de estudos clínicos e pré-clínicos (BRENDLER-SCHWAAB et al., 1994; LIMONCIEL, 2014). Ao mesmo tempo, é desejável que as avaliações de citotoxicidade *in vitro* sejam suficientemente rápidas e de baixo custo para permitir a triagem de um grande número de potenciais candidatos a medicamentos (BRENDLER-SCHWAAB et al., 1994; LIMONCIEL, 2014).

Figura 4 - Esquema representativo da diretiva dos 3Rs ("Replacement", "Reduction" e "Refinement").

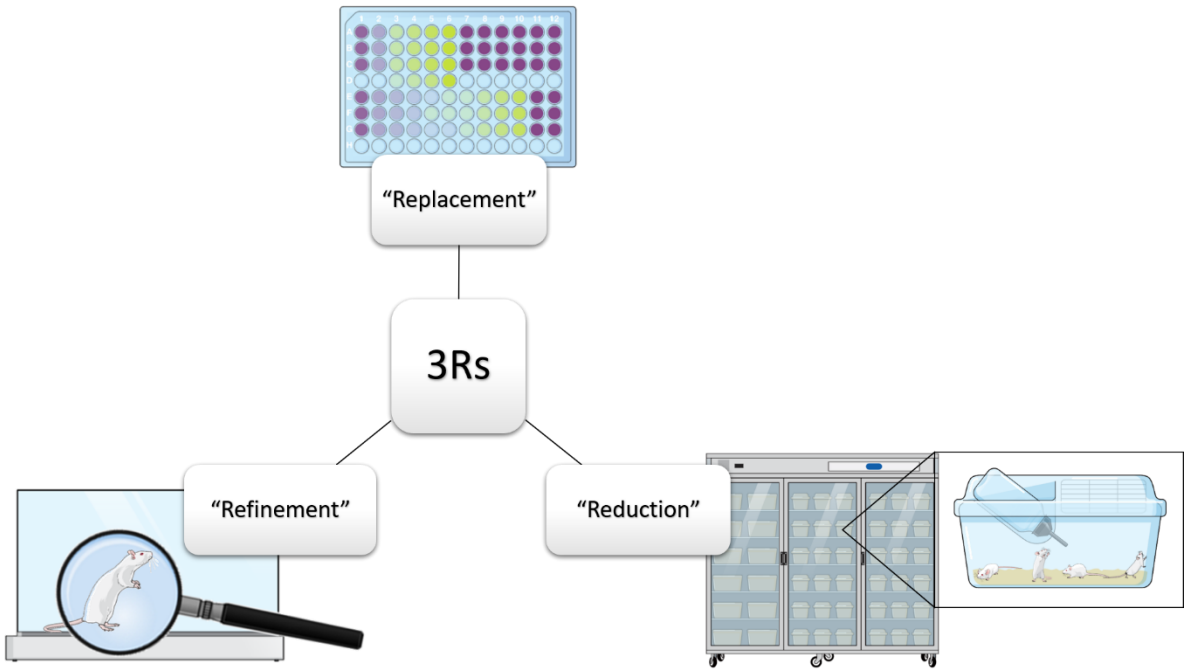

"Replacement" refere-se à substituição de vertebrados, através da utilização de modelos alternativos, ensaios *in vitro* ou *in silico*. "Reduction" compreende a redução no número de animais utilizados quando necessário e "Refinement" é o refinamento das técnicas aplicadas a modelos de vertebrados evitando o estresse desnecessário e repetições experimentais. FONTE: o autor.

O *docking molecular*, é uma potente ferramenta utilizada mundialmente e tem a capacidade de prever a conformação (orientação) de um ligante de interesse quando este interage com um receptor ou uma enzima (CHEN, 2015; FERREIRA et al., 2015). Os programas usados na docagem molecular para descoberta de candidatos a fármacos em sua fase inicial elucidam as interações entre essas moléculas e o local alvo (DAINA; MICHIELIN; ZOETE, 2017; HU et al., 2020; PIRES; BLUNDELL; ASCHER, 2015). Da mesma forma, análises de triagem virtual de farmacocinética e a toxicidade também podem incluir abordagens computacionais utilizando plataformas online que possuem a capacidade

de prever se a substância avançará para o próximo estágio de pesquisa e será realmente usada como terapia no futuro. Estas plataformas detêm um banco de dados com embasamento em resultados prévios publicados utilizando modelos *in vivo* (DAINA; MICHIELIN; ZOETE, 2017; HU et al., 2020; PIRES; BLUNDELL; ASCHER, 2015; PIRES; KAMINSKAS; ASCHER, 2018).

1.1 JUSTIFICATIVA

O interesse por moléculas biologicamente ativas e com propriedades multialvo, capazes de desempenhar efeitos simultâneos frente a diferentes patologias é de grande relevância. Nesse contexto, o JM-20 é uma molécula nova que possui diferentes propriedades farmacológicas de interesse científico. Entretanto, ainda não foi totalmente elucidada quanto seu mecanismo de ação e a toxicidade. Assim, torna-se importante avaliar o efeito desse composto no sistema colinérgico neuronal e não-neuronal, via de diferentes patologias (principalmente neurodegenerativas), bem como, o potencial antioxidante do JM-20, pois o estresse oxidativo pode estar diretamente envolvido a causas ou consequências de diferentes doenças. Além disso, o estudo da citotoxicidade do JM-20 em células humanas saudáveis é de grande interesse. Neste sentido, o JM-20 também poderia inibir enzimas especificas, proteger do estresse oxidativo e quiçá apresentar efeitos adversos mínimos.

1.2 OBJETIVO GERAL

Avaliar o potencial multialvo do composto JM-20 como potencial antioxidante e seus efeitos na atividade de colinesterases e na toxicidade *in vitro* e *in silico.*

1.2.1 Objetivos específicos

→ Avaliar o efeito do composto JM-20 na atividade da enzima acetilcolinesterase de diferentes fontes.

→ Determinar o tipo de inibição enzimática causada pelo JM-20**.**

→ Avaliar o efeito do JM-20 na atividade da enzima butirilcolinesterase de diferentes fontes.

→ Realizar analises *in sílico de docking molecular* afim de elucidar as interações entre o JM-20 e as enzimas.

→ Verificar o potencial antioxidante do composto, bem como efeito protetor em relação estresse oxidativo induzido por Fe^{2+}.

→ Avaliar a toxicidade do JM-20 em hemácias e leucócitos humanos saudáveis.

→ Prever a farmacocinética e toxicidade do JM-20 em através de um *screening virtual* utilizando ferramentas computacionais de simulação.

2.1 ARTIGO PUBLICADO – Molecular docking and *in vitro* evaluation of a new hybrid molecule (JM-20) on cholinesterase activity from different sources

Biochimie 168 (2020) 297–306

Contents lists available at ScienceDirect

Biochimie

journal homepage: www.elsevier.com/locate/biochi

Research paper

Molecular docking and in vitro evaluation of a new hybrid molecule (JM-20) on cholinesterase activity from different sources

Fernanda D'Avila da Silva [a], Pablo Andrei Nogara [a], Estael Ochoa-Rodríguez [b], Yanier Nuñez-Figueredo [b], Maylin Wong-Guerra [b], Denis Broock Rosemberg [a], João Batista Teixeira da Rocha [a, *]

[a] Programa de Pós-graduação Em Ciências Biológicas: Bioquímica Toxicológica, Universidade Federal de Santa Maria, 97105-900, Santa Maria, RS, Brazil
[b] Centro de Investigación y Desarrollo de Medicamentos, Ave 26, N° 1605 Boyeros y Puentes Grandes, CP10600, La Habana, Cuba

ARTICLE INFO

Article history:
Received 3 May 2019
Accepted 20 November 2019
Available online 23 November 2019

Keywords:
Selectivity
Acetylcholinesterase
Benzodiazepine
Dihydropyridine
In silico
In vitro

ABSTRACT

The main function of AChE is the hydrolysis of the neurotransmitter acetylcholine (ACh) at the neuromuscular and in cholinergic brain synapses. In some pathologies, loss of cholinergic neurons may be associated with a deficiency of ACh in specific brain areas. Consequently, the study of new safe drugs that inhibit AChE is important, because they can increase ACh levels in the synaptic cleft without adverse effects. Here, we evaluated the effects of JM-20 (a benzodiazepine–dihydropyridine hybrid molecule) on cholinesterase (ChE) activities from distinct sources (AChE from *Electrophorus electricus* (*Ee*AChE), human erythrocyte membranes (*Hs*AChE (ghost)), total erythrocyte (*Hs*AChE (erythrocyte)) and BChE from plasma (*Hs*BChE) and purified enzyme from the horse (*Ec*BChE)). Kinetic parameters were determined in the presence of 0.05–1.6 mM of substrate concentration. The interactions ChEs with JM-20 were performed using molecular docking simulations. JM-20 inhibited all tested AChE but not BChE. The IC_{50} values were 123 nM ± 0.2 (*Ee*AChE), 158 nM ± 0.1 (ghost *Hs*AChE), and 172 nM ± 0.2 (erythrocytic *Hs*AChE). JM-20 caused a mixed type of inhibition (it altered K_m and V_{max} of AChE). The molecular docking indicated the binding poses and the most plausible active isomer of JM-20. Besides giving important data for future drug design, our results help us understand the mode of action of JM-20 as a specific inhibitor of AChE enzymes.

© 2019 Elsevier B.V. and Société Française de Biochimie et Biologie Moléculaire (SFBBM). All rights reserved.

1. Introduction

Acetylcholine (ACh) is a neurotransmitter present in the central nervous system (CNS), peripheral nervous system (PNS) and at the neuromuscular junction [1–3]. ACh is synthesized by a specific enzyme (choline acetyltransferase) from choline and coenzyme A, transferred to vesicles and then released into the synaptic cleft, acting on muscarinic and/or nicotinic ACh receptors [1–4]. Physiologically, the interruption of cholinergic neurotransmission is performed by cholinesterases [1]. In humans, both butyrylcholinesterase (BChE) and acetylcholinesterase (AChE) can hydrolyze ACh [1–4].

AChE is the enzyme responsible for regulating ACh levels at synapse cleft by hydrolyzing ACh into choline and acetate [3–7]. However, in some pathologies (for example in Alzheimer's disease), dysfunctions in brain regions that contain cholinergic neurons can occur, resulting in the loss of cholinergic neurotransmission [2,8]. Thus, the discovery of new drugs that can inhibit AChE activity and increase ACh levels in the synaptic cleft (without causing adverse effects) is relevant. Multiple variants of AChE can be produced by alternative splicing, for instance, the synaptic, erythrocytic and readthrough AChE isoforms [3,6,9]. Thus, extensive research of the cholinergic system has been used to unravel novel therapeutic medicines for neurological and psychiatric pathologies, which present dysfunction in the cholinergic system [2,5,10,11].

JM-20 (3-ethoxycarbonyl-2-methyl-4- (2-nitrophenyl) –4,11-dihydro-1H-pyrido [2,3-b] [1,5] benzodiazepine) is a compound which derives from 1,5-benzodiazepines, by adding the 1,4-dihydropyridine moiety fused to the benzodiazepine ring (Fig. 1)

* Corresponding author. Universidade Federal de Santa Maria, Camobi, 97105-900, RS, Brazil.
E-mail addresses: jbtrocha@yahoo.com.br, jbtrocha@pesquisador.cnpq.br (J.B.T. Rocha).

https://doi.org/10.1016/j.biochi.2019.11.011
0300-9084/© 2019 Elsevier B.V. and Société Française de Biochimie et Biologie Moléculaire (SFBBM). All rights reserved.

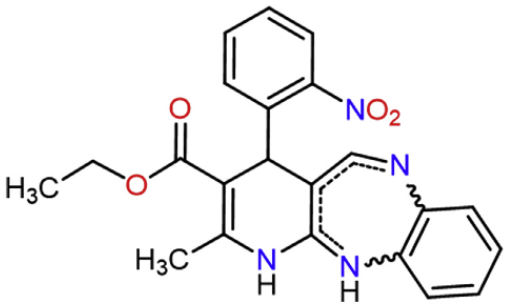

Fig. 1. Structural formula of the compound 3-ethoxycarbonyl-2-methyl-4-(2-nitrophenyl) -4-11-dihydro-1H-pyrido [2,3- b] [1,5] benzodiazepine (JM-20).

[12,13]. JM-20 reduces the aggressive behavior of socially isolated mice and increases the latency period for the beginning of the tonic crisis and the percentage of survival of animals with seizures caused by pentylenetetrazole [14]. JM-20 reduces anxiolytic-like responses in mice or rats treated orally with 2–10 mg/kg of the compound [15]. Furthermore, JM-20 may act as a multi-target neuroprotective agent by reducing the neuronal excitotoxic injury and protecting the mitochondria from Ca^{2+}-induced toxicity, thereby preserving the cellular energy balance [13,16–18]. Importantly, JM-20 does not induce mortality, suggesting the absence of toxic effects [15] which leads us to consider its use as a promising compound for therapeutic use. Here, we evaluated in vitro, the effect of JM-20 on AChE activity from different sources, e.g., the purified enzyme from *Electrophorus electricus* (*Ee*AChE), human erythrocyte membranes (*Hs*AChE (ghost)) and, human total erythrocyte (*Hs*AChE (erythrocyte)). We also verified the effect of JM-20 in the BChE activity purified from *Equus caballos* (*Ec*BChE) and in non-purified BChE from human plasma (*Hs*BChE). Moreover, kinetic analyses and *in silico* molecular docking were performed to elucidate the interactions between the compound and the enzymes, as well as the type of inhibition.

2. Material and methods

2.1. Compounds and reagents

JM-20 was synthesized, purified and characterized as reported elsewhere [15]. The compound was dissolved in dimethyl sulfoxide (DMSO). All chemicals and purified enzymes used were purchased from Sigma-Aldrich (St. Louis, MO, USA).

2.2. Sample preparation

2.2.1. Isolation of human erythrocyte membrane (ghost)

Humans erythrocyte were obtained from a healthy volunteer from the toxicological biochemistry laboratory at the Universidade Federal de Santa Maria. The Ethical Committee of the UFSM approved the protocol (nº 3.471.823) used in this study. Freshly drawn heparinized human blood was centrifuged at 200×*g* for 10 min. Plasma was removed, isotonic KCl (150 mM) was added, and the sample was centrifuged at 200×*g*. This procedure was repeated thrice. Red cells were maintained at 0–4 °C for the erythrocyte ghosts preparation, according to Bjerrum, 1979 [19]. Cells (20 mL) were lysed by the addition of 20 mL hemolyzing buffer A (4 mM $MgSO_4$, 3.8 mM CH_3COOH, pH 3.6), resulting in 50% hematocrit. After 1 min incubation, the cellular suspension was centrifuged at 23.000×*g* for 12 min, and posteriorly the supernatant was removed. In this procedure, the erythrocyte ghosts content was reduced to ~3% (wt/wt). At this stage, samples can present a pink color. The tonicity of the 3% (wt/wt) hemoglobin containing packed ghost was increased by addition 100 μL of buffer C (KCl 2 M) per mL of erythrocyte ghosts suspension. The suspension was incubated for 2 min, and then washed through the addition of 220 mL of medium B (4 mM $MgSO_4$, 1.2 mM CH_3COONa, 2 mM NaH_2PO_4/Na_2HPO_4, pH 7.0) and centrifuged at 23.000×*g* for 12 min. This procedure was repeated four times until the erythrocyte ghosts had a greyish white color. The erythrocyte ghosts were resuspended in isotonic KCl (150 mM). *Hs*AChE assays using these membranes were realized immediately after erythrocyte ghosts isolation. Protein was adjusted to approximately 165 μg/mL and the final content of protein in the AChE reaction system was 3–4 μg per well (0.2 mL).

2.2.2. Plasma and erythrocyte preparation

Freshly drawn heparinized human blood was centrifuged at 200×*g* for 10 min. Plasma was separated and diluted 40 times and the erythrocyte were washed using saline solution and centrifuged at 200×*g* for 10 min, this procedure was repeated 3 times. After washing, red blood cells were diluted 600 times. *Hs*BChE and *Hs*AChE assays were performed immediately after dilution of the samples. The procedure was performed as described elsewhere [11,20].

2.2.3. ChE enzymatic assay

ChE activity was measured according to the method proposed by Ellman et al. [21]. The reaction medium consisted of the following reagents at final concentration: 10 mM of potassium phosphate buffer (pH 7.4), 1 mM DTNB [5,5′-dithio-bis(2-nitrobenzoic acid)], AChE enzyme (0.0125 U of *Ee*AChE/0.2 mL, i.e., the final volume in the wells; 3–4 μg protein of *Hs*AChE from human erythrocyte membranes/0.2 mL, 10–15 μg protein of *Hs*AChE from human total erythrocyte/0.2 mL, 15–20 μg protein of *Hs*BChE from human plasma/0.2 mL or 0.005 U of purified *Ec*BChE/0.2 mL), and JM-20 (25 nM - 40 μM) or 0.05% DMSO (control group). This system was preincubated for 30 min at room temperature (26 °C ± 2). Then, we added acetylthiocholine iodide (0.4 mM, final concentration) to start the reaction. The increase in absorbance was monitored in a BioRad iMark microplate reader (Japan) at 415 nm using a plate of 96 wells. Some experiments were also performed in a cuvette (1 ml; in a Shimadzu UV-1800 spectrophotometer, Japan) for determining the effect of JM-20 in the *Ee*AChE and *Ec*BChE in the absence of pre-incubation. The final concentrations of protein used in the cuvette assays were the same used in 96 well plates.

2.2.4. Determination of IC_{50} values

The Half-maximal inhibitory concentration (IC_{50}) was determined by nonlinear regression log (inhibitor) vs. response – variable slope in accordance to equation (1), using GraphPad, Prism 6.01.

$$Y = Bottom + (Top - Bottom) / (1 + 10\hat{}((LogIC50 - X) * HillSlope)); \quad (1)$$

HillSlope describes the steepness of the family of curves (A HillSlope of −1.0 is standard).

Top and Bottom are plateaus in the units of the Y-axis.

2.2.5. Kinetic analysis

Kinetic parameters of the AChE activity were measured according to the method proposed by Ellman et al. [21] previously described by varying the concentration of acetylthiocholine as a

substrate (0.05, 0.1, 0.2, 0.4, and 1.6 mM) in the presence and absence of JM-20 (0, 75, 150, 250, and 400 nM) using a plate of 96 wells. Different plots were constructed for assessing the type of inhibition. The V_{max} constant was obtained through nonlinear regression enzyme kinetic – inhibition, substrate inhibition using GraphPad, Prism 6.01, and K_i were obtained through nonlinear regression enzyme kinetic – inhibition, mixed inhibition in accordance to equation (2), using GraphPad, Prism 6.01.

$$V_0 = V_{max}/(1 + I/(Alpha*K_i))*[S]/K_m*(1 + I/K_i)/(1 + I/ \times (Alpha*K_i)) + [S]; \quad (2)$$

Alpha determines the mechanism. Its value determines the degree to which the binding of inhibitor changes the affinity of the enzyme for the substrate.

K_i is the inhibition constant.

2.2.6. In silico analysis

To simulate the binding mode of interactions between the JM-20 molecules and the cholinesterase enzymes, Vina 1.1.1 program was used [22], with exhaustiveness of 200, using two docking protocols: a) one in the presence of water molecules [23–25] (the methodologies and results from the docking performed in the absence of water are presented as supplementary materials in supporting information) and b) other with the highly-conserved network of water molecules in the human acetyl- and butiryl-cholinesterases [26]. In the first moment, a blind docking was carried out with the enzymes, where were observed the binding of the ligands (JM-20 isomers) in the respective active sites. To improve the interactions between the enzyme and ligands, a local docking was further made. By the *Hs*AChE structure from the Protein Data Bank – PDB – with the code 4EY6 [27], the gridbox was centered on the coordinates: x = −13.25, y = −46.76 and z = 33.52, with the dimensions: 30 × 30 × 30 Å. For *Hs*BChE docking, the structure PBD: 4BDS from the Protein Data Bank [28] was used. The gridbox was centered on the coordinates: x = 138.8, y = 111.5 and z = 39.9, with the dimensions: 30 × 30 × 30 Å. For the protein structures, ions, ligands, and water were removed, while the hydrogens were added using the CHIMERA 1.8 program [29]. In the docking with water, and for *Hs*AChE the HOH molecules 704, 705, 707, 773, 803, 805 and 815 were kept; while for *Hs*BChE, the water molecules were 2045, 2064, 2089, 2090, 2093, 2131, and 2140 [26]. JM-20 molecules, galantamine, and tacrine were created using the Avogadro 1.1.1 software [30] followed by semi-empirical PM6 [31] geometry optimization using the MOPAC2016 program [32]. The ChE enzymes and the ligands were prepared for the docking using AutoDock Tools 4.2 [33], in which the compounds were considered flexible (with PM6 charges) and the enzymes rigid (with Gasteiger charges). The non-polar hydrogens were omitted. The structures with the most favorable binding free energy were selected and analyzed using Accelrys Discovery Studio 3.5 [34]. For more details, see the Supporting information.

2.2.7. Statistical analyses

Statistics have been performed using the GraphPad Prism 6 (version 6.01, GraphPad Software, Inc., USA). Results were expressed as the mean ± standard error of the mean (SEM). ChE activity data were analyzed using nonlinear regression enzyme kinetic – inhibition, substrate inhibition (comparisons with parameters obtained with Michaelis-Menten see Supplementary Material Table S2) and tested when slopes and intercepts were significantly different. Values of $p < 0.05$ were considered significantly different.

3. Results and discussion

Here, we expand the knowledge regarding the JM-20 compound, a new alternative as AChE inhibitor, which belongs to a new family of 1,5-benzodiazepines, structurally different from currently available 1,5-benzodiazepines by the presence of a 1,4-dihydropyridine moiety fused to the benzodiazepine ring [12,14]. JM-20 has been evaluated as a possible inhibitor of *Ee*AChE, *Hs*AChE (ghost), *Hs*AChE (erythrocyte) and of *Ec*BChE and *Hs*BChE. Regardless of the origin of AChE, compound JM-20 acts as an AChE inhibitor at nanomolar range and, surprisingly, IC_{50} values (Table 1) were lower than those previously reported for tacrine (reference drug in inhibition of AChE) that present IC_{50} around 180 nM ± 10 for *Ee*AChE and 150 nM ± 10 for *Hs*AChE [35–37]. The IC_{50} values give an indication about the potency of a substance in inhibiting AChE activity [38]. The IC_{50} and K_i values obtained here for JM-20 is within the range previously reported for tacrine using either the *Hs*AChE or *Ee*AChE [35,39–41].

Additionally, studies using compounds structurally similar to JM-20 (containing dihydropyridine or benzodiazepine group) demonstrated a potential inhibitory effect on *Ee*AChE activity [35,37,42,43]. To understand the inhibitory mechanism of the JM-20 compound on AChE activity, reactions were measured in the presence of different concentrations of substrate and data were analyzed according to the nonlinear regression enzyme kinetic – inhibition (substrate inhibition; GraphPad, Prism), Lineweaver-Burke, Eadie Hofstee, and Dixon method. Three different concentrations of inhibitor were used. K_m and V_{max} values were calculated from the slope of regression (Table 2 and Table 3, respectively).

JM-20 inhibited the enzyme activity proportionally to the increase in the concentration of the compound. Besides, JM-20 increased the K_m values as a function of its concentration (Table 2); while V_{max} decreased in the presence of increasing JM-20 concentrations (Table 3). These data suggest a mixed type of enzymatic inhibition [39,44]. The same kinetic assay approach was used for other sources of AChE. We used DMSO (0.05%) as control or JM-20 at a final concentration of 75, 150 and 250 nM in *Ee*AChE (Fig. 2). Nonlinear regression of the Lineweaver-Burke plot indicated significant differences between the slopes in the absence or presence of JM-20 ($F = 122.21$, $p < 0.0001$). Similar results were observed with Eadie Hofstee plot ($F = 27.94$, $p < 0.0001$).

*Hs*AChE (ghost) (Fig. 3) was also inhibited by JM-20, but in this test, we used 100 nM, 250 nM and 400 nM of inhibitor. The statistical analysis also indicated a significant difference between slopes obtained in the absence and presence of JM-20 ($F = 30.18$, $p < 0.0001$ for the Lineweaver-Burk plot and $F = 3.58$, $p < 0.0001$ for the Eadie Hofstee plot). For *Hs*AChE (erythrocyte), we tested 75, 150 and 250 nM of JM-20 (Fig. 4). The difference between the slops in the absence or presence of JM-20 was significant ($F = 12.93$, $p < 0,0001$ for the Lineweaver-Burk plot and $F = 3.29$, $p = 0.0254$ for the Eadie Hofstee plot). Furthermore, JM-20 was specific for AChE because it did not alter *Hs*BChE and *Ec*BChE activities when

Table 1
JM-20 IC_{50} and K_i values for ChE activity. IC_{50} was determined by nonlinear regression (log inhibitor vs response) in accordance to equation Y = Bottom + (Top-Bottom)/(1 + 10 ^((LogIC$_{50}$ -X) * HillSlope)), using GraphPad, Prism 6.01, and K_i values were obtained through nonlinear regression enzyme kinetic – inhibition, mixed inhibition in accordance to equation $V_0 = V_{max}/(1 + I/(Alpha * K_i)) * [S]/K_m * (1 + I/K_i)/(1 + I/(Alpha * K_i)) + [S]$.

ChE	IC_{50} (nM)	K_i (nM)
*Ee*AChE	123 ± 0.2	18 ± 2.5
*Hs*AChE (ghost)	158 ± 0.1	165 ± 25
*Hs*AChE (erythrocyte)	172 ± 0.2	99 ± 24

Table 2
K_m values for cholinesterase (ChE activity) from different sources in the presence or absence of JM-20. K_m expressed in mM (acetylthiocholine as substrate).

Concentration (nM)	*Ee*AChE	*Hs*AChE (ghost)	*Hs*AChE (erythrocyte)	*Hs*BChE (plasma)
Control	0.15 ± 0.03	0.28 ± 0.08	0.13 ± 0.02	0.27 ± 0.03
75	0.25 ± 0.09	–	0.21 ± 0.06	0.29 ± 0.06
100	–	0.32 ± 0.13	–	–
150	0.53 ± 0.13	–	0.17 ± 0.02	0.17 ± 0.05
250	0.38 ± 0.09	0.41 ± 0.24	0.43 ± 0.13	0.24 ± 0.03
400	0.36 ± 0.05	0.34 ± 0.05	–	0.25 ± 0.02

Table 3
V_{max} values for ChE activity from different sources in the presence or absence of JM-20. V_{max} activity expressed as Δ absorbance at 415 nm/s/mg protein (for *Ee*AChE); Δ absorbance at 415 nm/min/mg protein (for *Hs*AChE-Ghost); and, Δ absorbance at 415 nm/h/mg protein (for *Hs*AChE-erythrocyte and *Hs*BChE-plasma). Absorbance was determined in wells containing 0.2 ml of enzyme incubation media (for details see Material and Methods) in a BioRad iMark microplate reader (Japan).

Concentration (nM)	*Ee*AChE	*Hs*AChE (Ghost)	*Hs*AChE (erythrocyte)	*Hs*BChE (plasma)
Control	42 ± 4	78 ± 13	50 ± 2	156± 10
75	. 20± 4	–	50 ± 8	152 ± 20
100	–	60 ± 15	–	–
150	16 ± 2	–	32 ± 2	124 ± 11
250	9 ± 1	47 ± 18	31 ± 4	130 ± 5
400	5 ± 1	30 ± 2	-	139 ± 3

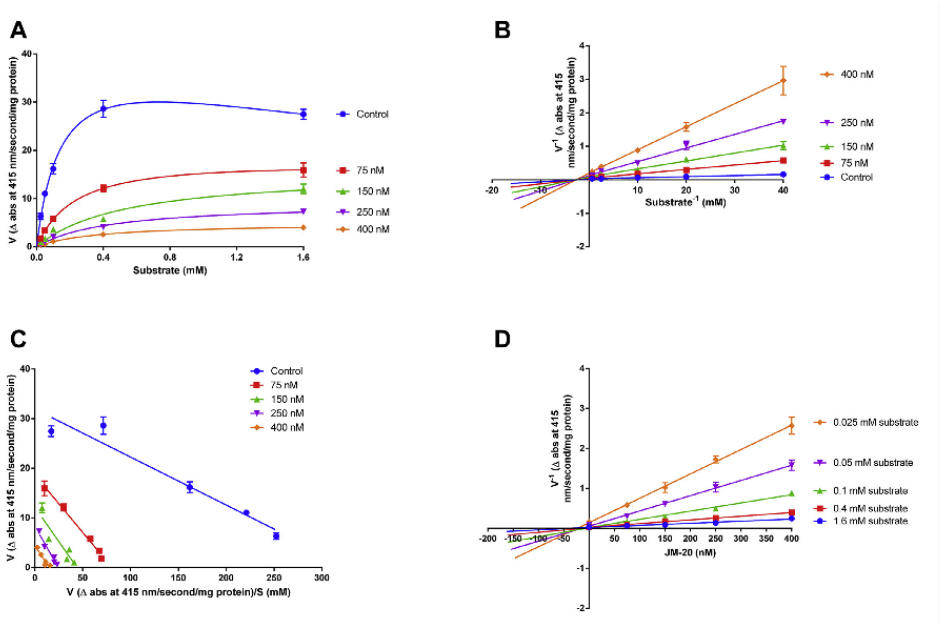

Fig. 2. Enzyme kinetic plots for acetylcholinesterase from the fish *Electrophorus electricus*: Nonlinear regression was calculated taken into consideration the substrate inhibition (acetylthiocholine) (A), Lineweaver-Burke (B), Eadie Hofstee (C) and Dixon plot (D) of *Ee*AChE. The data were expressed as mean ± SEM. The differences between the slopes are statistically significant.

tested in the nM range (Fig. 5A and Fig. 5B, respectively). To our knowledge, we showed for the first time the inhibition profile of JM-20 on AChE activity using kinetic analyses. The value of K_m indicates a substrate concentration that is required to reach half the maximum reaction velocity [44,45]. Mixed-type inhibitors modify both the binding of substrate and the velocity of the catalyzed reactions. Consequently, in our case, the type of inhibition of AChE by JM-20 was of the mixed type, because it changed both kinetic parameters [44,45]. We also observed that the highest concentration of the substrate used here (1.6 mM) reduced the velocity of the reaction catalyzed by *Ee*AChE (Fig. 2A). The inhibition possibly resulted from the binding of more than one substrate molecule (acetylthiocholine) in the active site of *Ee*AChE [46].

The effects of JM-20 (in the absence of pre-incubation) with *Ee*AChE and *Ec*BChE activities were also determined using a cuvette (Fig. 6). The results confirmed the specificity of JM-20 for AChE activity (Fig. 6A). Indeed, an inhibitory effect of *Ec*BChE (Fig. 6B) enzyme was obtained only using μM concentrations of JM-20 and

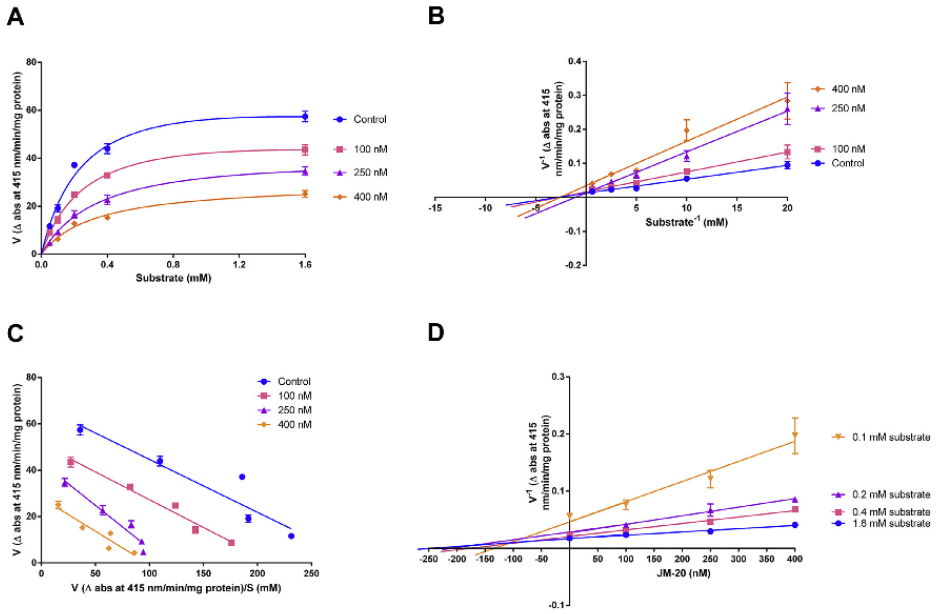

Fig. 3. Enzyme kinetic plots for acetylcholinesterase from the human erythrocyte ghosts: Nonlinear regression was calculated taken into consideration the substrate inhibition (acetylthiocholine) (A), Lineweaver-Burke (B), Eadie Hofstee (C) and Dixon plot (D) of *Hs*AChE (ghost). The data were expressed as mean ± SEM. The differences between the slopes are statistically significant.

the maximal inhibition was only about 50%, which was obtained with 10–20 μM of JM-20 (Fig. 6B).

Analyzing the structure of JM-20, we observe a chiral carbon on the position 4 (position that binds the 2-nitrophenyl group), and also it could present resonance in this structure, with the hydrogen atom from the amine group of the diazepine ring interchanging between the positions 6 and 11, being thus a tautomer. Furthermore, the diazepine ring has a nitrogen atom in the sp^3 hybridization (in position 6 or 11), which makes this ring nonplanar. In this case, due to the non-planarity of the diazepine ring, the benzene moiety can present two different conformations in the JM-20 molecule, like to an atropisomer [47]. A similar observation was found to the diazepam analogs, where the R isomers present the highest recognition for the benzodiazepine receptor complex [48,49]. All possibilities of the isomers of JM-20 and the nomenclature used for its identification are showed in Fig. S1.

Because isomers may vary in binding specificity and activity, the determination of the active form is crucial to elucidate the mechanism of action and potential pharmacological strategies [50–55]. Considering the importance of the structure and conformation of the molecules that interact in a determined target, we perform the molecular docking with the isomers of JM-20 (a–h) and the cholinesterases enzymes (AChE from *Homo sapiens* (*Hs*AChE) and *Electrophorus electricus* (*Ee*AChE), and BChE from *Homo sapiens* (*Hs*BChE) and *Equus caballus* (*Ec*BChE)) to determine the binding pose of them and the probability of the most active isomer.

Here, we applied two docking protocols, one without water molecules [23–25] and other taking into account the highly-conserved network of water molecules [26] (Fig. S2). In the molecular docking in the absence of water molecules (using the *Hs*AChE, *Ee*AChE, *Hs*BChE, and *Ec*BChE), all JM-20 isomers (a–h) can access the active site of the enzymes, with a specific pattern of interactions, where the isomers that varied the amine group (NH) position of 6–11 showed similar binding modes, generally (Fig. S3). In the absence of water, the JM-20 binds in the bottom of the gorge, near to the catalytic triad of both *Hs*AChE and *Hs*BChE enzymes.

Molecular docking simulations in the presence of the water molecules network (using the *Hs*AChE and *Hs*BChE), also demonstrated that the JM-20 interact in the active site of both cholinesterase, but with different binding pose when compared with the docking without water molecules (Figs. 7 and 8). These results are in accordance with the observations of Rosenberry et al. 2017 [26], where the exclusion of highly-conserved water molecules in the cholinesterase docking simulations resulted in unreliable binding poses. Furthermore, water molecules have potential importance in the catalysis of cholinesterases [26,56–58]. In this way, here we highlight the results from the docking in the presence of water. In the *Hs*AChE the JM-20 isomers interact mainly in the Peripheral Anionic Subsite (PAS), interacting with the W286 by H-bonds and anion-π interaction, with Y341 and L289 by hydrophobic π-π and alkyl-π interactions, respectively, and with the S293 by H-bonds (Fig. 7). The analysis of the interactions and the ΔG_{bind} (Table 4) shown that the isomers a, b, e, and f present a very similar binding pose, and more favorable binding energy when compared with the isomers c, d, g, and h, indicating that the 4-R isomers interact better with the *Hs*AChE. Besides, the benzodiazepine ring conformation in b and f allows a hydrophobic interaction with the L289 residue (Fig. 7B and F), which is correlated with its better binding energy (Table 4).

In the *Hs*BChE docking, the JM-20 isomers interacted in the Peripheral Anionic Subsite (PAS), in Acyl Binding Pocket (ABP), and the Catalytic Triad (CT) subsites. Here, we observed that the water 2093 has an important role in the interactions with the inhibitor, by the H-bonds with the acetyl and nitro moieties from JM-20 (Fig. 8). The isomers a and e showed a very similar binding pose, while the other isomers demonstrated a more diverse binding mode (Fig. 8),

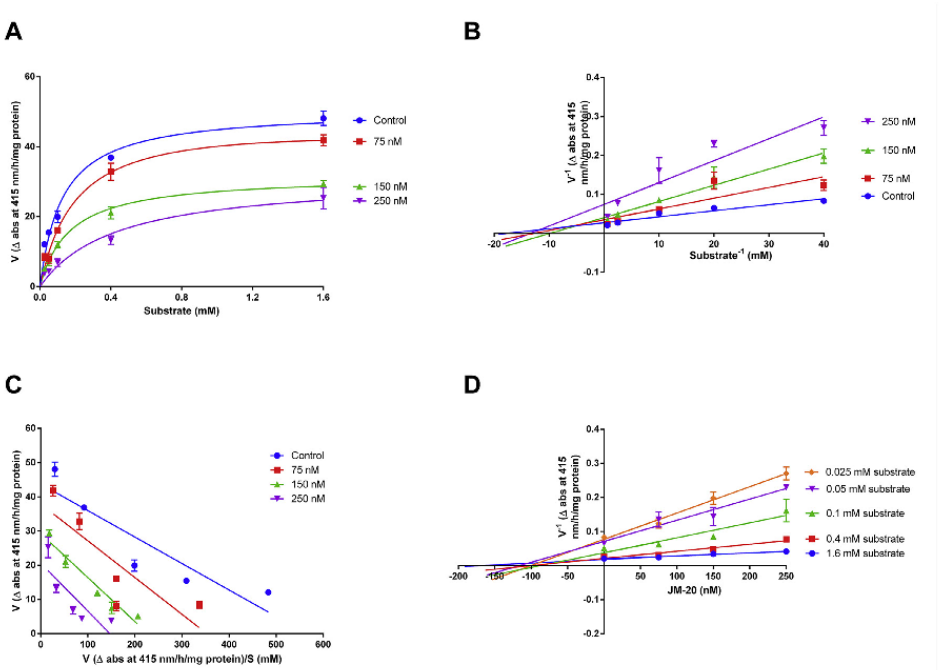

Fig. 4. Enzyme kinetic plots for acetylcholinesterase from the human erythrocyte: Nonlinear regression was calculated taken into consideration the enzyme inhibition by excess of substrate inhibition (A), Lineweaver-Burke (B), Eadie Hofstee (C) and Dixon plot (D) of *Hs*AChE (erythrocyte). The data were expressed as mean ± SEM. The differences between the slopes are statistically significant.

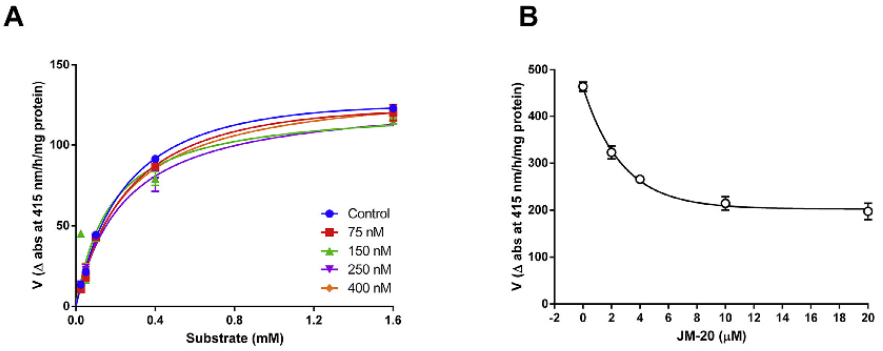

Fig. 5. *Hs*BChE (A) and *Ec*BChE (B) activities.

and as observed by the *Hs*AChE, the isomers a and e presented a better ΔG_{bind} (Table 4). The isomers with the lowest ΔG indicate a more favorable interaction with the proteins and consequently could have a major contribution to the enzyme inhibition. However, the other isomers also could have an important role in the enzyme inactivation. In the case of a and e, they interact with the *Hs*BChE mainly by hydrophobic interactions with the L286, F329, A328, and Y332 residues, and by H-bonds with S198, H438, and HOH2093 (Fig. 8A and E).

In general, position 4 (chiral center) of the JM-20 presented many binding modes in the *Hs*AChE and *Hs*BChE, while the tautomerism of the amine group affects less the *Hs*AChE than the *Hs*BChE. Docking simulations also revealed that the planarity of the benzodiazepine group affects the binding pose of JM-20 in the enzymes (Figs. 7 and 8). JM-20 bind in the PAS region on *Hs*AChE, while in the *Hs*BChE it could interact in the bottom of the gorge, close to the CT. This distinct binding pose occurs probably due to the BChE active site are more voluminous than the AChE (a difference of about 200 $Å^3$) [26,59,60]. The comparison between the residues of the AChEs and BChEs active sites shows specific amino acid replacements, such as the replacement of bigger and hydrophobic residues (Phe, Tyr, Trp) for smaller and hydrophobic

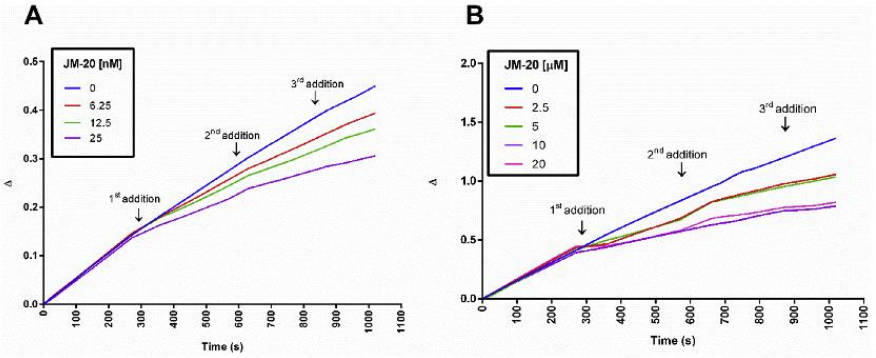

Fig. 6. *Ee*AChE (A) and *Ec*BChE (B). Each indicated point corresponds to the addition of JM-20 to the final concentration indicated for each addition. For instance, in the red line for AChE (A) the first addition corresponds to a final concentration of 6.25 nM of JM-20, the second, 12.5 nM and after the third 18.75 nM of JM-20. The *Ee*AChE (A) activity was determined in a cuvette (volume of 1 ml) at 412 nm (Shimadzu UV-1800 spectrophotometer, Japan) in the presence of 12 µg of purified enzyme. The *Ec*BChE (B) was determined in a cuvette (volume of 1 ml) at 412 nm (Shimadzu UV-1800 spectrophotometer, Japan) in the presence of 5 µg of purified enzyme.

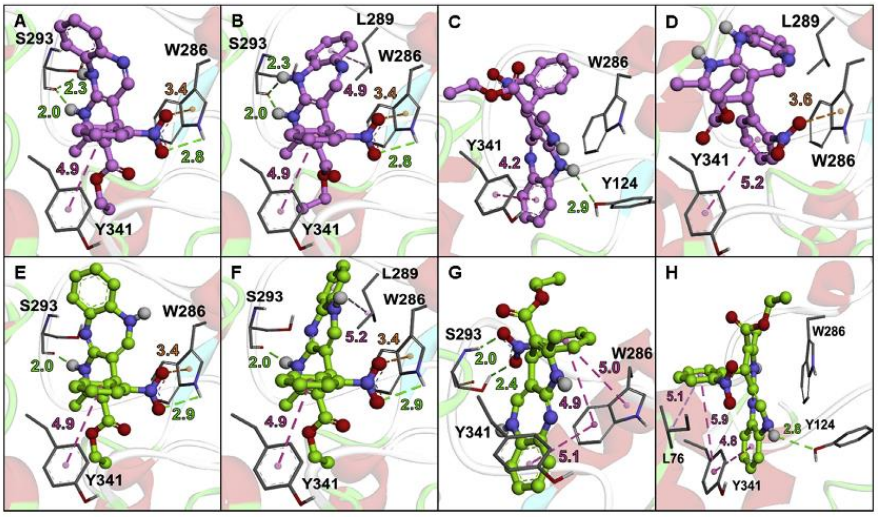

Fig. 7. Binding poses of JM-20 isomers a–h (A–H) in the *Hs*AChE enzyme, from molecular docking in the presence of highly-conserved water molecules. The JM-20 isomers (a–h) are in a ball and stick model, with the carbon atoms from the isomers a–d and e–h in the pink and green color, respectively. Only the main residues involved in the interactions are shown in stick model. The respective interactions, H-bonds (in green), electrostatic π-anion (in orange), and hydrophobic π-π and alkyl-π (in pink) are represented by colored dot lines. The interaction distances are in Å.

residues (Leu, Ala, Val) (Fig. S4 and Table S1). The elucidation of these features is important to determine how these molecules interact with a specific target and help us in the development of new drugs. According to the docking simulations, in the case of the JM-20, the isomer b demonstrated to be the main structure involved in the AChE inhibition, but the coexisting isomers may allow a synergistic activity.

The inclusion of highly-conserved water molecules in the docking simulations lead to a different binding pose of ligands when compared with the docking without water, despite the ΔG (Table 4) and the redocking showed similar values (Fig. S5). However, the results obtained by the inclusion of water molecules method are more realistic [26]. JM-20 binding pose is similar to tacrine-dihydropyridine hybrids [35,36,61], where the R-isomers appear to be more active and shown π-π stacking with W286, besides present IC_{50} for *Hs*AChE in the range of nM. Coumarin hybrids also demonstrated important interactions with the PAS, which could help in the prevention of pro-aggregation of AChE toward beta-amyloid protein (Aβ) [62]. These data indicate that the interaction with the W286 in PAS is essential for these classes of molecules. As proposed by Leon et al. [35], the lack of the tryptophan residue in the *Hs*BChE PAS (replaced by A277, Table S1) could explain the poor inhibition of this enzyme.

4. Conclusion

In conclusion, JM-20 can be an alternative therapy to treat neurological disorders related to cholinergic system disturbances because it has a potential inhibitory effect on AChE. Importantly, we reinforce that other studies are required to assess whether the

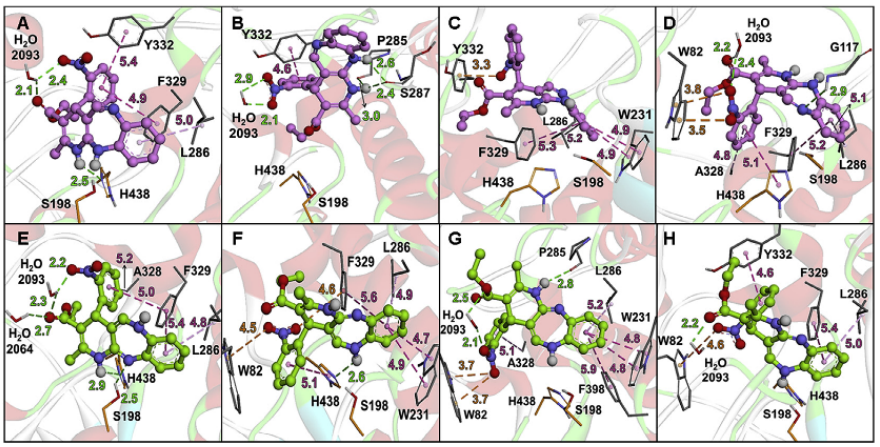

Fig. 8. Binding poses of JM-20 isomers a–h (A–H) in the *Hs*BChE enzyme, from molecular docking in the presence of highly-conserved water molecules. The JM-20 isomers (a–h) are in a ball and stick model, with the carbon atoms from the isomers a–d and e–h in the pink and green color, respectively. Only the main residues involved in the interactions are shown in stick model. The respective interactions, H-bonds (in green), electrostatic π-anion (in orange), and hydrophobic π-π and alkyl-π (in pink) are represented by colored dot lines. The interaction distances are in Å.

Table 4
Predicted ΔG_{bind} (kcal/mol) data from molecular docking between ChE and the JM-20 isomers (a–h).

	a	b	c	d	e	f	g	h	Rd.
With water									
*Hs*AChE	−9.2	−10.0	−8.1	−7.3	−9.0	−9.8	−8.3	−8.3	−10.5
*Hs*BChE	−10.6	−9.1	−9.9	−10.6	−11.0	−9.7	−9.9	−9.8	−8.5
Without water									
*Hs*AChE	−9.5	−11.1	−9.0	−7.3	−9.0	−10.5	−10.5	−10.5	−10.4
*Hs*BChE	−10.3	−10.8	−10.2	−10.2	−10.2	−10.3	−10.3	−10.5	−8.1
*Ee*AChE	−8.2	−10.6	−7.3	−7.7	−8.0	−9.2	−9.6	−10.0	−8.7
*Ec*BChE	−9.8	−10.1	−9.6	−9.8	−10.4	−9.9	−10.1	−10.6	−8.1

Rd: redocking, for AChE the ligand is galantamine, and for BChE is tacrine.

AChE inhibitor will be maintained *in vivo*, as well as toxicity studies following different routes, doses and time of exposure. Besides, simulations by molecular docking indicate that the 4-R isomers (a, b, e, and f) interact better with the *Hs*AChE, in the PAS region. These results help understand the mode of action of JM-20 on AChE, allowing more precise evidence for future pharmacological approaches.

Author contributions

Fernanda D'Avila da Silva: conceived and designed the analysis, collected the data, contributed data or analysis tools, performed the analysis, wrote the paper.

Pablo Andrei Nogara: collected the data, contributed data or analysis tools, performed the analysis, wrote the paper.

Estael Ochoa-Rodríguez: wrote the paper, synthesis and characterization of JM-20.

Yanier Nuñez-Figueredo: conceived and designed the analysis, wrote the paper, synthesis and characterization of JM-20.

Maylin Wong-Guerra: wrote the paper, synthesis and characterization of JM-20.

Denis Broock Rosemberg: contributed data or analysis tools, wrote the paper.

João Batista Teixeira Rocha: conceived and designed the analysis, contributed data or analysis tools, wrote the paper.

Declaration of competing interest

Material submitted entitled "Molecular docking and in vitro evaluation of a new hybrid molecule (JM-20) on cholinesterase activity from different sources" is original. This manuscript has not been published previously and it is not under consideration elsewhere. There is no conflict of interest. All authors agree to have the article published.

Acknowledgments

This work was financially supported by FAPERGS/CNPq 12/2014-PRONEX: no 16/2551-0000, CAPES/PROEX (no 23038.004173/2019–93; no 0493/2019; no 88882.182125/2018–01; 88882.182123/2018–01), and INCT-EN: for Cerebral Diseases, Excitotoxicity, and Neuroprotection.

Appendix A. Supplementary data

Supplementary data to this article can be found online at https://doi.org/10.1016/j.biochi.2019.11.011.

References

[1] L.K. McCorry, Physiology of the autonomic nervous system, Acta Anaesthesiol. Scand. 8 (2007) 17–20, https://doi.org/10.1111/j.1399-6576.1964.tb00252.x.
[2] T.H. Ferreira-Vieira, I.M. Guimaraes, F.R. Silva, F.M. Ribeiro, Alzheimer's

disease: targeting the cholinergic system, Curr. Neuropharmacol. 14 (2016) 101–115, https://doi.org/10.2174/1570159X13666150716165726.
[3] J. Wiesner, Z. Kříž, K. Kuča, D. Jun, J. Koča, Acetylcholinesterases – the structural similarities and differences, J. Enzym. Inhib. Med. Chem. 22 (2007) 417–424, https://doi.org/10.1080/14756360701421294.
[4] M.R. Picciotto, M.J. Higley, Y.S. Mineur, Acetylcholine as a neuromodulator: cholinergic signaling shapes nervous system function and behavior, Neuron 76 (2013) 116–129, https://doi.org/10.1016/j.neuron.2012.08.036.Acetylcholine.
[5] M.B. Colovic, D.Z. Krstic, T.D. Lazarevic-Pasti, A.M. Bondzic, V.M. Vasic, Acetylcholinesterase inhibitors: pharmacology and toxicology, Curr. Neuropharmacol. 11 (2013) 315–335, https://doi.org/10.2174/1570159X11311030006.
[6] D. Grisaru, M. Sternfeld, A. Eldor, D. Glick, H. Soreq, Structural roles of acetylcholinesterase variants in biology and pathology, Eur. J. Biochem. 264 (1999) 672–686, https://doi.org/10.1046/j.1432-1327.1999.00693.x.
[7] H. Dvir, I. Silman, M. Harel, T.L. Rosenberry, J.L. Sussman, Acetycholinesterase: from 3D structure to function, Chem. Biol. Interact. 187 (2010) 10–22, https://doi.org/10.1016/j.cbi.2010.01.042.
[8] Alzheimer's Association, Alzheimer's disease facts and figures, Alzheimers Dement. 13 (2017) 325–373, https://doi.org/10.1016/j.jalz.2017.02.001.
[9] L.D.C. Mannelli, A. Bartolini, C. Ghelardini, Neuropathy-induced Apoptosis : protective effect of physostigmine, J. Neurosci. Res. 1876 (2009) 1871–1876, https://doi.org/10.1002/jnr.22007.
[10] M. Pohanka, Acetylcholinesterase inhibitors: a patent review (2008 – present), Expert Opin. Ther. Pat. 22 (2012) 871–886, https://doi.org/10.1517/13543776.2012.701620.
[11] F. Worek, U. Mast, D. Kiderlen, C. Diepold, P. Eyer, Improved determination of acetylcholinesterase activity in human whole blood, Clin. Chim. Acta 288 (1999) 73–90, https://doi.org/10.1016/S0009-8981(99)00144-8.
[12] Y. Nuñez-Figueredo, J. Ramírez-Sánchez, G. Hansel, E.N. Simões Pires, N. Merino, O. Valdes, R. Delgado-Hernández, A.L. Parra, E. Ochoa-Rodríguez, Y. Verdecia-Reyes, C. Salbego, S.L. Costa, D.O. Souza, G.L. Pardo-Andreu, A novel multi-target ligand (JM-20) protects mitochondrial integrity, inhibits brain excitatory amino acid release and reduces cerebral ischemia injury in vitro and in vivo, Neuropharmacology 85 (2014) 517–527, https://doi.org/10.1016/j.neuropharm.2014.06.009.
[13] Y. Nuñez-Figueredo, G.L. Pardo-Andreu, J. Ramírez-Sánchez, R. Delgado-Hernández, E. Ochoa-Rodríguez, Y. Verdecia-Reyes, Z. Naal, A.P. Muller, L.V. Portela, D.O. Souza, Antioxidant effects of JM-20 on rat brain mitochondria and synaptosomes: mitoprotection against Ca2+-induced mitochondrial impairment, Brain Res. Bull. 109 (2014) 68–76, https://doi.org/10.1016/j.brainresbull.2014.10.001.
[14] Y. Nuñez-Figueredo, J. Ramírez-Sánchez, R. Delgado-Hernández, M. Porto-Verdecia, E. Ochoa-Rodríguez, Y. Verdecia-Reyes, J. Marin-Prida, M. González-Durruthy, S.A. Uyemura, F.P. Rodrigues, C. Curti, D.O. Souza, G.L. Pardo-Andreu, JM-20, a novel benzodiazepine-dihydropyridine hybrid molecule, protects mitochondria and prevents ischemic insult-mediated neural cell death in vitro, Eur. J. Pharmacol. 726 (2014) 57–65, https://doi.org/10.1016/j.ejphar.2014.01.021.
[15] Y.N. Figueredo, E.O. Rodríguez, Y.V. Reyes, C.C. Domínguez, A.L. Parra, J.R. Sánchez, R.D. Hernández, M.P. Verdecia, G.L. Pardo Andreu, Characterization of the anxiolytic and sedative profile of JM-20: a novel benzodiazepine–dihydropyridine hybrid molecule, Neurol. Res. 35 (2013) 804–812, https://doi.org/10.1179/1743132813Y.0000000216.
[16] J. Ramírez-Sánchez, E.N. Simões Pires, Y. Nuñez-Figueredo, G.L. Pardo-Andreu, L.A. Fonseca-Fonseca, A. Ruiz-Reyes, E. Ochoa-Rodríguez, Y. Verdecia-Reyes, R. Delgado-Hernández, D.O. Souza, C. Salbego, Neuroprotection by JM-20 against oxygen-glucose deprivation in rat hippocampal slices: involvement of the Akt/GSK-3β pathway, Neurochem. Int. 90 (2015) 215–223, https://doi.org/10.1016/j.neuint.2015.09.003.
[17] Y. Nuñez-Figueredo, G.L. Pardo Andreu, S. Oliveira Loureiro, M. Ganzella, J. Ramírez-Sánchez, E. Ochoa-Rodríguez, Y. Verdecia-Reyes, R. Delgado-Hernández, D.O. Souza, The effects of JM-20 on the glutamatergic system in synaptic vesicles, synaptosomes and neural cells cultured from rat brain, Neurochem. Int. 81 (2015) 41–47, https://doi.org/10.1016/j.neuint.2015.01.006.
[18] M. Wong-guerra, J. Jiménez-martin, L.A. Fonseca-fonseca, J. Ramírez-sánchez, Y. Montano-peguero, J.B. Rocha, F.D. Avila, A.M. De Assis, D.O. Souza, L. Gilberto, R.M. Valle, G.A. Lopez, O.V. Martínez, N.M. García, A. Mondelo-rodríguez, A.S. Padrón-yaquis, Y. Nuñez-figueredo, J. Jiménez-martin, L.A. Fonseca-fonseca, J. Ramírez-sánchez, Y. Montano-peguero, J.B. Rocha, F.D. Avila, A.M. De Assis, D.O. Souza, G.L. Pardo-andreu, R. Menéndez-soto, G.A. Lopez, O.V. Martínez, N.M. García, A. Mondelo, A.S. Padrón-yaquis, Y.N. Jm, JM-20 protects memory acquisition and consolidation on scopolamine model of cognitive impairment, Neurol. Res. 00 (2019) 1–14, https://doi.org/10.1080/01616412.2019.1573285.
[19] P.J. Bjerrum, Hemoglobin-depleted human erythrocyte ghosts: characterization of morphology and transport functions, J. Membr. Biol. 48 (1979) 43–67, https://doi.org/10.1007/BF01869256.
[20] F. Worek, P. Eyer, D. Kiderlen, H. Thiermann, L. Szinicz, Effect of human plasma on the reactivation of sarin-inhibited human erythrocyte acetylcholinesterase, Arch. Toxicol. 74 (2000) 21–26, https://doi.org/10.1007/s002040050647.
[21] G.L. Ellman, K.D. Courtney, V. Andres, R.M. Featherstone, A new and rapid colorimetric determination of acetylcholinesterase activity, Biochem. Pharmacol. 7 (1961) 88–95, https://doi.org/10.1016/0006-2952(61)90145-9.
[22] O. Trott, A. Olson, AutoDock Vina, Improving the speed and accuracy of docking with a new scoring function, efficient optimization and multithreading, J. Comput. Chem. 31 (2010) 455–461, https://doi.org/10.1002/jcc.21334.AutoDock.
[23] P.A. Nogara, R.D.A. Saraiva, D. Caeran Bueno, L.J. Lissner, C. Lenz Dalla Corte, M.M. Braga, D.B. Rosemberg, J.B.T. Rocha, Virtual screening of acetylcholinesterase inhibitors using the lipinski's rule of five and ZINC databank, BioMed Res. Int. 2015 (2015), https://doi.org/10.1155/2015/870389.
[24] F.D. da Silva, P.A. Nogara, M.M. Braga, J.B.T. da Rocha, Molecular docking analysis of acetylcholinesterase supports the protective effect of pralidoxime on toxic action of chlorpyrifos in behavior and neurochemistry of Nauphoeta cinerea, Comput. Toxicol. (2018), https://doi.org/10.1016/j.comtox.2018.07.003.
[25] J. Chlebek, J. Korábecný, R. Doležal, Š. Štepánková, D.I. Pérez, A. Hoštálková, L. Opletal, L. Cahlíková, K. Macáková, T. Kucera, M. Hrabinová, D. Jun, In vitro and in silico acetylcholinesterase inhibitory activity of thalictricavine and canadine and their predicted penetration across the blood-brain barrier, Molecules 24 (2019) 1–11, https://doi.org/10.3390/molecules24071340.
[26] T.L. Rosenberry, X.B. Id, I.R. Macdonald, M. Wandhammer, M. Trovaslet-leroy, S. Darvesh, F. Nachon, Comparison of the binding of reversible inhibitors to human butyrylcholinesterase and acetylcholinesterase: ACrystallographic, kinetic and calorimetric study, Molecules (2017) 1–21, https://doi.org/10.3390/molecules22122098.
[27] J. Cheung, M.J. Rudolph, F. Burshteyn, M.S. Cassidy, E.N. Gary, J. Love, M.C. Franklin, J.J. Height, Structures of human acetylcholinesterase in complex with pharmacologically important ligands, J. Med. Chem. 55 (2012) 10282–10286, https://doi.org/10.1021/jm300871x.
[28] M. Wandhammer, M. De Koning, M. Van Grol, M. Loiodice, L. Saurel, D. Noort, M. Goeldner, F. Nachon, A step toward the reactivation of aged cholinesterases-Crystal structure of ligands binding to aged human butyrylcholinesterase, Chem. Biol. Interact. 203 (2013) 19–23, https://doi.org/10.1016/j.cbi.2012.08.005.
[29] E.F. Pettersen, T.D. Goddard, C.C. Huang, G.S. Couch, D.M. Greenblatt, E.C. Meng, T.E. Ferrin, UCSF Chimera - a visualization system for exploratory research and analysis, J. Comput. Chem. 25 (2004) 1605–1612, https://doi.org/10.1002/jcc.20084.
[30] M.D. Hanwell, D.E. Curtis, D.C. Lonie, T. Vandermeerschd, E. Zurek, G.R. Hutchison, Avogadro: an advanced semantic chemical editor, visualization, and analysis platform, J. Cheminf. 4 (2012) 1–17, https://doi.org/10.1186/1758-2946-4-17.
[31] J.J.P. Stewart, Optimization of parameters for semiempirical methods V: modification of NDDO approximations and application to 70 elements, J. Mol. Model. 13 (2007) 1173–1213, https://doi.org/10.1007/s00894-007-0233-4.
[32] James J.P. Stewart, Stewart computational chemistry - MOPAC home page. http://openmopac.net/, 2016.
[33] G.M. Morris, R. Huey, W. Lindstrom, M.F. Sanner, R.K. Belew, D.S. Goodsell, A.J. Olson, Software news and updates AutoDock4 and AutoDockTools4 : automated docking with selective receptor flexibility, J. Comput. Chem. (2009) 2785–2791, https://doi.org/10.1002/jcc.
[34] D.S. BIOVIA, Accelrys Discovery Studio, 2017.
[35] R. León, C.D.L. Ríos, J. Marco-contelles, O. Huertas, X. Barril, F.J. Luque, M.G. López, A.G. García, M. Villarroya, New tacrine-dihydropyridine hybrids that inhibit acetylcholinesterase , calcium entry , and exhibit neuroprotection properties, Bioorg. Med. Chem. 16 (2008) 7759–7769, https://doi.org/10.1016/j.bmc.2008.07.005.
[36] J. Marco-Contelles, R. León, C. de los Ríos, A. Samadi, M. Bartolini, V. Andrisano, O. Huertas, X. Barril, F.J. Luque, M.I. Rodríguez-Franco, B. López, M.G. López, A.G. Garcia, M. do C. Carreiras, M. Villarroya, Tacripyrines, the first tacrine-dihydropyridine hybrids, as multitarget-directed ligands for the treatment of alzheimer's disease, J. Med. Chem. 52 (2009) 2724–2732, https://doi.org/10.1021/jm801292b.
[37] J. Marco-Contelles, R. León, C. De Los Ríos, A. Guglietta, J. Terencio, M.G. Lòpez, A.G. Garcìa, M. Villarroya, Novel multipotent tacrine-dihydropyridine hybrids with improved acetylcholinesterase inhibitory and neuroprotective activities as potential drugs for the treatment of Alzheimer's disease, J. Med. Chem. 49 (2006) 7607–7610, https://doi.org/10.1021/jm061047j.
[38] G.W. Caldwell, Z. Yan, W. Lang, J.A. Masucci, The IC 50 concept revisited, Curr. Top. Med. Chem. (2012) 1282–1290.
[39] F.H. Darras, Y. Pang, On the use of the experimentally determined enzyme inhibition constant as a measure of absolute binding affinity, Biochem. Biophys. Res. Commun. 489 (2017) 451–454, https://doi.org/10.1016/j.bbrc.2017.05.168.
[40] W.M. Li, K.K.W. Kan, P.R. Carlier, Y.P. Pang, Y.F. Han, East meets west in the search for alzheimer ' s therapeutics - novel di- meric inhibitors from tacrine and huperzine A, Curr. Alzheimer Res. (2007) 386–396.
[41] S. Gemma, E. Gabellieri, P. Huleatt, C. Fattorusso, M. Borriello, B. Catalanotti, S. Butini, M. De Angelis, E. Novellino, V. Nacci, T. Belinskaya, A. Saxena, G. Campiani, Discovery of huperzine A – tacrine hybrids as potent inhibitors of human cholinesterases targeting their midgorge recognition sites, J. Med. Chem. (2006) 3421–3425.
[42] M. Mehta, A. Adem, M. Sabbagh, New acetylcholinesterase inhibitors for alzheimer's disease, Int. J. Alzheimer's Dis. 2012 (2012), https://doi.org/10.1155/2012/728983.
[43] K. Spilovska, J. Korabecny, E. Nepovimova, R. Dolezal, E. Mezeiova, O. Soukup,

K. Kuca, Multitarget tacrine hybrids with neuroprotective properties to confront alzheimer's disease, Curr. Top. Med. Chem. 17 (2017) 1006–1026, https://doi.org/10.2174/1568026605666160927152728.
[44] S. Nagar, U.A. Argikar, D.J. Tweedie, Enzyme Kinetics in Drug Metabolism, Hertfordshire, 2014, https://doi.org/10.1007/978-1-62703-758-7.
[45] A.A. Al-jafari, M.A. Kamal, N.H. Greig, A.S. Alhomida, E.R. Perry, Kinetics of human erythrocyte acetylcholinesterase inhibition by a novel derivative of Physostigmine : phenserine, Biochem. Biophys. Res. Commun. 185 (1998) 180–185.
[46] Z. Radic, N.A. Pickering, D.C. Vellom, S. Camp, P. Taylor, Three distinct domains in the cholinesterase molecule confer selectivity for, Biochemistry (1993) 12074–12084, https://doi.org/10.1021/bi00096a018.
[47] J.E. Smyth, N.M. Butler, P.A. Keller, A twist of nature – the significance of atropisomers in biological systems, Nat. Prod. Rep. (2015) 1562–1583, https://doi.org/10.1039/c4np00121d.
[48] N.W. Gilman, P. Rosen, J. V Earley, C.M. Cook, J.F. Blount, L.J. Todaro, Atropisomers of 1,4-benzodiazepines. 2. Synthesis and resolution of imidazo[l,5-a][l,4]Benzodiazepines, J. Org. Chem. (1993) 3285–3298, https://doi.org/10.1021/jo00064a014.
[49] A.R. Dos Santos, A.C. Pinheiro, A.C.R. Sodero, A.S. Da Cunha, M.C. Padilha, P.M. De Sousa, S.P. Fontes, M.P. Veloso, C.A.M. Fraga, Atropoisomerismo: O efeito da quiralidade axial em substâncias bioativas, Quim. Nova 30 (2007) 125–135, https://doi.org/10.1590/S0100-40422007000100024.
[50] C. Jang, D.K. Yadav, L. Subedi, R. Venkatesan, A. Venkanna, S. Afzal, E. Lee, J. Yoo, E. Ji, S.Y. Kim, M. Kim, Identification of novel acetylcholinesterase inhibitors designed by pharmacophore- based virtual screening , molecular docking and bioassay, Sci. Rep. (2018) 1–21, https://doi.org/10.1038/s41598-018-33354-6.
[51] M. Aarthy, U. Panwar, C. Selvaraj, S.K. Singh, Advantages of structure-based drug design approaches in neurological disorders, Curr. Neuropharmacol. (2017) 1136–1155, https://doi.org/10.2174/1570159X15666170102145257.
[52] M.R. Arkin, J.A. Wells, S.S. Francisco, Small-molecule inhibitors of protein – protein interactions : progressing towards the dream, Nat. Rev. 3 (2004) 301–317, https://doi.org/10.1038/nrd1343.
[53] A.L. Hopkins, Network pharmacology : the next paradigm in drug discovery, Nat. Chem. Biol. 4 (2008) 682–690, https://doi.org/10.1038/nchembio.118.
[54] M.M. Makola, I.A. Dubery, G. Koorsen, P.A. Steenkamp, M.M. Kabanda, L.L. Preez, N.E. Madala, The effect of geometrical isomerism of 3 , 5-dicaffeoylquinic acid on its binding affinity to HIV-integrase Enzyme : a molecular docking study, evidence-based complement, Altern. Med. 2016 (2016) 1–10, https://doi.org/10.1155/2016/4138263.
[55] G. Sinko, Z. Kovarik, E. Reiner, V. Simeon-rudolf, J. Stojan, Mechanism of stereoselective interaction between butyrylcholinesterase and ethopropazine enantiomers, Biochimie 93 (2011) 1797–1807, https://doi.org/10.1016/j.biochi.2011.06.023.
[56] Y. Nicolet, O. Lockridge, P. Masson, J.C. Fontecilla-camps, F. Nachon, Crystal structure of human butyrylcholinesterase and of its complexes with substrate and products, J. Biol. Chem. 278 (2003) 41141–41147, https://doi.org/10.1074/jbc.M210241200.
[57] G. Koellner, G. Kryger, C.B. Millard, I. Silman, J.L. Sussman, T. Steiner, Active-site gorge and buried water molecules in crystal structures of acetylcholinesterase from Torpedo californica, J. Mol. Biol. 296 (2) (2000) 713–735.
[58] H. Dvir, D.M. Wong, M. Harel, X. Barril, M. Orozco, F.J. Luque, D. Munoz-Torrero, P. Camps, T.L. Rosenberry, I. Silman, J.L. Sussman, 3D structure of Torpedo californica acetylcholinesterase complexed with huprine X at 2 . 1 Å Resolution : kinetic and molecular dynamic correlates, Biochemistry 41 (2002) 2970–2981, https://doi.org/10.1021/bi011652i.
[59] A. Saxena, A.M.G. Redman, X. Jiang, O. Lockridge, B.P. Doctor, Differences in active-site gorge dimensions of cholinesterases revealed by binding of inhibitors to human butyrylcholinesterase, Chem. Biol. Interact. c (1999) 61–69, https://doi.org/10.1016/s0009-2797(99)00014-9.
[60] M. Bajda, A. Wi, M. Hebda, N. Guzior, Structure-Based search for new inhibitors of cholinesterases, Int. J. Mol. Sci. (2013) 5608–5632, https://doi.org/10.3390/ijms14035608.
[61] P. Kishore, D. Anuradha, P. Piplani, R. Rao, Molecular docking and receptor-specific 3D-QSAR studies of acetylcholinesterase inhibitors, Mol. Divers. (2012) 803–823, https://doi.org/10.1007/s11030-012-9394-x.
[62] S.K. Yusufzai, M.S. Khan, O. Sulaiman, H. Osman, D.N. Lamjin, Molecular docking studies of coumarin hybrids as potential acetylcholinesterase, butyrylcholinesterase, monoamine oxidase A/B and β- amyloid inhibitors for Alzheimer ' s disease, Chem. Cent. J. 12 (2018) 1–57, https://doi.org/10.1186/s13065-018-0497-z.

2.1.1 Material de apoio do artigo - Molecular docking and *in vitro* evaluation of a new hybrid molecule (JM-20) on cholinesterase activity from different sources

Supporting Information

Molecular docking and in vitro evaluation of a new hybrid molecule (JM-20) on cholinesterase activity from different sources

Fernanda D'Avila da Silva[a], Pablo Andrei Nogara[a], Estael Ochoa-Rodríguez[b], Yanier Nuñez-Figueredo[b], Denis Broock Rosemberg[a], João Batista Teixeira da Rocha[a*]

Molecular docking and protein homology modelling of AChE from *Electrophorus electricus* (*Ee*AChE) and BChE from *Equus caballus* (*Ec*BChE)

Three-dimensional structures of *Ee*AChE and *Ec*BChE were obtained by the protein homology modeling [1], and the Swiss-Model (https://swissmodel.expasy.org) was used to build them, using the amino acid sequence of the *Ee*AChE and *Ec*BChE taken from the National Center for Biotechnology Information – NCBI (https://www.ncbi.nlm.nih.gov/pubmed/) with the codes XP_026871422.1 and AAF61480.1, respectively. As the protein template, the *Tetronarce californica* AChE (PDB 3I6M) [2] and the *Hs*BChE (PDB 4BDS) were used. The validation of the protein models by PROCHECK, Verify 3D and ProSA programs showed that the structures presented conformation similar to the native proteins (Table S3) [3–5]. For docking simulations, the *Ee*AChE gridbox was centered on the coordinates: x = 3.53; y = 65.57; z = 66.74; with the dimensions 30^3 Å, while the *Ec*BChE gridbox was centered on the coordinates: x = 3.76; y = 13.45; z = 13.57; with the dimensions 30^3 Å. Considering that the ChE models do not present water molecules, we used these structures in the docking simulations in the absence of water, only. For more details, see the section 2.3.6. *In silico analysis*.

JM-20

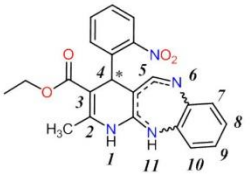

Comp.	isomer
a	4-R-11-NH-S_N
b	4-R-11-NH-R_N
c	4-S-11-NH-S_N
d	4-S-11-NH-R_N
e	4-R-6-NH-S_N
f	4-R-6-NH-R_N
g	4-S-6-NH-S_N
h	4-S-6-NH-R_N

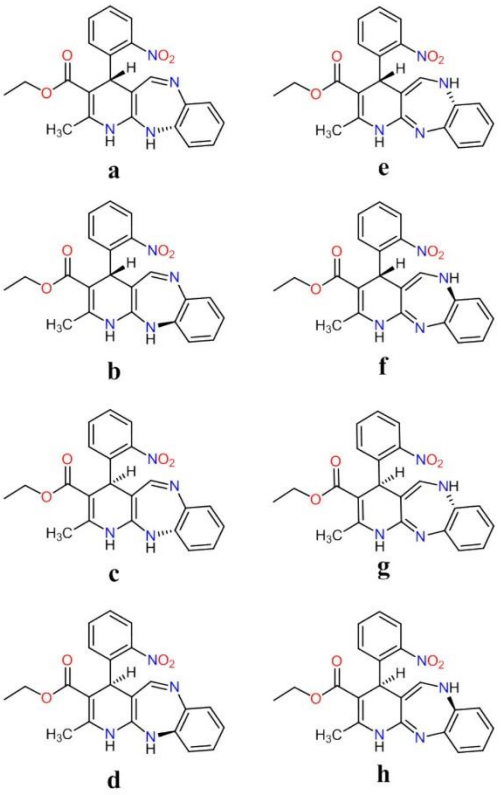

Figure S1. JM-20 isomers and the nomenclature used for their identification. To determine the configuration of the N sp3 of the diazepine ring, the N atom was considered a chiral center, with the dihydropyridine moiety and H atom in the plan, and the electron pair with low priority.

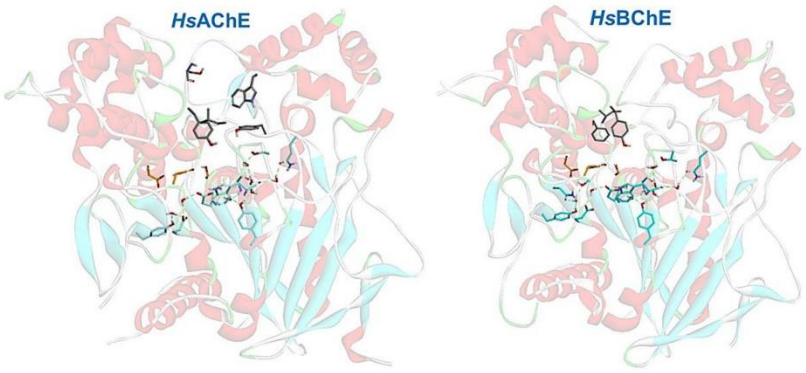

Figure S2. Structures of *Hs*AChE (PDB 4EY6) and *Hs*BChE (PDB 4BDS). The catalytic triad (Glu, His and Ser) are showed with carbon atoms in orange color, and the residues involved in the water molecules network with carbon atoms in blue color (*Hs*AChE: Gln71, Trp86, Gly120, Ser125, Tyr133, Glu202, Tyr428, and Glu450; *Hs*BChE: Gln67, Trp82, Gly115, Thr120, Tyr128, Glu197, Ser224, Asn322, Tyr419, and Glu441). For the *Hs*AChE (4EY6) the water molecules are 704, 705, 707, 773, 803, 805 and 815, and for *Hs*BChE (4BDS): 2045, 2064, 2089, 2090, 2093, 2131, and 2140. Some residues from Peripheral Anionic Subsite, PAS (*Hs*AChE: Tyr124, Trp286, and Tyr341; *Hs*BChE: Tyr332) and Acyl Binding Pocket, ABP (*Hs*BChE: Leu286 and Phe329) are represented by grey carbon atoms.

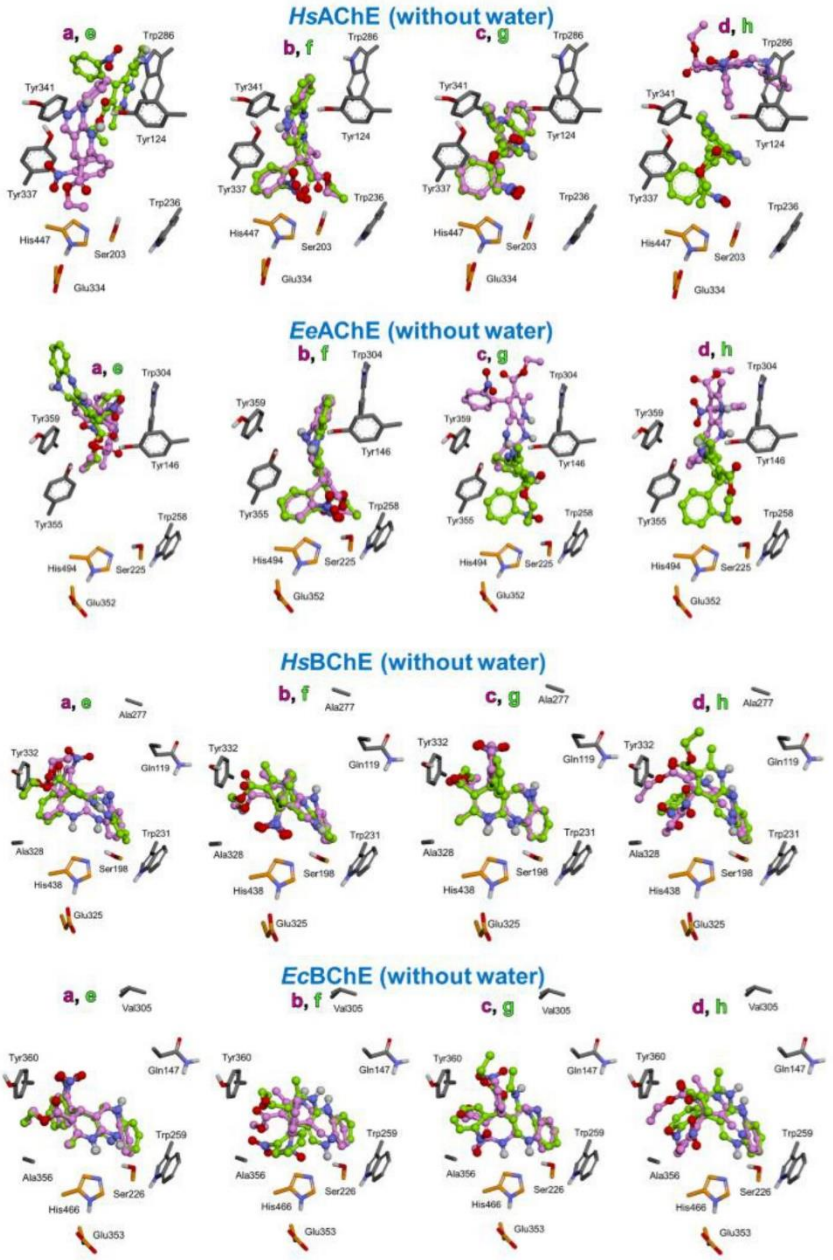

Figure S3. Comparison between the binding modes of each JM-20 isomer (**a-h**) in the cholinesterase enzymes (*Hs*AChE, *Ee*AChE, *Hs*BChE and *Ec*BChE), from molecular docking without water molecules. The JM-20 isomers (**a**–**h**) are in a ball and stick model, with the carbon atoms from the isomers **a**–**d** and **e**–**h** in the pink and green colors, respectively. The cholinesterase's catalytic triad is represented by Ser, His, and Glu residues (with the carbon atoms in the orange color).

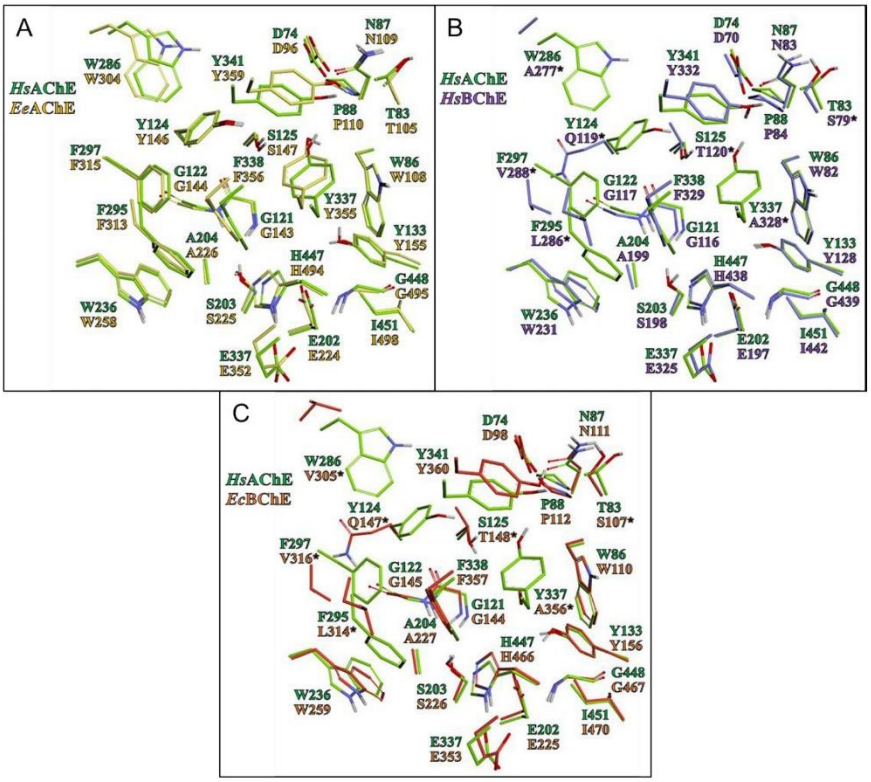

Figure S4. Comparison between the active site of *Hs*AChE *vs Ee*AChE (A), *Hs*AChE *vs Hs*BChE (B), and *Hs*AChE *vs Ec*BChE (C). The structures overlapping was made by the Discovery Studio Visualizer program (https://www.3ds biovia.com). * Indicates different amino acid residues.

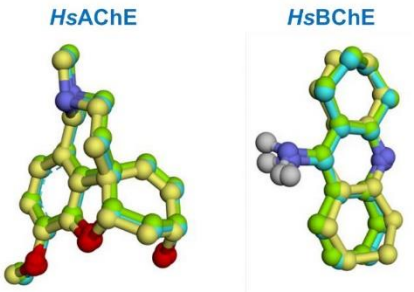

Figure S5. Root-mean-square deviation (RMSD) between X-ray structures (*Hs*AChE (PDB 4ey6) and *Hs*BChE (PDB 4bds)) and the molecular docking in the absence or presence of water molecules (with the carbons atoms shown in yellow, green and blue, respectively). For *Hs*AChE, the galantamine presented the RMSD value of 0.36 Å (*Hs*AChE x-ray structure *vs* docking without water) and 0.23 Å (*Hs*AChE x-ray structure *vs* docking with water). For *Hs*BChE, the tacrine presented the RMSD value of 0.48 Å (*Hs*BChE x-ray structure *vs* docking without water) and 0.41 Å (*Hs*BChE x-ray structure *vs* docking with water). A redocking with an RMSD value lower than 2.0 Å is considered a good docking protocol [6,7]. Only the heavy atoms are shown.

Table S1. Comparison between the amino acid residues from the active site of *Hs*AChE, *Ee*AChE, *Hs*BChE, and *Ec*BChE. For the visualization of each amino acid position, please see Figure S4.

Subsite	*Hs*AChE	*Ee*AChE	*Dr*AChE	*Hs*BChE	*Ec*BChE
Catalytic triad (CT)	Ser203	Ser225	Ser225	Ser198	Ser226
	Glu334	Glu352	Glu352	Glu325	Glu353
	His447	His494	His495	His438	His466
Oxyanion Hole (OH)	Gly121	Gly143	Gly143	Gly116	Gly144
	Gly122	Gly144	Gly144	Gly117	Gly145
	Ala204	Ala226	Ala226	Ala199	Ala227
Anionic Subsite (AS)	Trp86	Trp108	Trp108	Trp82	Trp110
	Tyr133	Tyr155	Tyr155	Tyr128	Tyr156
	Glu202	Glu224	Glu224	Glu197	Glu225
	Gly448	Gly495	Gly496	Gly439	Gly467
	Ile451	Ile498	Ile499	Ile442	Ile470
Acyl Binding Pocket (ABP)	Trp236	Trp258	Trp258	Trp231	Trp259
	Phe295	Phe313	Phe313	Leu286	Leu314
	Phe297	Phe315	Phe315	Val288	Val316
	Phe338	Phe356	Phe356	Phe329	Phe357
Omega Loop (OL)	Thr83	Thr105	Ile105	Ser79	Ser107
	Asn87	Asn109	Asn109	Asn83	Asn111
	Pro88	Pro110	Pro110	Pro84	Pro112
Peripheral Anionic Subsite (PAS)	Asp74	Asp96	Asp96	Asp70	Asp98
	Tyr124	Tyr146	Tyr146	Gln119	Gln147
	Ser125	Ser147	Ser147	Thr120	Thr148
	Trp286	Trp304	Trp304	Ala277	Val305
	Tyr337	Tyr355	Tyr355	Ala328	Ala356
	Tyr341	Tyr359	Tyr359	Tyr332	Tyr360

Table S2. Comparison between enzyme kinetic parameters (Vmax and Km values) obtained by non-linear regression – inhibition (substrate inhibition) vs Michelis-Menten, using the Graph Pad Prisma.

		Enzyme kinetic – inhibition (substrate inhibition) (nM)						Michaelis-Menten (nM)					
		Control	75	100	150	250	400	Control	75	100	150	250	400
*Ee*AChE	Vmax (Δabs 415 nm/s/ mg protein)	42.12 ± 4.32	19.74 ± 4.13	-	15.64 ± 1.56	9.12 ± 0.71	4.93 ± 0.25	31.06 ± 1.34	18.19 ± 0.97	-	15.64 ± 1.52	9.12 ± 0.68	4.93 ± 0.25
	Km	0.15 ± 0.03	0.25 ± 0.09	-	0.53 ± 0.13	0.38 ± 0.09	0.36 ± 0.05	0.09 ± 0.01	0.21 ± 0.03	-	0.53 ± 0.13	0.43 ± 0.09	0.36 ± 0.05
*Hs*AChE (Ghost)	Vmax (Δabs 415 nm/min/ mg protein)	78.53 ± 13.38	-	60.17 ± 14.79	-	46.80 ± 18.07	30.18 ± 1.81	65.50 ± 2.44	-	50.02 ± 2.04	-	41.94± 2.52	29.92 ± 1.78
	Km	0.28 ± 0.08	-	0.32 ± 0.13	-	0.41 ± 0.24	0.34 ± 0.05	0.20 ± 0.02	-	0.22 ± 0.03	-	0.33 ± 0.05	0. 33± 0.05
*Hs*AChE (Erythorcytes)	Vmax (Δabs 415 nm/h/ mg protein)	50.51 ± 1.94	50.03 ± 8.14	-	31.71 ± 1.48	31.33 ± 3.58	-	50.51 ± 1.88	46.91 ± 2.13	-	31.71 ± 1.44	31.33 ± 3.48	-
	Km	0.13 ± 0.02	0.21 ± 0.06	-	0.17 ± 0.02	0.43 ± 0.13	-	0.13 ± 0.02	0.18 ± 0.03	-	0.17 ± 0.02	0.43 ± 0.13	-
*Hs*BChE	Vmax (Δabs 415 nm/h/ mg protein)	156.0 ± 9.77	152.1 ± 20.34	-	124.3 ± 11.06	129.9 ± 5.25	138.6 ± 3.24	141.6 ± 2.27	139.7 ± 4.31	-	124.3 ± 10.73	129.9 ± 5.09	138.6 ± 3.15
	Km	0.27 ± 0.03	0.29 ± 0.06	-	0.17 ± 0.05	0.24 ± 0.03	0.25 ± 0.02	0.23 ± 0.01	0.25 ± 0.02	-	0.17 ± 0. 05	0.24 ± 0.03	0.25 ± 0.02

Table S3. Validation of ChE structure models from protein homology modelling.

Enzyme	PROCHECK (most favorable regions)	Verify 3D	ProSa
*Ee*AChE	87.1%	93.1%	-10.2
*Ec*BChE	92.6%	90.1%	-10.8

References

[1] Z. Xiang, Advances in Homology Protein Structure Modeling, Curr. Protein Pept. Sci. 7 (2006) 217–227. doi:10.2174/138920306777452312.

[2] C. Bartolucci, L.A. Haller, U. Jordis, G. Fels, D. Lamba, Probing Torpedo californica Acetylcholinesterase Catalytic Gorge with Two Novel Bis-functional, J. Med. Chem. (2010) 745–751. doi:10.1021/jm901296p.

[3] R.A. Laskowski, PDBsum new things, Nucleic Acids Res. 37 (2009) 355–359. doi:10.1093/nar/gkn860.

[4] D. Eisenberg, R. Lüthy, J.U. Bowie, VERIFY3D: Assessment of protein models with three-dimensional profiles, Methods Enzymol. 277 (1997) 396–406. doi:10.1016/S0076-6879(97)77022-8.

[5] M. Wiederstein, M.J. Sippl, ProSA-web: Interactive web service for the recognition of errors in three-dimensional structures of proteins, Nucleic Acids Res. 35 (2007) 407–410. doi:10.1093/nar/gkm290.

[6] J.L. Stigliani, V. Bernardes-Génisson, J. Bernadou, G. Pratviel, Cross-docking study on InhA inhibitors: A combination of Autodock Vina and PM6-DH2 simulations to retrieve bio-active conformations, Org. Biomol. Chem. 10 (2012) 6341–6349. doi:10.1039/c2ob25602a.

[7] C.P. Vianna, W.F. De Azevedo, Identification of new potential Mycobacterium tuberculosis shikimate kinase inhibitors through molecular docking simulations, J. Mol. Model. 18 (2012) 755–764. doi:10.1007/s00894-011-1113-5.

2.2 MANUSCRITO – Cytotoxic, antioxidative prospects and virtual screening of the new hybrid molecule (JM-20) on human blood cells

Cytotoxic, antioxidative prospects and virtual screening of the new hybrid molecule (JM-20) on human blood cells

Silva, F. D.[a], Galiciolli, M. E. A.[b,c], Irioda, A. C. [b,c], Oliveira, C. S.[a,b,c], Piccoli, B. C.[a], Ochoa-Rodríguez, E.[d], Nuñez-Figueredo, Y.[d], Rocha, J.B.T.[a*]

[a]*Programa de Pós-graduação em Ciências Biológicas: Bioquímica Toxicológica, Universidade Federal de Santa Maria, 97105-900 Santa Maria, RS, Brazil.*

[b]*Programa de Pós-Graduação Stricto Sensu em Biotecnologia Aplicada a Saúde da Criança e do Adolescente, Instituto de Pesquisa Pelé Pequeno Príncipe, Rua Silva Jardim, 1632, Curitiba, Paraná, Brazil.*

[c]*Faculdade Pequeno Príncipe, Avenida Iguaçu, 333, Curitiba, Paraná, Brazil.*

[d]*Centro de Investigación y Desarrollo de Medicamentos, Ave 26, Nº 1605,e /Boyeros y Puentes Grandes, CP10600, La Habana, Cuba.*

*João Batista Teixeira da Rocha, Universidade Federal de Santa Maria, Camobi, 97105-900, RS, Brazil. Tel.: +55 55 3220 9462; E-mail address: jbtrocha@yahoo.com.br.

Abstract

Previous studies have shown that JM-20, a new 1,5-benzodiazepine fused to a dihydropyridine fraction, has different pharmacological properties of clinical interest. However, considering that studies on its possible toxic effects on blood cells have not yet been reported, the present study aimed to investigate for the first-time cytotoxicity through cell viability, and morphological changes on leukocytes. Additionally, we evaluated the production of reactive species and possible changes in the cell cycle (in human leukocytes), as well as its hemolytic effect in human erythrocytes. JM-20 antioxidant effects are still scarce in the literature; therefore, we verified the protective effect on the oxidative stress induced by Fe^{2+} in the leukocyte and the scavenger activity of free radicals. Besides, we predict ADMET parameters using *in silico* virtual screening tools. Human blood was obtained from healthy volunteers. Immediately after the blood collection the leukocytes or erythrocytes were isolated and treated with different concentrations of JM-20. The results showed no cytotoxic effect for red blood cells and no alterations in the cell cycle. A potent protective effect of JM-20 lipid peroxidation was also evidenced with an IC_{50} value of around 1.0 µM. The *in silico* pharmacokinetic and toxicological properties of JM-20, derivatives, and nifedipine were studied. Our findings demonstrated that the JM-20 and its putative metabolites present similar characteristics to the nifedipine, as similar absorption by gastrointestinal tract (orally), distribution by permeation through BBB and in the CNS, metabolism, and toxicity. The in vitro and silico data support the low toxicity of JM-20 in mammals.

key words: toxicity, oxidative stress, *in vitro*, *in silico*, *swiss*ADME, *pk*CSM

1. Introduction

The new molecule derived from a benzodiazepine and a pyridine fusion, JM-20 (3-ethoxycarbonyl-2-methyl-4- (2-nitrophenyl) 4,11-dihydro-1H-pyrido [2,3-b] benzodiazepine) (Figure 1) is arousing interest based on their pharmacological effects. For example, JM-20 has been demonstrated to reduce the aggressive behavior of socially isolated mice, increase the latency period for the beginning of the tonic crisis, and the lethality induced by pentylenetetrazol (Nuñez-Figueredo et al., 2014b). Besides, the JM-20 treatment (2-10 mg/kg *p.o.*) reduces anxiolytic-like responses in mice (Nuñez-figueredo et al., 2013).

JM-20 has also been described to exhibit *in vitro* and *in vivo* multi-target neuroprotective effects by reducing the neuronal excitotoxic injury and protecting the mitochondria from Ca^{2+}-induced toxicity (Nuñez-Figueredo et al., 2014a; Ramírez-Sánchez et al., 2015; Wong-guerra et al., 2019). Recently, Silva et al (Silva et al., 2020) demonstrated that JM-20 is a potent *in vitro* acetylcholinesterase inhibitor; suggesting that this compound could be an option in the treatment of neurodegenerative pathologies.

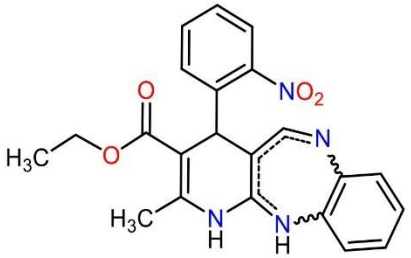

Figure 1. Structural formula of the compound 3-ethoxycarbonyl-2-methyl-4-(2-nitrophenyl)-4-11-dihydro-1H-pyrido [2,3- b] [1,5] benzodiazepine (JM-20).

Oxidative stress has been implicated in several pathological conditions, including cancer (Khansari et al., 2009), neurological disorders (Pohanka, 2014; Uttara et al., 2009), atherosclerosis (Li et al., 2014; Victor et al., 2009), hypertension (Briones and Touyz, 2010; Schulz et al., 2011), ischemia (Love, 1999; Misra et al., 2009), diabetes (Maritim et al., 2003), acute respiratory distress syndrome (Bartens et al., 1999), idiopathic pulmonary fibrosis (Kliment and Oury, 2010; Rahman et al., 1999), chronic obstructive pulmonary disease (Repine et al., 1997), and asthma (Nadeem et al., 2003).

In this context, reactive oxygen species (ROS) are physiologically produced by living organisms as a result of cellular metabolism, but at high concentrations, they cause damage to cell components, such as lipids, proteins, and DNA (Birben et al., 2012). Although aerobic organisms have natural antioxidant systems, which include enzymatic and nonenzymatic antioxidants that are, in normal conditions, effective in blocking the ROS harmful effects, the imbalance favoring oxidant species is termed, oxidative stress (Birben et al., 2012; Rahal et al., 2014).

In addition to the beneficial effects, synthetic compounds must be present minimal toxic effects for the cells and the organism in general. Thus, there is a need for reliable *in vitro* cytotoxicity tests to properly evaluated the toxicity of new compounds before *in vivo* pre-clinical or clinical studies (Hughes et al., 2011). Likewise, an accurate *in vitro* toxicity test can reduce the number of animal studies (Bhanushali et al., 2015). At the same time, *in vitro* cytotoxicity assessments can rapidly allow the screening of a large number of potential drug candidates (Hughes et al., 2011).

Another alternative developed to study de pharmacokinetics and toxicity of new compounds comprises computational approaches with the main function to guide compounds design and the modifications during the drug development process (Hu et al., 2020; Pires et al., 2018, 2015). The *in silico* programs used to discover drugs have a focus on the elucidation of the interaction between molecules and target proteins of interest (Daina et al., 2017; Hu et al., 2020; Pires et al., 2015). In addition, the *in silico* analysis of pharmacokinetics and toxicity can help in predicting the safety of new molecules (Daina et al., 2017; Hu et al., 2020; Pires et al., 2018, 2015).

Considering the pharmacological potential of JM-20 and the fact that no studies on its potential toxic effect on human blood cells have been reported so far, the present study was undertaken to investigate for the first time the cytotoxicity (in human leukocytes), as well as its potential hemolytic effect in human erythrocytes. Furthermore, we also investigated the antioxidant effect of the compound against Fe^{2+}-induced lipid peroxidation in isolated leukocytes. Moreover, we also evaluated and predict a range of ADMET (absorption, distribution, metabolism, excretion, and toxicity) properties for the JM-20 and its derivative compounds.

2. Material and methods

2.1 Compound and reagents

JM-20 was synthesized, purified, and characterized as previously reported (Nuñez-figueredo et al., 2013). The compound was dissolved in dimethyl sulfoxide (DMSO). The chemicals reagents used in this work were purchased from Sigma-Aldrich (St. Louis, MO, USA).

2.2 Blood samples

Human blood was obtained from healthy male and female voluntary donors aged 20 to 60 years from the toxicological biochemistry laboratory at the Universidade Federal de Santa Maria (UFSM) for TBARS, cell viability, and hemolysis studies. The Ethical Committee of the UFSM approved the protocol (3.471.823) used in these studies. For the flow cytometry analysis (cell cycle arrest and reactive species production), human blood was obtained from healthy male and female voluntary donors aged 20 to 60 years from Instituto de Pesquisa Pelé Pequeno Príncipe (IPPP). The experiments carried out at IPPPP were approved by the Ethical Committee of the Faculdades Pequeno Príncipe (3.977.300). In all experiments, we used blood from different donors (n=3).

2.2.1 Isolated human leukocytes

Immediately after the blood collection, 2 mL of 5% dextran was added and the tubes with blood, and dextran were maintained in rest for 1h. After that, the supernatant was removed and centrifuged at 200 *g* for 10 min. The pellet was washed with 1 mL of lyse solution (150 mM NH_4Cl, 10 mM $NaHCO_3$, and 1mM EDTA), after this procedure the leukocytes were solubilized in Hank's buffer (5.4 mM KCl, 0.3 mM Na_2HPO_4, 0.4 mM KH_2PO_4, 4.2 mM $NaHCO_3$, 0.5 mM $MgCl_2$, 122.6 mM NaCl, 0.01 mM D-glucose, 10 mM Tris-HCl, and 1.3 mM $CaCl_2$, pH = 7.4). The samples were used for cell viability, TBARS, cell cycle arrest and ROS production.

2.3 Cytotoxicity assays

2.3.1 Hemolysis determination

Heparinized human blood was immediately centrifuged 200 *g* for 10 min and hemolysis evaluation was realized as reported elsewhere (Duarte et al., 2016; Menezes et al., 2014). The plasma was discarded, and the cell pellets were washed three times with phosphate-buffered saline (6.1 mM, 150 mM NaCl, pH 7.4). The hemolysis was estimated by measuring the resistance of red blood cells to the rupturing (lysis) and the release of their contents (cytoplasm) in a salt solution. Three hundred microliters of erythrocytes, 0.2 µL of JM-20 solution (5–20 µM), and 699.8 µL of phosphate buffer saline (PBS) (6.1 mM, 150 mM NaCl, pH 7.4) were incubated for 3 h at 28 °C in a shaker. After incubation, samples were mixed and centrifuged at 2500 rpm for 10 min and the supernatant was transferred to a microplate and the erythrocytes lysis were measured using a spectrophotometer Spectra Max plate reader at 540 nm. The results were expressed as a percentage of the positive control (triton 0.05%). We discount the possible hemolysis caused by vehicle (DMSO) and used PBS like negative control.

2.3.2 Cell viability

The cell viability was determined using the Trypan blue exclusion method, which assumes that nonviable cells are stained in blue (Mishell et al., 1980). In summary, 1 µL of JM-20 (10–50 µM final concentration) was added to 249 µL of leukocytes suspension (2000 cells/µL) and incubated at 37 °C for 3 h. Dimethyl sulfoxide (DMSO – 0.4%) was used as the control, tert-butyl hydroperoxide (1 mM) was used as the positive control, and water was used as blank. Thereafter, 50 µL of this system were mixed with 50 µL of 0.4% trypan blue and incubated for 5 min at room temperature. From the mixture, an aliquot of 10 µL was placed in a Neubauer chamber and the viable cells were counted microscopically. The viability was expressed as viable cells in percent of the total cells.

2.3.3 Cell Cycle arrest

The DNA content of the cells was measured by flow cytometry using 7-amino actinomycin D (7-AAD) solution (BD via probe™). Leukocytes ($2x10^5$ cells/100 µL) were incubated with JM-20 (10-50 µM) for 3h at 37 ºC. After the incubation, cells were carefully washed with PBS and fixed in cold ethanol (70%) for 30 minutes at -20 ºC. Again, cells were washed with PBS and human albumin (2%) and incubated in 7-Aminoactinomycin D (7AA-D) (20 µg/mL), RNAse (350 µg/mL), and Triton-X (0.1%) solution for 15 min under an ice bath. Cells were evaluated (10,000 events/sample in the granulocytes gate) in the PERCP channel (Ex_{max} 482 nm/Em_{max} 678 nm; blue laser) by FACSCanto II (BD Biosciences) cytometer and data were processed by Infinicyt Software V1.6.0.

2.3.4 RS formation

The RS generation was analyzed by flow cytometry using 2,7-dichlorodihydrofluorescein diacetate (DCFH-DA). Leukocytes ($2x10^5$ cells/100 µL) were incubated with JM-20 (10-50 µM) for 3h at 37 ºC. After the incubation, cells were washed two times with PBS and incubated with 35 µM DCFH-DA for 15 min at 37 ºC in the dark. Cells were evaluated (10,000 events/sample in the granulocytes gate) in the FITC channel (Ex_{max} 494 nm/Em_{max} 520 nm; blue laser) by FACSCanto II (BD Biosciences) cytometer and data were processed by Infinicyt Software V1.6.0.

2.4 Antioxidant activity

2.4.1 Thiobarbituric Acid Reactive Substances (TBARS) Production

The TBARS production was performed as described by Ohkawa *et al*. (Ohkawa et al., 1979). Isolated leukocytes were incubated with 100 µM $FeSO_4$ in the presence or absence of JM-20 (0.5 – 5.0 µM final concentration) at 37 °C for 1 h. Subsequently, 40 µL of sodium dodecyl sulfate (8.1%), 100 µL of acetic acid buffer (pH 3.4), and 100 µL of 0.6% thiobarbituric acid (TBA) were added and incubated at 100 °C for 1 h. After cooling, the absorbance of the samples was measured at 532 nm using a

spectrophotometer Spectra Max plate reader. The quantification of protein in the isolated leukocyte samples was performed using a Nanodrop-1000 spectrophotometer. The average amount of protein was 4.82 mg / mL.

2.4.2 DPPH radical scavenging assay

The method proposed by Pereira et al (2014) (Pereira et al., 2014) was used for this test. For the time-dependent curve, the JM-20 compound was dissolved in DMSO and mixed with 0.3 mM DPPH in ethanol. To perform the concentration curve 0, 10, 20, 50, and 100 μM of JM-20 were used; and mixed with 0.3 mM DPPH in ethanol. The reaction was divided into two parts. At the first moment, we monitored the absorbance in spectrophotometer SpectraMax at 518 nm for 30 minutes with an interval of 30 seconds, we called it a fast phase reaction. In the second moment, the slow phase reaction, the absorbance was recorded every 30 minutes for 180 minutes. α-tocopherol (100 μM) was used as a positive control.

2.5 ADMET predictions

The platforms pkCSM and swissADME analyze pharmacokinetic and toxicological properties that rely on distance-based graph signatures in a free online system. This tool can be a powerful tracking and guidance mechanism showing the balance between power and security for researchers. The online platforms SwissADME (absorption, distribution, metabolism, and excretion) and pkCSM were used for ADMET (absorption, distribution, metabolism, excretion, and toxicity) profile determination of JM-20 and its putative metabolites. We compared the results of the two platforms with nifedipine (which is a therapeutically used antihypertensive drug and a Ca^{2+} channel blocker) and structurally like the JM-20 moiety. We also use the nifedipine metabolites described in the literature (Lee et al., 2014) to predict the possible metabolites of JM-20.

2.6 Statistical Analysis

Statistical analyses were performed using the GraphPad Prism 6 (version 6.01, GraphPad Software, Inc., USA). Results were expressed as the mean ± standard error of the mean (SEM). Data were analyzed by one-way ANOVA followed by Newman Keuls post-hoc test. Results from TBARS were also calculated as the half-maximal inhibitory concentration (IC_{50}) according to nonlinear regression log (inhibitor) vs. response – variable slope in accordance with equation 1, using GraphPad, Prism 6.01.

Equation 1: $Y=Bottom+(Top-Bottom)/(1+10^{((LogIC_{50}-X)*HillSlope)})$;

HillSlope describes the steepness of the family of curves (A HillSlope of -1.0 is standard).
Top and Bottom are plateaus in the units of the Y-axis.
Values of $p \leq 0.05$ were considered significantly different.

3. Results

Here we demonstrated the antioxidant activity of the JM-20 compound, as well as elucidating the low toxicity of this compound in human blood cells *in vitro*. Our results showed that JM-20 (even at high concentrations, i.e., 10-20 µM) did not cause hemolysis [F (3, 8) = 3.053; p = 0.0919] (Table 1). We consider positive control (triton 0.05%) to be 100% hemolysis.

Table 1. Determination of hemolysis after exposure to different concentration of JM-20 (1 – 20 µM).

	Hemolysis (% of positive control)
PBS (negative control)	11.02 ± 0.22
JM-20 (1 µM)	5.66 ± 1.76
JM-20 (10 µM)	6.76 ± 1.54
JM-20 (20 µM)	8.38 ± 1.27

Data were expressed as mean ± SEM (n = 3) and analyzed by One-way ANOVA followed by Newman Keuls post hoc test. No significant differences were observed (p > 0.05).

In the cell viability assay, we used leukocytes isolated from fresh whole blood from voluntary donors. The tert-butyl hydroperoxide (1 mM) was used as a positive control and damaged about 40% of the cells (i.e., 60% of leukocytes were viable) when compared to the vehicle (DMSO) group (Figure 2). At the lowest concentration tested (10 µM), JM-20 did not change cell viability; but at the higher concentrations tested, 20 and 50 µM, JM-20 caused a decrease of about 20% and 50% in leukocyte viability, respectively, when compared to the vehicle (DMSO) group (Figure 2). This result is also in accordance with the observed morphology of the leukocytes treated with JM-20 (Figure 3), in which the concentrations of 20 and 50 µM seem to modify cell populations.

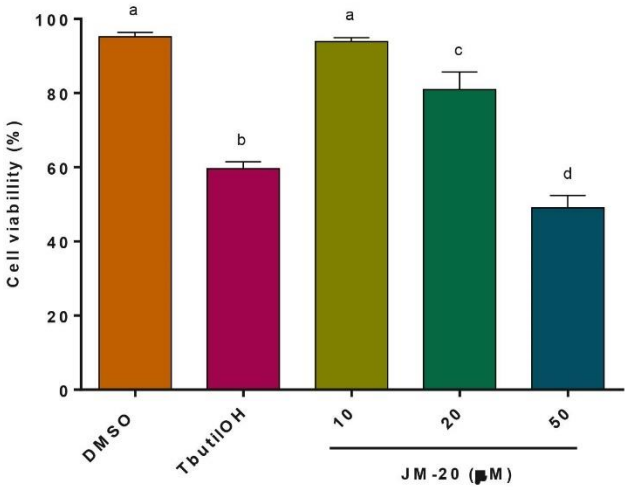

Figure 2. Cell viability after incubating different concentrations of JM-20 (10 – 50 µM) with leukocytes. DMSO (0.4%) was used as the control, and tert-butyl hydroperoxide (TbutilOH-1mM) was used as the positive control. Data were expressed as mean ± SEM (n = 3) and analyzed by One-way ANOVA followed by Newman Keuls post hoc test. Different letters indicated the differences between the compounds and/or JM-20 concentrations ($p \leq 0.05$).

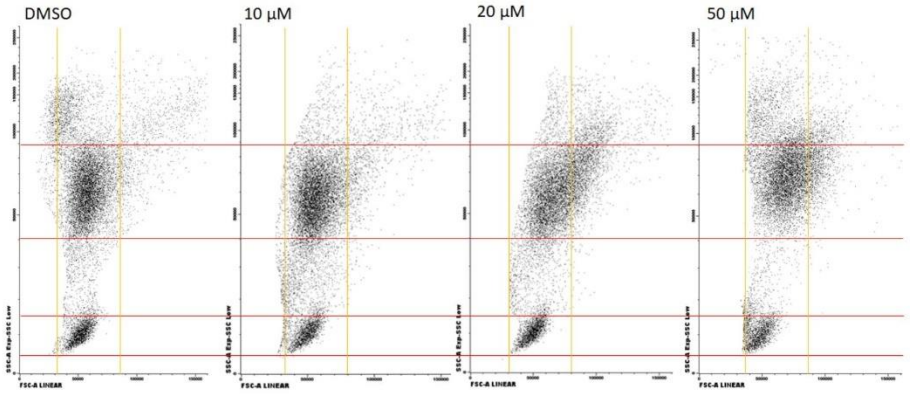

Figure 3. Morphological visualization of leukocytes exposed to JM-20 (10-50 µM). The leukocytes populations used to measure RS production via DCFH oxidation in this study.

The exposure to all JM-20 concentrations tested (10-50 µM) caused a significant increase in the intracellular reactive species (RS) levels (Figure 4). Although a decrease in the cell viability and an increase in the RS production was observed, the exposure to JM-20 (10-50 µM) did not alter the cell cycle (Figure 5).

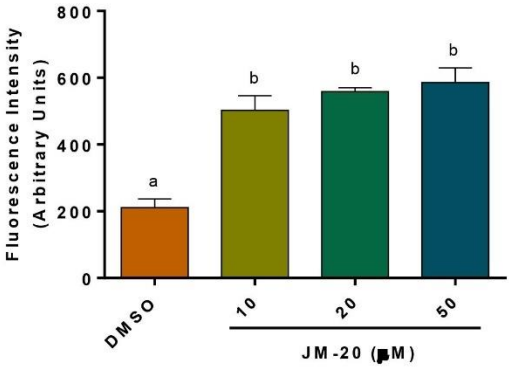

Figure 4: RS generation after incubating different concentrations of JM-20 (10 – 50 µM) with leukocytes. DMSO (0.4%) was used as the control. Data were expressed as mean ± SEM (n = 4) and analyzed by One-way ANOVA followed by Newman Keuls post hoc test. Different letters indicated the differences between the DMSO and/or JM-20 concentrations ($p \leq 0.05$).

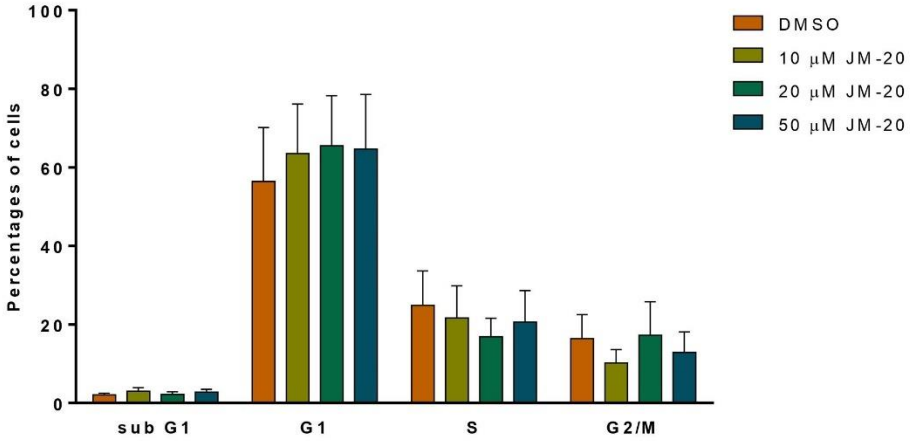

Figure 5: Cell cycle distribution after incubating different concentrations of JM-20 (10 – 50 µM) with leukocytes. DMSO (0.4%) was used as the control. Data were expressed as mean ± SEM (n = 6) and analyzed by One-way ANOVA followed by Newman Keuls post hoc test.

We also evaluate the inhibition of lipid peroxidation by JM-20. JM-20 inhibited the lipid peroxidation of isolated leukocytes induced by Fe^{2+} in almost all concentrations tested and was effective such as the positive control (α-tocopherol) (Figure 6). The calculated IC_{50} value for the inhibition of lipid peroxidation was 1.051 ± 0.21µM (Table 2). This result indicates that this compound is effective in preventing lipid peroxidation, even at low concentrations. Based on the TBARS results, we decided to test the compound for Fe-chelating activity, but it did not show significant effects (data not shown), suggesting another mechanism of action for the antioxidant effect observed in lipid peroxidation induced by Fe^{2+} probably related to the protection of this compound the cell membrane.

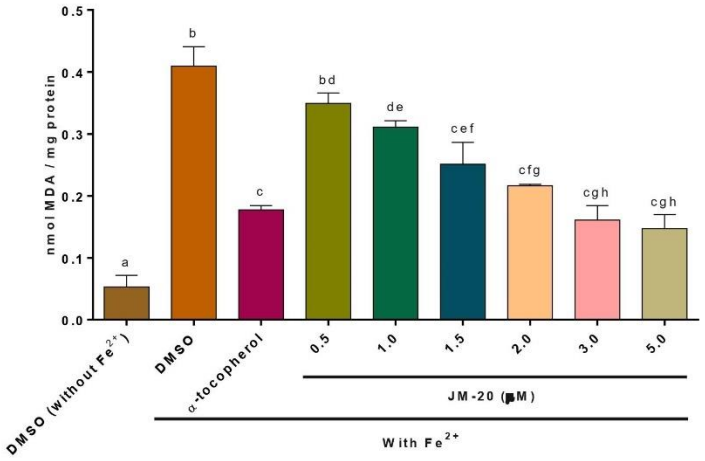

Figure 6. Effect of different concentrations of JM-20 (0.5 – 5 μM) on lipid peroxidation induced by iron. α-tocopherol (10 μM) was used as positive control. Data were expressed as mean ± SEM (n = 3) and analyzed by One-way ANOVA followed by Newman Keuls post hoc test. Different letters indicated the differences between the compounds ($p \leq 0.05$).

Table 2. IC_{50} values for inhibition of lipid peroxidation induced by Fe^{2+}.

Compound	TBARS IC_{50} (μM)
α-tocopherol	1.065 ± 0.34
JM-20	1.051 ± 0.21

Regarding DPPH radical scavenging assay, JM-20 scavenged the DPPH radical at nearly all the tested concentrations (Figure 7). The calculated IC_{50} value for DPPH quenching color was 16.25 ± 0.23 μM in the slow phase (12.600 seconds).

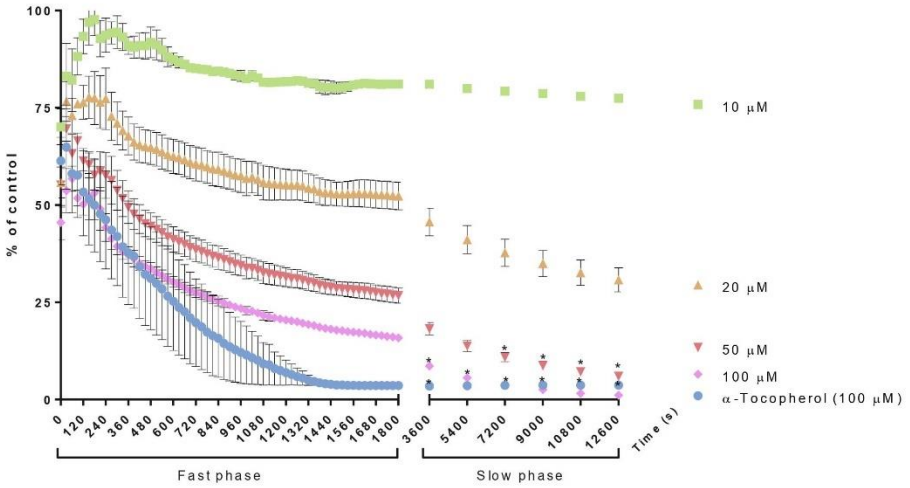

Figure 7. Time-dependent curve of JM-20 in the DPPH test. α-tocopherol was used as a positive control. Results were expressed as mean ± S.E.M. (n = 3). Data were analyzed by repeated measurements Two-way ANOVA followed by Bonferroni post hoc test and differences are considered significant at $p < 0.05$. *Indicates equal values for α-tocopherol and JM-20 (50 and 100 μM) in the respective times ($p \leq 0.05$).

Here, for the first time, we demonstrate the *in silico* ADMET screening of JM-20 (Figure 8A) and some of its putative metabolites (Figure 9) using two different platforms (swissADME and pkCSM).

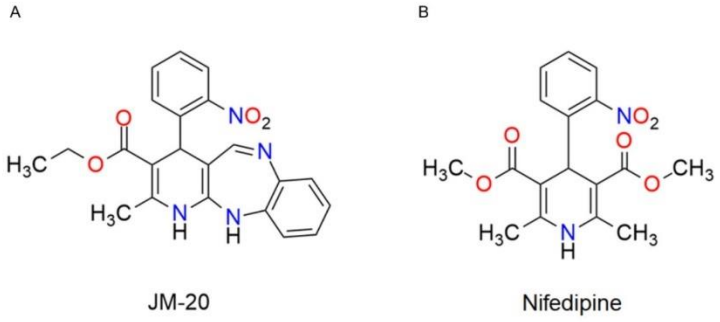

Figure 8. JM-20 and Nifedipine structure.

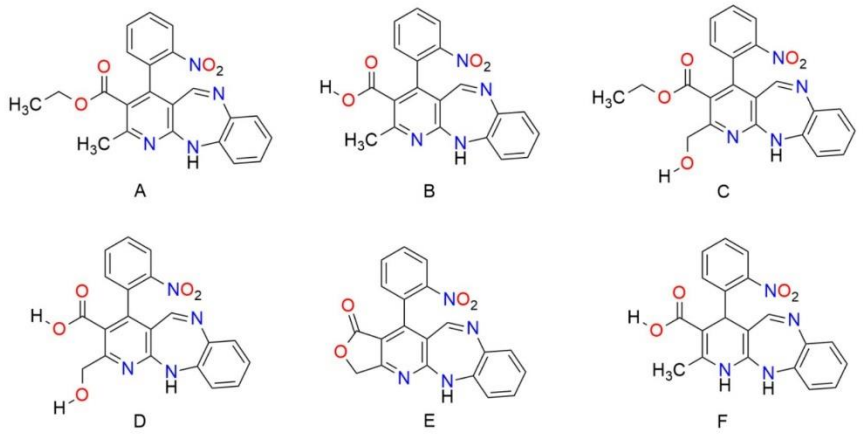

Figure 9: JM-20 putative metabolites. The metabolites were theoretically built considering the nifedipine.

We select the main parameters that represent the ADMET profile. On absorption, we consider water-solubility, Caco2 permeability, intestinal absorption (human), skin permeability, and p-glycoprotein substrate. Regarding distribution parameters, we observed two permeation processes: brain-blood barrier (BBB) and CNS. On metabolism, we highlight the effects on cytochrome P450 isoforms, which can be a substrate or responsible for the inhibition of isoforms. The excretion was predicted by total clearance and Renal OCT2 substrate. And finally, the toxicity, we regard the maximum tolerated dose (human) and total acute toxicity (LD50). The comparison between JM-20 and nifedipine in terms of ADMET is displayed in Table 3. We can also point out that JM-20 obtained values referring to good absorption by administration by the oral route, observed through CaCo-2 permeability and human intestinal absorption that refers to low absorption for drugs with a percentage below 30, here JM-20 and its metabolites showed intestinal absorption greater than 65%. The BBB permeability and in the CNS our compound also seems to be effective, logBB > 0.3 are capable of crossing the BBB, and logPS > -2 are penetrating substances in the CNS, the JM-20 had 0.23 logBB and -1.92 log PS. With regard to metabolism, exogenous substances are expected to have a certain degree of inhibition of enzymes responsible for the detoxification of the organism. Here we show that JM-20 was not an inhibitor of the CYP2D6 isoform, in the same way as nifedipine. We can also point out that our results are promising when compared to nifedipine. Although, we can see some

differences between swissADME and pkCSM we can observe that the JM-20 is very similar to Nifedipine.

Table 3. ADMET prediction of compound JM-20 and Nifedipine by SWISSADME and pkCSM.

	JM-20		Nifedipine	
	pkCSM	**SwissADME**	**pkCSM**	**SwissADME**
Water solubility	-4.23 log mol/L	3.26e-05 mol/L	-4.23 log mol/L	7.00e-04 mol/L
Caco2 permeability	1.24 log Papp in 10^{-6} cm/s	High	1.19 log Papp in 10^{-6} cm/s	High
Intestinal absorption (human)	93.53 % Absorbed	-	87.12 % Absorbed	-
Skin permeability	-2.74 log Kp	-6.32 cm/s	-2.82 log Kp	-6.85 cm/s
P-glycoprotein substrate	Yes	No	Yes	No
BBB permeability	0.23 log BB	No	-0.59 log BB	No
CNS permeability	-1.92 log PS	-	-2.53 log PS	-
CYP2D6 substrate	No	-	No	-
CYP3A4 substrate	Yes	-	Yes	-
CYP1A2 inhibitor	No	No	Yes	Yes
CYP2C19 inhibitor	Yes	No	No	Yes
CYP2C9 inhibitor	Yes	Yes	No	Yes
CYP2D6 inhibitor	No	No	No	No
CYP3A4 inhibitor	Yes	Yes	Yes	No
Total clearance	0.34 log mL/min/Kg	-	0.81 log mL/min/Kg	-
Renal OCT2 substrate	No	-	No	-
Max tolerated dose (human)	-0.08 log mg/Kg/day	-	-0.44 log mg/Kg/day	-
Oral acute toxicity (LD_{50})	2.53 mol/Kg	-	2.8 mol/Kg	-

4. Discussion

In vitro methodologies have advantages when compared to *in vivo* tests, for instance, reduction of the number of experimental variables, such as - weight, sex, and age of the experimental animals, as well as the stress of manipulation. Also, it is possible to obtain significant data in a short time (Dias et al., 2017; Emami, 2006; Hara et al., 1998). Here we used some techniques to evaluate the JM-20 in relation to antioxidant effects and toxicity. According to other studies that also focused on evaluating the toxicity of substances unknown, we analyzed hemolysis and cell viability in red blood cells and leukocytes, respectively (Bueno et al., 2018, 2013; Duarte et al., 2016; Prestes et al., 2019). The leukocytes isolated from fresh human blood as

previously described (Bueno et al., 2013; Duarte et al., 2016; Waczuk et al., 2015) were used to test the cytotoxicity and antioxidant effects of the JM-20 compound.

Toxic agents can trigger the hemolysis process, consequently causing hemoglobin release into the plasma (Anadón et al., 2014; Bowen et al., 2010; Çimen, 2008; Harvey, 1997). The hemolytic effect has been used as one of the screening methodologies for substances of clinical interest (Anadón et al., 2014; Bowen et al., 2010). Here, JM-20 exposure did not alter the hemoglobin homeostasis. The trypan blue exclusion methodology is widely used to assess cytotoxicity by measuring cell viability and cell membrane integrity (Adan et al., 2016; Weyermann et al., 2005). The test is based on the trypan blue absorption into the cytoplasm of damaged cells due to the plasma membrane loss of selectivity, while the living cells remain intact (Adan et al., 2016; Duarte et al., 2016; Menezes et al., 2014; Weyermann et al., 2005). Our results clearly showed that the JM-20 did not present toxic effects for erythrocytes and leukocytes except for the highest concentrations tested (20 and 50 μM). In addition, we evaluated the toxicity of the compound at considerably higher concentrations (micromolar) than the therapeutic concentrations, such as for the inhibition of acetylcholinesterase, which had an effect was on the range of nanomolar (Silva et al., 2020).

Moreover, other analyzes are important to determine the profile of a compound, such as the increases in the intracellular RS levels that are responsible for lipid, protein, and DNA damage leading to cellular death (Birben et al., 2012). Similarly, Fisher et al. 2004 (Fischer et al., 2004) demonstrated that an increase in the RS leukocyte generation occurred concomitantly with a decrease in cell viability. The main hypothesis is that the excessive production of RS causes the reduction of cell viability in leukocytes directly or indirectly (Bueno et al., 2018). Unexpectedly, in our study, the concentration of 10 μM JM-20 caused a significant increase in the RS species but did not alter the cell viability. These results call for attention and need to be explored.

Nevertheless, some synthetic antioxidant compounds showed a pro-oxidant effect at high concentrations (Nogueira and Rocha, 2010). In this context, we decided to test the antioxidant effect of the compound JM-20. Oxidative stress can lead to cell damage through lipid peroxidation of cell membranes (Kudryavtseva et al., 2015). The cell membrane consists mainly of phospholipids, which undergo peroxidation forms aldehydes, such as malondialdehyde (Kanno et al., 2009). The lipid peroxidation products react with thiobarbituric acid, forming a pink complex that can be quantified in

the TBARS assay (Ohkawa et al., 1979). In this case, JM-20 at concentrations of 3 and 5 μM was as effective as tocopherol (10 μM).

Furthermore, the study of ADMET of a given compound is important to understand or predict its potential toxicity and the future use of the clinical practice (Daina et al., 2017; Hu et al., 2020; Pires et al., 2018, 2015). Through the results of the analysis regarding absorption such as CaCo-2 permeability and intestinal absorption, it is possible to predict the absorption of a drug administered orally, for example (Pires et al., 2015). Besides, cytochrome P450 is the main detoxification enzyme present in the body and is found in the liver (Gregg, 2004; Shankar and Mehendale, 2014). Here we evaluated the inhibition for each isoform of this enzyme and point out that the CYP2D6 and CYP3A2 isoforms are the main ones involved in drug metabolism (Shankar and Mehendale, 2014). Moreover, the isoform CYP2D6 was not inhibited by our compound. In the analysis of toxicity in silico, we highlight the maximum tolerated dose, which predicts the limit of a toxic dose of chemical substances in humans, and the LD_{50}, which is a standard measure of acute toxicity. In this case, JM-20 was similar to nifedipine.

We also compared our results with nifedipine (Figure 8B) and its metabolites (Figure 10, Table S1, Table S2) (Lee et al., 2014). The choice of nifedipine to compare with JM-20 was based on the similarity between the nifedipine and nifedipine-like portion of the JM-20 structure. Likewise, we use published data from nifedipine and its known metabolites to propose the metabolites of our compound (Lee et al., 2014). As expected, the JM-20 showed an ADMET profile like nifedipine. Thus, emphasizing the potential therapeutic use of JM-20.

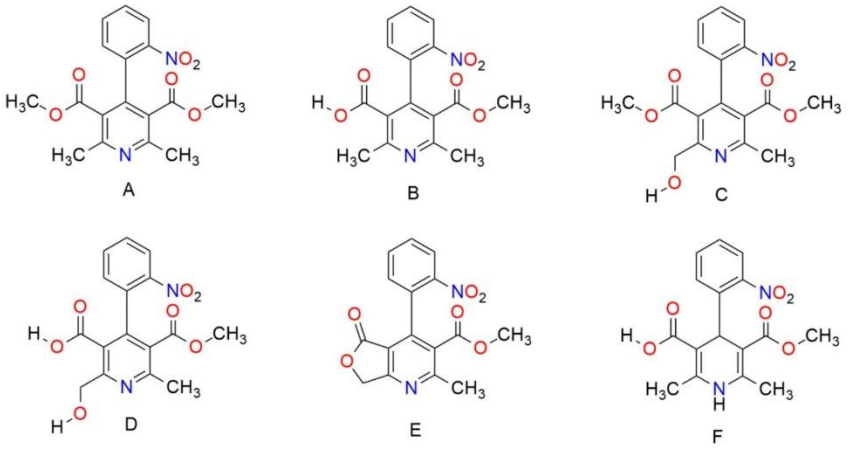

Figure 10: Nifedipine metabolites.

Conclusion

In conclusion, the results presented in this study demonstrated the in vitro antioxidant activity of JM-20 in human leukocytes, and the scavenger effect of free radicals. JM-20 was not cytotoxic to human erythrocytes at high concentrations nor altered the cell cycle in leukocytes. We also propose the metabolites of the compound based on previous studies in similar structures present in the literature and elucidate the pharmacokinetic and toxicological effects of the compound and its metabolites. Thus, our findings here with human cells in vitro and in silico give further support to new in vitro and in vivo studies from this using other types of cells and complex organisms such as rodent models.

Acknowledgment

This work was financially supported by FAPERGS/CNPq 12/2014-PRONEX: nº 16/2551-0000, CAPES/PROEX (n° 23038.004173/2019-93; n° 0493/2019; n°

88882.182125/2018-01; 88882.182123/2018-01), and INCT-EN: for Cerebral Diseases, Excitotoxicity, and Neuroprotection.

References

Adan, A., Kiraz, Y., Baran, Y., 2016. Cell Proliferation and Cytotoxicity Assays. Curr. Pharm. Biotechnol. 17, 1213–1221. https://doi.org/10.2174/1389201017666160808160 5

Anadón, A., Martínez, M.A., Castellano, V., Martínez-Larrañaga, M.R., 2014. The role of in vitro methods as alternatives to animals in toxicity testing. Expert Opin. Drug Metab. Toxicol. 67–79.

Bartens, C., Fischer, M., Fridrich, P., Steltzer, H., 1999. Antioxidant status in patients with acute respiratory distress syndrome. Intensive Care Med 25, 180–185.

Bhanushali, M., Bagale, V., Shirode, A., Joshi, Y., Kadam, V., 2015. An in-vitro toxicity testing - A reliable alternative to toxicity testing by reduction , replacement and refinement of animals International Journal of Advances in Pharmaceutical Sciences An in-vitro toxicity testing - a reliable alternative to toxicity t. Int. J. Adv. Pharm. Sci. 1, 15–31. https://doi.org/10.5138/ijaps.2010.0976.1055.01002

Birben, E., Sahiner, U.M., Sackesen, C., Erzurum, S., Kalayci, O., 2012. Oxidative Stress and Antioxidant Defense. World Allergy Organ. J. 9–19.

Bowen, R.A.R., Hortin, G.L., Csako, G., Otañez, O.H., Remaley, A.T., 2010. Impact of blood collection devices on clinical chemistry assays. Clin. Biochem. 43, 4–25. https://doi.org/10.1016/j.clinbiochem.2009.10.001

Briones, A.M., Touyz, R.M., 2010. Oxidative Stress and Hypertension : Current Concepts. Curr Hypertens Rep 12, 135–142. https://doi.org/10.1007/s11906-010-0100-z

Bueno, D., Meinerz, D., Waczuk, E., Souza, D. De, Batista, J., 2018. Toxicity of organochalcogens in human leukocytes is associated , but not directly related with reactive species production , apoptosis and changes in antioxidant gene expression. Free Radic. Res. 52, 1158–1169. https://doi.org/10.1080/10715762.2018.1536824

Bueno, D.C., Meinerz, D.F., Allebrandt, J., Waczuk, E.P., Bonfanti, D., Oscar, D., Mariano, C., Batista, J., Rocha, T., 2013. Cytotoxicity and Genotoxicity Evaluation of Organochalcogens in Human Leucocytes : A Comparative Study between Ebselen , Diphenyl Diselenide , and Diphenyl Ditelluride. Biomed Res. Int. 2013, 1–6.

Çimen, M.Y.B., 2008. Free radical metabolism in human erythrocytes. Clin. Chim. Acta 390, 1–11. https://doi.org/10.1016/j.cca.2007.12.025

Daina, A., Michielin, O., Zoete, V., 2017. SwissADME: a free web tool to evaluate pharmacokinetics, drug- likeness and medicinal chemistry friendliness of small molecules. Nat. Publ. Gr. 1–13. https://doi.org/10.1038/srep42717

Dias, D.M., Maria, N., Costa, B., Nutti, M.R., 2017. Advantages and limitations of in vitro and in vivo methods of iron and zinc bioavailability evaluation in the assessment of biofortification program effectiveness. Crit. Rev. Food Sci. Nutr. ISSN 8398, 23–43. https://doi.org/10.1080/10408398.2017.1306484

Duarte, A.E., Waczuk, E.P., Roversi, K., Arlene, M., Barros, L.M., Assis, F., Rose, I., Menezes, A. De, Galberto, J., Boligon, A.A., Ademiluyi, A.O., Kamdem, J.P., Batista, J., Rocha, T., 2016. Polyphenolic Composition and Evaluation of Antioxidant Activity , Osmotic Fragility and Cytotoxic Effects of Raphiodon echinus (Nees & Mart .) Schauer 1–15. https://doi.org/10.3390/molecules21010002

Emami, J., 2006. In vitro - In vivo Correlation : From Theory to Applications. J Pharm Pharm. Sci 9, 169–189.

Fischer, T.W., Scholz, G., Knöll, B., Hipler, U.C., Eisner, P., 2004. Melatonin suppresses reactive oxygen species induced by UV irradiation in leukocytes. J. Pineal Res. 37, 107–112. https://doi.org/10.1111/j.1600-079X.2004.00142.x

Gregg, C.R., 2004. Cytochrome P450. Compr. Coord. Chem. II 8, 281–307. https://doi.org/10.1016/B0-08-043748-6/08145-7

Hara, T.O., Dunne, A., Butler, J., Devane, J., Butler, J., Devane, J., 1998. A review of methods used to compare dissolution profile data. Pharm. Sci. Technolo. Today 1, 214–223.

Harvey, J.W., 1997. The Erythrocyte : and Biochemical Disorders, in: Clinical Biochemistry of Domestic Animals. pp. 157–203.

Hu, B., Joseph, J., Geng, X., Wu, Y., Suleiman, M.R., Liu, X., Shi, J., Wang, X., He, Z., Wang, J., Cheng, M., 2020. Refined pharmacophore features for virtual screening of human thromboxane A2 receptor antagonists. Comput. Biol. Chem. 86, 107249. https://doi.org/10.1016/j.compbiolchem.2020.107249

Hughes, J.P., Rees, S., Kalindjian, S.B., Philpott, K.L., 2011. Principles of early drug. Br. J. Pharmacol. 162, 1239–1249. https://doi.org/10.1111/j.1476-5381.2010.01127.x

Kanno, K., Wu, M.K., Scapa, E.F., Roderick, S.L., Cohen, D.E., 2009. Structure and Function of Phosphatidylcholine Transfer Protein (PC-TP)/StarD2. Biochim Biophys Acta 1771, 654–662. https://doi.org/10.1016/j.bbalip.2007.04.003.Structure

Khansari, N., Shakiba, Y., Mahmoudi, M., 2009. Chronic inflammation and oxidative stress as a major cause of age-related diseases and cancer. Recent Pat. Inflamm. Allergy Drug Discov. 3, 73–80. https://doi.org/10.2174/187221309787158371

Kliment, C.R., Oury, T.D., 2010. Oxidative stress , extracellular matrix targets , and idiopathic pulmonary fibrosis. Free Radic. Biol. Med. 49, 707–717. https://doi.org/10.1016/j.freeradbiomed.2010.04.036

Kudryavtseva, A. V, Krasnov, G.S., Dmitriev, A.A., Alekseev, B.Y., Kardymon, O.L., Sadritdinova, A.F., Fedorova, M.S., Pkrovsky, A. V., Melnikova, N. V, Kaprin, A.D., Moskalev, A.A., Snezhkina, A. V, 2015. Mitochondrial dysfunction and oxidative stress in aging and cancer. Oncotarget 7, 44879–44905.

Lee, P.W., Aizawa, H., Gan, L.L., Prakash, C., Zhong, D., 2014. Nifedipine, in: Handbook of Metabolic Pathways of Xenobiotics, First Edition. pp. 1–4.

Li, H., Horke, S., Ulrich, F., 2014. Vascular oxidative stress , nitric oxide and atherosclerosis 237, 208–219. https://doi.org/10.1016/j.atherosclerosis.2014.09.001

Love, S., 1999. Oxidative Stress in Brain Ischemia. Brain Pathol. 131, 119–131.

Maritim, A.C., Sanders, R.A., Watkins, J.B.I., 2003. Diabetes , Oxidative Stress , and Antioxidants : A Review. J Biochem Mol. Toxicol. 17, 24–38. https://doi.org/10.1002/jbt.10058

Menezes, V., Filho, B., Pansera, E., Paul, J., Olalekan, A., Rodrigues, S., Galberto, J., Rose, I., Menezes, A. De, Augusti, A., Linde, M., Batista, J., Posser, T., 2014. Phytochemical constituents , antioxidant activity , cytotoxicity and osmotic fragility effects of Caju (Anacardium microcarpum). Ind. Crop. Prod. 55, 280–288. https://doi.org/10.1016/j.indcrop.2014.02.021

Mishell, R.I., Shiigi, J.M., Mishell, B.B., Grabstein, K.H., Shiigi, S.M., 1980. Prevention of the Immunosuppressive Effects of Glucocorticosteroids by Cell-free Factors from Adjuvant-activated Accessory Cells 245, 233–245.

Misra, M.K., Sarwat, M., Bhakuni, P., Tuteja, R., Tuteja, N., 2009. Oxidative stress and ischemic myocardial syndromes. Med Sci Monit 15, 209–219.

Nadeem, A., Chhabra, S.K., Masood, A., Raj, H.G., 2003. Increased oxidative stress and altered levels of antioxidants in asthma. J. Allergy Clin. Immunol. 111, 72–78. https://doi.org/10.1067/mai.2003.17

Nogueira, C.W., Rocha, J.B.T., 2010. Diphenyl diselenide a janus-faced molecule. J. Braz. Chem. Soc. 21, 2055–2071. https://doi.org/10.1590/S0103-50532010001100006

Nuñez-Figueredo, Y., Pardo-Andreu, G.L., Ramírez-Sánchez, J., Delgado-Hernández, R., Ochoa-rodríguez, E., Verdecia-Reyes, Y., Naal, Z., Muller, A.P., Portela, L.V., Souza, D.O., Pastoris, A., Valmor, L., Souza, D.O., 2014a. Antioxidant effects of JM-20 on rat brain mitochondria and synaptosomes: Mitoprotection against Ca2+-induced mitochondrial impairment. Brain Res. Bull. 109, 68–76. https://doi.org/10.1016/j.brainresbull.2014.10.001

Nuñez-Figueredo, Y., Ramírez-Sánchez, J., Delgado-Hernández, R., Porto-Verdecia, M., Ochoa-Rodríguez, E., Verdecia-Reyes, Y., Marin-Prida, J., González-Durruthy, M., Uyemura, S.A., Rodrigues, F.P., Curti, C., Souza, D.O., Pardo-Andreu, G.L., 2014b. JM-20, a novel benzodiazepine-dihydropyridine hybrid molecule, protects mitochondria and prevents ischemic insult-mediated neural cell death in vitro. Eur. J. Pharmacol. 726, 57–65. https://doi.org/10.1016/j.ejphar.2014.01.021

Nuñez-figueredo, Y., Rodríguez, E.O., Reyes, Y.V., Domínguez, C.C., Parra, A.L., Sánchez, J.R., Hernández, R.D., Verdecia, M.P., Pardo Andreu, G.L., 2013. Characterization of the anxiolytic and sedative profile of JM-20: a novel benzodiazepine–dihydropyridine hybrid molecule. Neurol. Res. 35, 804–812. https://doi.org/10.1179/1743132813Y.0000000216

Ohkawa, H., Ohishi, N., Yagi, K., 1979. Assay for Lipid Peroxides in Animal Tissues

Thiobarbituric Acid Reaction 358, 351–358.

Pereira, R.P., Boligon, A.A., Appel, A.S., Fachinetto, R., Ceron, C.S., Tanus-Santos, J.E., Athayde, M.L., Rocha, J.B.T., 2014. Chemical composition , antioxidant and anticholinesterase activity of Melissa officinalis. Ind. Crop. Prod. 53, 34–45. https://doi.org/10.1016/j.indcrop.2013.12.007

Pires, D.E. V, Blundell, T.L., Ascher, D.B., 2015. pkCSM: Predicting Small-Molecule Pharmacokinetic and Toxicity Properties Using Graph-Based Signatures. J. Med. Chem. 4066–4072. https://doi.org/10.1021/acs.jmedchem.5b00104

Pires, D.E. V, Kaminskas, L.M., Ascher, D.B., 2018. Prediction and Optimization of Pharmacokinetic and Toxicity Properties of the Ligand, in: Computational Drug Discovery and Design, Methods in Molecular Biology. pp. 271–284.

Pohanka, M., 2014. Alzheimer´s Disease and Oxidative Stress : A Review. Curr. Med. Chem. 21, 356–364.

Prestes, A. de S., Santos, M.M. dos, Ecker, A., Macedo, G.T. de, Fachinetto, R., Bressan, G.N., Rocha, J.B.T., Barbosa, N.V., 2019. Toxicology in Vitro Methylglyoxal disturbs the expression of antioxidant , apoptotic and glycation responsive genes and triggers programmed cell death in human leukocytes. Toxicol. Vitr. 55, 33–42. https://doi.org/10.1016/j.tiv.2018.11.001

Rahal, A., Kumar, A., Singh, V., Yadav, B., Tiwari, R., Chakraborty, S., Dhama, K., 2014. Oxidative Stress, Prooxidants, and Antioxidants: The Interplay. Biomed Res. Int. 2014, 1–19.

Rahman, I., Skwarska, E., Henry, M., Davis, M., O'connor, clare m, Fitzgerald, muiris x., Greening, A., Macnee, W., 1999. Systemic and pulmonary oxidative stress in idiopathic pulmonary fibrosis. Free Radic. Biol. Med. 27, 60–68.

Ramírez-Sánchez, J., Simões Pires, E.N., Nuñez-Figueredo, Y., Pardo-Andreu, G.L., Fonseca-Fonseca, L.A., Ruiz-Reyes, A., Ochoa-Rodríguez, E., Verdecia-Reyes, Y., Delgado-Hernández, R., Souza, D.O., Salbego, C., 2015. Neuroprotection by JM-20 against oxygen-glucose deprivation in rat hippocampal slices: Involvement of the Akt/GSK-3β pathway. Neurochem. Int. 90, 215–223. https://doi.org/10.1016/j.neuint.2015.09.003

Repine, J.E., Bast, A., Lankhorst, I., Group, T.O.S.S., 1997. Oxidative Stress in Chronic Obstructive. Am J Respir Crit Care Med 156.

Schulz, E., Gori, T., Mu, T., 2011. Oxidative stress and endothelial dysfunction in hypertension. Hypertens. Res. 34, 665–673. https://doi.org/10.1038/hr.2011.39

Shankar, K., Mehendale, H.M., 2014. Cytochrome P450. Encycl. Toxicol. Third Ed. 1, 1125–1127. https://doi.org/10.1016/B978-0-12-386454-3.00299-2

Silva, F.D., Nogara, P.A., Ochoa-rodríguez, E., Nuñez-Figueredo, Y., Wong-guerra, M., Rosemberg, D.B., Rocha, J.B.T. da, 2020. Biochimie Molecular docking and in vitro evaluation of a new hybrid molecule (JM-20) on cholinesterase activity from different sources Yanier Nu n. Biochimie 168, 297–306. https://doi.org/10.1016/j.biochi.2019.11.011

Uttara, B., Singh, A. V, Zamboni, P., Mahajan, R.T., 2009. Oxidative Stress and

Neurodegenerative Diseases : A Review of Upstream and Downstream Antioxidant Therapeutic Options. Curr. Neuropharmacol. 7, 65–74.

Victor, V.M., Rocha, M., Solá, E., Bañuls, C., Garcia-malpartida, K., Mijares, A.H.-, 2009. Oxidative Stress , Endothelial Dysfunction and Atherosclerosis. Curr. Pharm. Des. 15, 2988–3002.

Waczuk, E.P., Kamdem, J.P., Amos Olalekan Abolaji, Meinerz, D.F., Bueno, D.C., Gonzaga, T.K.S. do N., Dorow, T.S. do C., Boligon, A.A., Athayde, M.L., Rocha, J.B.T. da, Ávila, D.S., 2015. Euphorbia tirucalli aqueous extract induces cytotoxicity, genotoxicity and changes in antioxidant gene expression in human leukocytes. Toxicol. Res. (Camb). 739–748. https://doi.org/10.1039/c4tx00122b

Weyermann, J., Lochmann, D., Zimmer, A., 2005. A practical note on the use of cytotoxicity assays. Int. J. Pharm. 288, 369–376. https://doi.org/10.1016/j.ijpharm.2004.09.018

Wong-guerra, M., Jiménez-martin, J., Fonseca-fonseca, L.A., Ramírez-sánchez, J., Montano-peguero, Y., Rocha, J.B., Avila, F.D., Assis, A.M. De, Souza, D.O., Gilberto, L., Valle, R.M., Lopez, G.A., Martínez, O.V., García, N.M., Mondelo-rodríguez, A., Padrón-yaquis, A.S., Nuñez-figueredo, Y., Jiménez-martin, J., Fonseca-fonseca, L.A., Ramírez-sánchez, J., Montano-peguero, Y., Rocha, J.B., Avila, F.D., Assis, A.M. De, Souza, D.O., Pardo-andreu, G.L., Menéndez-soto, R., Lopez, G.A., Martínez, O.V., García, N.M., Mondelo-, A., Padrón-yaquis, A.S., Jm-, Y.N., 2019. JM-20 protects memory acquisition and consolidation on scopolamine model of cognitive impairment. Neurol. Res. 00, 1–14. https://doi.org/10.1080/01616412.2019.1573285

2.2.1 Material de apoio do Manuscrito - Cytotoxic, antioxidative prospects and virtual screening of the new hybrid molecule (JM-20) on human blood cells

Cytotoxic and antioxidative prospects of the new hybrid molecule (JM-20) on human blood cells

Silva, F. D.[a], Galiciolli, M. E. A.[b,c], Irioda, A. C. [b,c], Oliveira, C. S.[a,b,c], Piccoli, B. C.[a], Ochoa-Rodríguez, E.[d], Nuñez-Figueredo, Y.[d], Rocha, J.B.T.[a*]

[a]*Programa de Pós-graduação em Ciências Biológicas: Bioquímica Toxicológica, Universidade Federal de Santa Maria, 97105-900 Santa Maria, RS, Brazil.*

[b]*Programa de Pós-Graduação Stricto Sensu em Biotecnologia Aplicada a Saúde da Criança e do Adolescente, Instituto de Pesquisa Pelé Pequeno Príncipe, Rua Silva Jardim, 1632, Curitiba, Paraná, Brazil.*

[c]*Faculdades Pequeno Príncipe, Avenida Iguaçu, 333, Curitiba, Paraná, Brazil.*

[d]*Centro de Investigación y Desarrollo de Medicamentos, Ave 26, Nº 1605,e /Boyeros y Puentes Grandes, CP10600, La Habana, Cuba.*

*João Batista Teixeira da Rocha, Universidade Federal de Santa Maria, Camobi, 97105-900, RS, Brazil. Tel.: +55 55 3220 9462; E-mail address: jbtrocha@yahoo.com.br.

The metabolites of JM-20 (Table S1) show high permeability for almost all, the exception to metabolite C and D, that platform swissADME consider low absorption. In addition, just metabolite D presents the value of intestinal absorption below 70% absorption. Table S2 shows the metabolites from nifedipine and like our compound, present high Caco2 permeability, except for metabolite D that present low absorption. The intestinal absorption we can see that the metabolite D e F presents a value below 70% absorption. The distribution profile observed through a blood-brain barrier membrane (BBB) permeability and CNS permeability was verified and the results showed that all structures were poor BBB permeability. The main enzymes responsible for the metabolism of drugs on the liver is the cytochrome P450 monooxygenase (CYP) enzymes superfamily. Here we evaluated different isoforms present in humans. According to the results for metabolites (Table S1, and Table S2), all molecules were seen to be negative to CYP2D6. However, our results show again disagreements between platforms pkCSM and swissADME for CYP1A2, CYP2C19, CYP2C9, and CYP3A4. In the same way, it is possible to observe that all molecules are substrates for CYP3A4, except metabolite B of JM-20. The total clearance determines the rates to achieve steady-state concentrations, which include hepatic clearance (metabolism in the liver and biliary clearance) and renal clearance (excretion via the kidneys). The values of JM-20 and your metabolites were lower than nifedipine and your metabolites (Table S1, and Table S2) for total clearance, but no molecule was substrate to renal OCT2. Toxicity has been a major concern to the safety of drug candidates and early identification of toxicity is of great relevance. Here we highlight that the values obtained for max tolerated dose (human) and oral acute toxicity (LD50) were similar for all molecules. In fact, it is possible to observe the similarity in the ADMET profile for the JM-20, Nifedipine, and its metabolites, although there are some disagreements between the platforms pkCSM and swissADME (Table S1, Table S2, and Table S3).

Table S1. ADMET prediction of the putative metabolites of JM-20 by SWISSADME and pkCSM.

	JM-20 metabolites											
	A		B		C		D		E		F	
	pkCSM	Swiss-ADME	pkCSM	Swiss-ADME	pkCSM	Swiss-ADME	pkCSM	Swiss-ADME	pkCSM	Swiss-ADME	pkCSM	Swiss-ADME
Water solubility	-4.64 log mol/L	6.19e-06 mol/L	-2.99 log mol/L	1.72e-05 mol/L	-4.07 log mol/L	3.63e-05 mol/L	-3.30 log mol/L	1.84e-04 mol/L	-4.35 log mol/L	3.01e-05 mol/L	-3.87 log mol/L	9.44e-05 mol/L
Caco2 permeability	0.09 log Papp in 10^{-6} cm/s	High	-0.29 log Papp in 10^{-6} cm/s	High	0.09 log Papp in 10^{-6} cm/s	Low	0.051 log Papp in 10^{-6} cm/s	Low	0.16 log Papp in 10^{-6} cm/s	High	-0.28 log Papp in 10^{-6} cm/s	High
Intestinal absorption (human)	100 % Absorbed	-	73.69 % Absorbed	-	93.55 % Absorbed	-	66.97 % Absorbed	-	100 % Absorbed	-	71.89 % Absorbed	-
Skin permeability	-2.73 log Kp	-5.64 cm/s	-2.73 log Kp	-5.96 cm/s	-2.73 log Kp	-6.63 cm/s	-2.73 log Kp	-7.24 cm/s	-2.73 log Kp	-6.29 cm/s	-2.73 log Kp	-6.64 cm/s
P-glycoprotein substrate	Yes	No	Yes	No	Yes	No	Yes	No	Yes	No	Yes	No
BBB permeability	-0.30 log BB	No	-0.08 log BB	No	-0.08 log BB	No	-1.38 log BB	No	-0.25 log BB	No	-0.71 log BB	No
CNS permeability	-1.94 log PS	-	-1.86 log PS	-	-2.30 log PS	-	-2.24 log PS	-	-1.92 log PS	-	-2.16 log PS	-
CYP2D6 substrate	No	-	No		No	-	No	-	No	-	No	-
CYP3A4 substrate	Yes	-	No		Yes	-	Yes	-	Yes	-	Yes	-
CYP1A2 inhibitor	Yes	No	Yes	No	Yes	No	No	No	Yes	Yes	No	No
CYP2C19 inhibitor	Yes	Yes	No	No	Yes	Yes	No	No	Yes	Yes	No	No
CYP2C9 inhibitor	Yes	Yes	Yes	Yes	Yes	Yes	No	Yes	Yes	Yes	No	Yes
CYP2D6 inhibitor	No	No	No	No	No	No	No	No	No	No	No	No
CYP3A4 inhibitor	No	Yes	No	No	No	Yes	No	No	No	Yes	No	No
Total clearance	0.17 log mL/min/Kg	-	0.07 log mL/min/Kg	-	0.112 log mL/min/Kg	-	0.067 log mL/min/Kg	-	0.031 log mL/min/Kg	-	0.27 log mL/min/Kg	-
Renal OCT2 substrate	No	-	No	-	No	-	No	-	No	-	No	-
Max tolerated dose (human)	0.28 log mg/Kg/day	-	0.65 log mg/Kg/day	-	0.44 log mg/Kg/day	-	0.76 log mg/Kg/day	-	0.11 log mg/Kg/day	-	-0.10 log mg/Kg/day	-
Oral acute toxicity (LD_{50})	2.85 mol/Kg	-	2.43 mol/Kg	-	2.68 mol/Kg	-	2.49 mol/Kg	-	2.79 mol/Kg	-	2.93 mol/Kg	-

Tables S2. ADMET prediction of metabolites of Nifedipine by SWISSADME and pkCSM.

	Nifedipine metabolites											
	A		B		C		D		E		F	
	pkCSM	Swiss-ADME	pkCSM	Swiss-ADME	pkCSM	Swiss-ADME	pkCSM	Swiss-ADME	pkCSM	Swiss-ADME	pkCSM	Swiss-ADME
Water solubility	-4.78 log mol/L	1.98e-04 mol/L	-4.21 log mol/L	3.19e-04 mol/L	-4.32 log mol/L	1.59e-04 mol/L	-4.33 log mol/L	2.57e-04 mol/L	-4.12 log mol/L	5.57e-04 mol/L	-3.55 log mol/L	1.17e-03 mol/L
Caco2 permeability	1.19 log Papp in 10-6 cm/s	High	1.20 log Papp in 10-6 cm/s	High	1.21 log Papp in 10-6 cm/s	High	0.021 log Papp in 10-6 cm/s	Low	1.44 log Papp in 10-6 cm/s	High	0.99 log Papp in 10-6 cm/s	High
Intestinal absorption (human)	90.11 % Absorbed	-	74.49 % Absorbed	-	78.19 % Absorbed	-	64.98 % Absorbed	-	96.34 % Absorbed	-	61.59 % Absorbed	-
Skin permeability	-2.72 log Kp	-6.41 cm/s	-2.74 log Kp	-6.55 cm/s	-2.74 log Kp	-6.32 cm/s	-2.74 log Kp	-6.47 cm/s	-2.74 log Kp	-6.87 cm/s	-2.73 log Kp	-7.00 cm/s
P-glycoprotein substrate	No	No	No	No	No	No	No	No	No	No	Yes	No
BBB permeability	-0.99 log BB	No	-1.03 log BB	No	-1.04 log BB	No	-0.87 log BB	No	-0.99 log BB	No	-0.53 log BB	No
CNS permeability	-2.53 log PS	-	-2.51 log PS	-	-3.45 log PS	-	-3.32 log PS	-	-2.56 log PS	-	-2.59 log PS	-
CYP2D6 substrate	No	-	No	-	No	-	No	-	No	-	No	-
CYP3A4 substrate	Yes	-	Yes	-	Yes	-	Yes	-	Yes	-	Yes	-
CYP1A2 inhibitor	No	Yes	No	No	No	Yes	No	No	No	Yes	No	No
CYP2C19 inhibitor	Yes	Yes	No	No	No	Yes	No	No	Yes	Yes	No	No
CYP2C9 inhibitor	Yes	Yes	No	Yes	No	Yes	No	No	No	Yes	No	Yes
CYP2D6 inhibitor	No	No	No	No	No	No	No	No	No	No	No	No
CYP3A4 inhibitor	No	No	No	No	No	No	No	No	No	No	No	No
Total clearance	0.76 log mL/min/Kg	-	0.74 log mL/min/Kg	-	0.68 log mL/min/Kg	-	0.73 log mL/min/Kg	-	0.63 log mL/min/Kg	-	0.81 log mL/min/Kg	-
Renal OCT2 substrate	No	-	No	-	No	-	No	-	No	-	No	-
Max tolerated dose (human)	0.23 log mg/Kg/day	-	0.06 log mg/Kg/day	-	0.53 log mg/Kg/day	-	0.06 log mg/Kg/day	-	0.08 log mg/Kg/day	-	-0.79 log mg/Kg/day	-
Oral acute toxicity (LD_{50})	2.84 mol/Kg	-	2.80 mol/Kg	-	2.06 mol/Kg	-	2.56 mol/Kg	-	2.84 mol/Kg	-	2.40 mol/Kg	-

Table S3. Physicochemical properties of JM-20, Nifedipine and respectively metabolites by pkCSM and swissADME.

	JM-20 and metabolites													
	JM-20		**A**		**B**		**C**		**D**		**E**		**F**	
	pkCSM	**Swiss-ADME**	**pkCSM**	**Swiss-ADME**	**pkCSM**	**Swiss-ADME**	**pkCSM**	**Swiss-ADME**	**pkCSM**	**Swiss-ADME**	**pkCSM**	**Swiss-ADME**	**pkCSM**	**Swiss-ADME**
MW	404.43 g/mol	404.42 g/mol	402.41 g/mol	402.40 g/mol	374.36 g/mol	374.35 g/mol	418.41 g/mol	418.40 g/mol	390.35 g/mol	390.35 g/mol	372.34 g/mol	372.33 g/mol	376.37 g/mol	376.37 g/mol
LogP	4.16	2.56	4.95	2.80	4.47	1.77	4.13	2.45	3.65	2.03	4.13	2.09	3.68	1.59
Rotatable bonds	4	5	4	5	3	3	5	6	4	4	2	2	3	3
Acceptors	7	5	7	6	6	6	8	7	7	7	7	6	6	5
Donors	2	2	1	1	2	2	2	2	3	3	1	1	3	3
Surface area	172.67	108.54 Å²	171.96	109.40 Å²	158.91	120.40 Å²	176.75	129.63 Å²	163.70	140.63 Å²	158.22	109.40 Å²	159.62	119.54 Å²
	Nifedipine and metabolites													
	Nifedipine		**A**		**B**		**C**		**D**		**E**		**F**	
	pkCSM	**Swiss-ADME**	**pkCSM**	**Swiss-ADME**	**pkCSM**	**Swiss-ADME**	**pkCSM**	**Swiss-ADME**	**pkCSM**	**Swiss-ADME**	**pkCSM**	**Swiss-ADME**	**pkCSM**	**Swiss-ADME**
MW	346.34 g/mol	346.33 g/mol	344.32 g/mol	344.32 g/mol	330.29 g/mol	330.29 g/mol	346.29 g/mol	346.29 g/mol	332.27 g/mol	332.26 g/mol	328.28 g/mol	238.28 g/mol	332.31 g/mol	332.31 g/mol
LogP	2.17	2.87	2.85	2.66	2.76	2.00	2.24	1.87	2.16	1.43	2.42	2.12	2.09	1.99
Rotatable bonds	4	6	4	6	4	5	4	6	4	5	3	4	4	5
Acceptors	7	6	7	7	6	7	8	8	7	8	7	7	6	6
Donors	1	1	0	0	1	1	1	1	2	2	0	0	2	2
Surface area	143.81	110.45 Å²	143.10	111.31 Å²	136.42	122.31 Å²	141.53	131.54 Å²	134.85	142.54 Å²	135.73	111.31 Å²	137.13	121.45 Å²

4 DISCUSSÃO

Esta tese buscou descrever o potencial multialvo de uma nova molécula denominada JM-20 como inibidora de enzimas colinesterases e antioxidante, determinar sua toxicidade em células sanguíneas humanas, assim como averiguar *in sílico* utilizando ferramentas de *docking molecular* e de *screening virtual* a conformação ideal do ligante para interação com a AChE e prever efeitos ADMET, respectivamente. Usando enzimas colinesterases de diferentes fontes, foi definido o mecanismo de ação do JM-20 nestas enzimas, a especificidade da molécula e o tipo de inibição enzimática que induz. Na busca de efeitos adicionais do JM-20, descrevemos o potencial antioxidante desta molécula como trapeadora de radicais livres e inibidora da peroxidação de fosfolipídios. A toxicidade do JM-20 foi avaliada através de abordagens *in vitro*, utilizando células sanguíneas saudáveis do organismo, *e in silico* (pkCSM e swissADME) predizendo além da toxicidade, a absorção, distribuição, metabolismo e excreção.

As substâncias capazes de inibir colinesterases são denominadas anticolinesterásicas, e são terapeuticamente administrados, por exemplo, para o tratamento dos sintomas de doenças neurodegenerativas como na doença de Alzheimer (DA) (H. FERREIRA-VIEIRA et al., 2016; POHANKA, 2012). Os medicamentos anticolinesterásicos incluem a tacrina, donepezil, galantamina e rivastigmina (YIANNOPOULOU; PAPAGEORGIOU, 2013). De acordo com a hipótese colinérgica da DA, a degeneração de neurônios colinérgicos localizados, principalmente, no córtex cerebral ocasionam um prejuízo na neurotransmissão colinérgica. Este prejuízo contribui significativamente para o déficit da função cognitiva observada em pacientes com DA (FRANCIS et al., 1999; ITO et al., 2010; WARREN; FLETCHER; GOLDEN, 2012; YAN et al., 2008). Portanto, um inibidor de colinesterase retardaria a degradação da ACh promovendo a permanência deste neurotransmissor na fenda sináptica, estimulando uma transmissão colinérgica mais intensificada (H. FERREIRA-VIEIRA et al., 2016; POHANKA, 2012). O fármaco de referência para inibição da colinesterase, a tacrina, apresenta efeitos adversos variados principalmente relacionados a hepatotoxicidade, inviabilizando seu uso na prática clínica atual (BAZSON et al., 1995; LANCTÔT; RAJARAM; HERRMANN, 2009; OSSENI et al., 1999). Neste sentido, essas novas substâncias devem ser eficazes e ao mesmo tempo apresentar de efeitos adversos mínimos.

Adicionalmente, a ACh também pode ser encontrada fora do sistema nervoso, fazendo parte do sistema colinérgico não-neuronal (WESSLER et al., 2003; WESSLER;

KIRKPATRICK, 2016, 2008; WESSLER; KIRKPATRICK; RACK, 1998). Seus efeitos podem ser mediados através de receptores nicotínicos e muscarínicos extracelulares, ligados à membrana celular da célula onde foi sintetizada ou de células vizinhas, ou ainda interagir diretamente com proteínas de sinalização intracelular (WESSLER; KIRKPATRICK; RACK, 1998). A enzima que inativa a ACh, a AChE, é abundantemente expressa nas células de mamíferos, isto é, células neuronais e não neuronais (WESSLER; KIRKPATRICK; RACK, 1998). Inicialmente, a AChE presente nos eritrócitos foi descrita como um biomarcador da integridade da membrana dessas células (SALDANHA, 2017). Entretanto, foram observadas alterações na atividade dessa enzima quando não estavam relacionadas com a integridade da membrana dos eritrócitos, por exemplo, a atividade da AChE aumentada em diferentes doenças e baixa atividade da AChE eritrocitária em pacientes expostos a pesticidas (SALDANHA, 2017).

Os primeiros estudos que tinham como objetivo avaliar a atividade da AChE utilizavam tecidos animais que continham a enzima e, somente a partir da década de 30, que a enzima isolada passou a ser utilizada por pesquisadores (NACHMANSOHN; ROTHENBERG, 1945). A técnica mais utilizada para determinação da atividade da ChE foi descrita por Ellman e colaboradores em 1961 (ELLMAN et al., 1961). O método proposto por Ellman e colaboradores baseia-se na taxa de hidrólise da acetiltiocolina (ACh modificada) pelas ChE, formando acetato e tiocolina. A tiocolina reage com o ânion carboxilato do DTNB produzindo o 2- nitrobenzoato 5-mercaptotiocolina e o 5-tio-2- nitrobenzoato (ânion de coloração amarela) que é quantificado por espectrofotômetro no comprimento de onda de 412 nm (ELLMAN et al., 1961).

Nesta tese, ampliamos o conhecimento sobre uma nova molécula, o JM-20, na inibição específica da enzima acetilcolinesterase. Estudos prévios demonstraram valores de IC_{50} para inibição da AChE iguais a 193.2 ± 10.4 nmol/L e 214.8 ± 3.1 nmol/L para *Hs*AChE e *Ee*AChE, respectivamente (WONG-GUERRA et al., 2019). Além do mais, pela primeira vez foi demonstrada uma análise cinética desse efeito em diferentes fontes da enzima (artigo 1). A cinética enzimática ou o estudo das velocidades das reações enzimáticas compreende informações indiretas sobre os mecanismos de ação catalítica, especificidade das enzimas, fatores que podem afetar a velocidade da reação e a determinação quantitativa de seus efeitos (MOTTA, 2003).

Nós utilizamos a acetilcolinesterase isolada e purificada do órgão elétrico do peixe *Electrophorus electricus*, isolada das membranas de eritrócitos humanos e dos eritrócitos

totais. Independentemente da fonte da enzima o composto foi capaz de inibir a atividade da AChE em concentrações nanomolares. Para avaliação cinética, utilizamos diferentes concentrações de substrato da reação (acetiltiocolina) e três concentrações do composto previamente selecionadas. Os resultados demonstraram que o composto foi capaz de inibir a atividade da AChE concentração-dependente. Além disso, o JM-20 aumentou os valores de K_m em função de sua concentração enquanto a V_{max} diminuiu, sugerindo um tipo de inibição mista. Os inibidores de tipo misto fazem parte dos inibidores reversíveis, os quais ligam-se a um sitio distinto do sitio ativo (local onde o substrato se liga) (NELSON; COX, 2014). O inibidor pode ligar-se tanto a enzima quanto ao complexo enzima-substrato. Neste tipo de inibição observamos a variação de K_m e V_{max} (NELSON; COX, 2014).

Para avaliar se a inibição do JM-20 era especificamente para a AChE ou se poderia inibir também a BChE, foi utilizada a enzima isolada e purificada de *Equus caballos* e de plasma humano (artigo 1). O JM-20 foi capaz de inibir a *Ec*BChE somente em concentrações micromolares (artigo 1). Por isso, consideramos que a inibição do JM-20 sob enzimas colinesterases é especifica para a AChE devido ao fato da ausência de inibição para a BChE na faixa nanomolar (artigo 1).

A fim de entendermos melhor a interação do composto com a AChE, realizamos análises *in silico* de simulação molecular (artigo 1). Essa tecnologia computacional é uma potente ferramenta capaz de prever a orientação de uma ligante quando este interage com um receptor ou uma enzima (CHEN, 2015). Surpreendentemente, a análise estrutural do JM-20 indicou a presença de um carbono quiral na quarta posição, o qual pode apresentar ressonância com o átomo de hidrogênio do grupo amina do anel diazepínico variando entre as posições 6 e 11, caracterizando um tautômero. Adicionalmente, a presença de um átomo de nitrogênio com hibridização sp^3 (posição 6 ou 11) no anel diazepínico revela uma geometria não planar, possibilitando duas conformações adicionais diferentes para a molécula. No total, existe a possibilidade de o JM-20 apresentar pelo menos oito isômeros que não haviam sido estudados até o momento (artigo 1).

Sabe-se que podem ocorrer variações entre os isômeros de acordo com a especificidade e a atividade de ligação em relação as enzimas, assim, a determinação do isômero com maior afinidade pela enzima é crucial para elucidar o mecanismo de ação e as estratégias farmacológicas potencias do composto (AARTHY et al., 2017; ARKIN; WELLS; FRANCISCO, 2004; HOPKINS, 2008; JANG et al., 2018; MAKOLA et al., 2016; SINKO et al., 2011). Por este motivo, realizamos a simulação molecular com cada um dos oito isômeros

do JM-20 interagindo com a AChE de *Homo sapiens* (*Hs*AChE) e de *Electrophorus electricus* (*Ee*AChE) e com a BChE de *Homo sapiens* (*Hs*BChE) e de *Equus caballus* (*Ec*BChE) (artigo 1) com a finalidade de determinar a postura de ligação de cada isômero e a probabilidade do isômero mais ativo.

Para as análises aplicamos dois protocolos distintos de *docking molecular*. O primeiro protocolo consistiu na ausência moléculas de água, o qual demonstrou que todos os isômeros do JM-20 podem acessar o sitio ativo das enzimas, com um padrão especifico de interações. Na ausência de água o JM-20 se liga ao fundo do *gorge* próximo a tríade catalítica das enzimas *Hs*AChE e *Hs*BChE. Por outro lado, o segundo protocolo que englobou simulações de docking molecular na presença de moléculas de água (utilizando o *Hs*AChE e *Hs*BChE), também demonstraram que o JM-20 interage no sítio ativo de ambas as colinesterases, mas com modo de ligação diferente quando comparado com o docking sem moléculas de água. ROSENBERRY et al., 2017 descrevem que a ausência de água em simulações moleculares com colinesterases resulta em posições de ligação não confiáveis e, além disso, as moléculas de água tem importância na catálise destas enzimas (DVIR et al., 2002; KOELLNER et al., 2000; NICOLET et al., 2003; ROSENBERRY et al., 2017). Desta forma, aqui destacamos os resultados da docagem na presença de água. As análises das interações e da energia de ligação mostraram que os isômeros a, b, e e f apresentam uma conformação de ligação muito semelhante, e energia de ligação mais favorável quando comparados com os isômeros c, d, g e h , indicando que os isômeros 4-R interagem melhor com o *Hs*AChE (material de apoio do artigo 1).

Além de inibidor de AChE, o JM-20 também possui efeito antioxidante através da inibição da peroxidação lipídica e trapeador de radicais livres, que foram avaliadas utilizando as técnicas colorimétricas de produção de substâncias reativas ao ácido tiobarbitúrico (TBARS) e de trapeamento do radical 2,2-difenilpicrilhidrazil (DPPH) (manuscrito 1). No teste de TBARS, foram utilizados leucócitos isolados do sangue periférico e foi induzida a peroxidação com Fe^{2+}. O JM-20 foi capaz de proteger os leucócitos da peroxidação lipídica. Para entender o mecanismo de ação do JM-20 sob a inibição da peroxidação lipídica, foi avaliada a capacidade deste composto em quelar ferro, entretanto, o JM-20 não apresentou efeitos significativos (dados não mostrados). Estes resultados sugerem outro mecanismo de ação do JM-20 como inibidor da peroxidação lipídica induzida pelo Fe^{2+}, provavelmente relacionado à proteção da membrana celular por este composto. A avaliação da capacidade de trapeamento do JM-20 foi verificada em duas partes. Na primeira parte, monitoramos a absorbância em espectrofotômetro SpectraMax a 518 nm durante 30 minutos com intervalo de

30 segundos, denominamos reação de fase rápida. No segundo momento, a reação de fase lenta, a absorbância foi registrada a cada 30 minutos durante 3 horas. O JM-20 teve efeito somente na fase lenta, nas concentrações de 50 e 100 µM.

Para torna-se um medicamento de uso clínico, uma substância precisa possuir efeito farmacológico e também apresentar baixa toxicidade ao organismo humano (PIRES; KAMINSKAS; ASCHER, 2018). É importante ressaltar que o JM-20 não induziu mortalidade em camundongos fêmeas tratados com o composto (2000 mg/Kg) por via intragástrica (gavagem) (NUÑEZ-FIGUEREDO et al., 2013). Desse modo, elucidamos a ausência de toxicidade do JM-20 *in vitro* em altas concentrações nos eritrócitos (manuscrito 1). Substâncias ou compostos desconhecidos podem desencadear o processo de ruptura de glóbulos vermelhos ou eritrócitos e, consequentemente, a liberação de seu conteúdo (hemoglobina) no plasma (AMIN; DANNENFELSER, 2006). Assim, o teste que visa avaliar o efeito hemolítico tem sido comumente utilizado como uma das metodologias de triagem para muitas substâncias de interesse clínico (AMIN; DANNENFELSER, 2006). Adicionalmente, o ensaio de viabilidade celular usando azul de tripan é um método amplamente descrito na literatura e usado para avaliar a citotoxicidade através da integridade da membrana (ADAN; KIRAZ; BARAN, 2016; ALTMAN; RANDERS; RAO, 1999; BHATIA; YETTER, 2008). O teste é baseado na absorção do azul de tripan no citoplasma das células mortas devido à perda de seletividade da membrana da mesma, enquanto as células vivas permanecem intactas (ALTMAN; RANDERS; RAO, 1999). Nossos resultados mostraram que o JM-20 não causou hemólise, entretanto, as concentrações 20 e 50 µM do composto foram responsáveis por uma diminuição de cerca de 20% e 50% na viabilidade dos leucócitos, respectivamente, quando comparado ao grupo controle (DMSO) (manuscrito 1).

Neste estudo também exploramos a existência de efeitos citotóxicos do JM-20 em leucócitos através da produção de espécies reativas (ER) e ausência de alterações no ciclo celular (manuscrito 1). A citometria de fluxo pode ser usada para a detecção de ER através de sondas fluorescentes (ERUSLANOV; KUSMARTSEV, 2010). A oxidação do diacetato de 2′-7′-diclorodihidrofluoresceína (DCFH-DA) é uma das técnicas amplamente utilizadas para detectar a produção de ER. Essa técnica apresenta algumas vantagens como reprodutibilidade, sensibilidade e preço acessível (ERUSLANOV; KUSMARTSEV, 2010). A exposição a todas as concentrações de JM-20 (10-50 µM) causou um aumento significativo nos níveis de espécies reativas intracelulares (ER). Embora tenha sido observada diminuição da viabilidade celular e aumento da produção de ER, a exposição ao JM-20 (10-50 µM) não alterou o ciclo

celular. Por outro lado, o JM-20 apresentou IC_{50} similar ao ∝-tocoferol na inibição da peroxidação lipídica, sendo 1,051 ± 0,21 e 1,065 ± 0,34 µM, respectivamente. Logo, apresentando um faixa de segurança ampla entre possíveis concentrações tóxicas e terapêuticas. Além do mais, como inibidor da AChE o JM-20 teve seu efeito em concentrações nanomolares.

Ferramentas computacionais também podem colaborar na triagem dos feitos de uma substância nova (HU et al., 2020; PIRES; KAMINSKAS; ASCHER, 2018). Neste contexto, nós avaliamos o perfil ADMET (absorção, distribuição, metabolismo, excreção e toxicidade) do JM-20 utilizando plataformas gratuitas online como o swissADME e o pkCSM. Por exemplo, parâmetros como permeabilidade CaCo-2 e absorção intestinal podem colaborar para elucidação sobre a absorção de drogas por via oral (DAINA; MICHIELIN; ZOETE, 2017; PIRES; BLUNDELL; ASCHER, 2015). Além disso, com relação ao metabolismo, é possível verificar efeitos de inibição em enzimas responsáveis pelo processo de desintoxicação do organismo, encontradas principalmente no fígado, como as isoformas do citocromo P450 (DAINA; MICHIELIN; ZOETE, 2017; PIRES; BLUNDELL; ASCHER, 2015). Adicionalmente comparamos o JM-20 com a nifedipina, uma molécula estruturalmente similar ao nosso composto e atualmente utilizada na prática clínica para tratar angina e hipertensão, compondo a lista de medicamentos essenciais da organização mundial da saúde (LEE et al., 2014; OMS, 2019). Conforme esperado, o JM-20 apresentou efeitos farmacocinéticos e toxicológicos similares a nifedipina de acordo com as análises computacionais, embora tenha havido divergências entre as plataformas utilizadas. Assim, também salientamos a importância da utilização de mais de um método computacional de avaliação.

4 CONCLUSÃO

Assim sendo, nosso trabalho demonstrou que o composto JM-20 foi eficaz na inibição da AChE, pois apresentou efeito em concentrações nanolares. Enquanto que na BChE não foi constatada inibição nas mesmas concentrações, logo, o JM-20 apresenta seletividade para a AChE. Os ensaios cinéticos mostraram que, provavelmente, o tipo de inibição enzimática é misto. O JM-20 também teve um potente efeito antioxidante como trapeador de radicais livres e inibidor da peroxidação lipídica induzida pelo Fe^{2+} nos leucócitos, entretanto esse efeito não ocorre pela atividade quelante de Fe^{2+}. Os ensaios de citotoxicidade utilizando células sanguíneas humanas indicaram que o JM-20 não causa hemólise, nem altera o ciclo celular,

porém, parece ser pró-oxidante em altas concentrações. Através de testes *in silico* comparamos a absorção, distribuição, metabolismo, excreção e toxicidade (ADMET) do JM-20, da nifedipina e de seus respectivos metabólitos e, conforme esperado, ambos os compostos apresentaram perfil ADMET semelhante. Por fim, nossos resultados reforçam a utilização do JM-20 como um composto multialvo na terapia, de distúrbios do SNC, principalmente.

REFERÊNCIAS BIBLIOGRÁFICAS

AARTHY, M. et al. Advantages of Structure-Based Drug Design Approaches in Neurological Disorders. **Current Neuropharmacology**, [s. l.], p. 1136–1155, 2017.

ADAN, A.; KIRAZ, Y.; BARAN, Y. Cell Proliferation and Cytotoxicity Assays. **Current Pharmaceutical Biotechnology**, [s. l.], v. 17, p. 1213–1221, 2016.

ALTMAN, S. A.; RANDERS, L.; RAO, G. Comparison of Trypan Blue Dye Exclusion and Fluorometric Assays for Mammalian Cell Viability Determinations. [s. l.], p. 871–874, 1999.

AMIN, K.; DANNENFELSER, R. In Vitro Hemolysis: Guidance for the Pharmaceutical Scientist. **Journal of pharmaceutical sciences**, [s. l.], v. 95, n. 6, p. 1173–1176, 2006.

ARKIN, M. R.; WELLS, J. A.; FRANCISCO, S. S. Small-molecule inhibitors of protein – protein interactions : progressing towards the dream. **Nature Reviews**, [s. l.], v. 3, n. April, p. 301–317, 2004.

ARUOMA, O. I. Free Radicals , Oxidative Stress , and Antioxidants in Human Health and Disease. **JAOCS**, [s. l.], v. 75, n. 2, p. 199–212, 1998.

BARTENS, C. et al. Antioxidant status in patients with acute respiratory distress syndrome. **Intensive Care Med**, [s. l.], v. 25, p. 180–185, 1999.

BAZSON, R. et al. Tacrine-Induced Hepatotoxicity. [s. l.], v. 4, n. 3, p. 168–181, 1995.

BHANUSHALI, M. et al. An in-vitro toxicity testing - A reliable alternative to toxicity testing by reduction , replacement and refinement of animals International Journal of Advances in Pharmaceutical Sciences An in-vitro toxicity testing - a reliable alternative to toxicity t. **International Journal of Advances in Pharmaceutical Sciences**, [s. l.], v. 1, n. March 2010, p. 15–31, 2015.

BHATIA, S. K.; YETTER, A. B. Correlation of visual in vitro cytotoxicity ratings of biomaterials with quantitative in vitro cell viability measurements. [s. l.], p. 315–319, 2008.

BIRBEN, E. et al. Oxidative Stress and Antioxidant Defense. **World Allergy Organization Journal**, [s. l.], n. January, p. 9–19, 2012.

BRENDLER-SCHWAAB, S. Y. et al. Cells of different tissues for in vitro and in vivo studies in toxicology: compilation of isolation methods. **Toxicology in Vitro**, [s. l.], v. 8, n. 6, p. 1285–1302, 1994.

BRIONES, A. M.; TOUYZ, R. M. Oxidative Stress and Hypertension : Current Concepts. **Curr Hypertens Rep**, [s. l.], v. 12, n. March, p. 135–142, 2010.

CHEN, Y. Beware of docking! **Trends in Pharmacological Sciences**, [s. l.], v. 36, n. 2, p. 78–95, 2015. Disponível em: <http://dx.doi.org/10.1016/j.tips.2014.12.001>

COLOVIC, M. B. et al. Acetylcholinesterase Inhibitors: Pharmacology and Toxicology. **Current Neuropharmacology**, [s. l.], v. 11, n. 3, p. 315–335, 2013. Disponível em: <http://www.eurekaselect.com/openurl/content.php?genre=article&issn=1570-159X&volume=11&issue=3&spage=315>

DA SILVA, F. D. et al. Molecular docking analysis of acetylcholinesterase supports the protective effect of pralidoxime on toxic action of chlorpyrifos in behavior and neurochemistry of Nauphoeta cinerea. **Computational Toxicology**, [s. l.], 2018. a.

DA SILVA, F. D. et al. Molecular docking analysis of acetylcholinesterase corroborates the protective e ff ect of pralidoxime against chlorpyrifos-induced behavioral and neurochemical impairments in Nauphoeta cinerea. **Computational Toxicology**, [s. l.], v. 8, n. March, p. 25–33, 2018. b. Disponível em: <https://doi.org/10.1016/j.comtox.2018.07.003>

DAINA, A.; MICHIELIN, O.; ZOETE, V. SwissADME: a free web tool to evaluate pharmacokinetics, drug- likeness and medicinal chemistry friendliness of small molecules. **Nature Publishing Group**, [s. l.], n. March, p. 1–13, 2017.

DIAS, K. S. T. et al. Artigo Aplicações Recentes da Abordagem de Fármacos Multialvo para o Tratamento da Doença de Alzheimer Recent Applications of the Multi-Target Directed Ligands Approach for the Treatment of Alzheimer ' s Disease Aplicações Recentes da Abordagem de Fármaco. **Revista Virtual de Quimica**, [s. l.], v. 7, n. 2, 2015.

DVIR, H. et al. 3D Structure of Torpedo californica Acetylcholinesterase Complexed with Huprine X at 2 . 1 Å Resolution : Kinetic and Molecular Dynamic Correlates. **Biochemistry**, [s. l.], v. 41, p. 2970–2981, 2002.

ELLMAN, L. G. et al. A new and rapid colorimetric of acetylcholinesterase determination. **Biochemical Pharmacolog**, [s. l.], v. 7, p. 88–95, 1961.

ERUSLANOV, E.; KUSMARTSEV, S. Identification of ROS using oxidazed DCFDA and flow-cytometry. In: **Advanced Protocols in Oxidative Stress II, Methods in Molecular Biology**. [s.l: s.n.]. v. 594p. 57–72.

FALSAFI, S. K. et al. Scopolamine administration modulates muscarinic, nicotinic and nmda receptor systems. **PLoS ONE**, [s. l.], v. 7, n. 2, 2012.

FERREIRA, L. G. et al. **Molecular docking and structure-based drug design strategies**. [s.l: s.n.]. v. 20

FLOYD, R. A.; HENSLEY, K. Oxidative stress in brain aging Implications for therapeutics of neurodegenerative diseases. **Neurobiology of Aging**, [s. l.], v. 23, p. 795–807, 2002.

FONSECA-FONSECA, L. A. et al. Neuroscience Letters JM-20 , a novel hybrid molecule , protects against rotenone-induced neurotoxicity in experimental model of Parkinson ' s disease. **Neuroscience Letters**, [s. l.], v. 690, n. July 2018, p. 29–35, 2019. a. Disponível em: <https://doi.org/10.1016/j.neulet.2018.10.008>

FONSECA-FONSECA, L. A. et al. JM-20, a novel hybrid molecule , protects against rotenone-induced neurotoxicity in experimental model of Parkinson's disease. **Neuroscience Letters**, [s. l.], v. 690, n. July 2018, p. 29–35, 2019. b. Disponível em: <https://doi.org/10.1016/j.neulet.2018.10.008>

FRANCIS, P. T. et al. The cholinergic hypothesis of Alzheimer ' s disease : a review of progress. **J Neurol Neurosurg Psychiatry**, [s. l.], v. 66, p. 137–147, 1999.

FUJII, T. et al. Expression and Function of the Cholinergic System in Immune Cells. **Frontiers in immunology**, [s. l.], v. 8, n. September, p. 1–18, 2017.

GRISARU, D. et al. Structural roles of acetylcholinesterase variants in biology and pathology. **European Journal of Biochemistry**, [s. l.], v. 264, n. 3, p. 672–686, 1999.

GWILT, C. R.; DONNELLY, L. E.; ROGERS, D. F. The non-neuronal cholinergic system in the airways : An unappreciated regulatory role in pulmonary inflammation ? **Pharmacology & Therapeutics**, [s. l.], v. 115, p. 208–222, 2007.

H. FERREIRA-VIEIRA, T. et al. Alzheimer's disease: Targeting the Cholinergic System. **Current Neuropharmacology**, [s. l.], v. 14, n. 1, p. 101–115, 2016. Disponível em: <http://www.eurekaselect.com/openurl/content.php?genre=article&issn=1570-159X&volume=14&issue=1&spage=101>

HOPKINS, A. L. Network pharmacology : the next paradigm in drug discovery. **Nature Chemical Biology**, [s. l.], v. 4, n. 11, p. 682–690, 2008.

HU, B. et al. Refined pharmacophore features for virtual screening of human thromboxane A2 receptor antagonists. **Computational Biology and Chemistry**, [s. l.], v. 86, n. September 2019, p. 107249, 2020. Disponível em: <https://doi.org/10.1016/j.compbiolchem.2020.107249>

ITO, K. et al. Disease progression meta-analysis model in Alzheimer's disease. **Alzheimer's and Dementia**, [s. l.], v. 6, n. 1, p. 39–53, 2010. Disponível em: <http://dx.doi.org/10.1016/j.jalz.2009.05.665>

JANG, C. et al. Identification of novel acetylcholinesterase inhibitors designed by pharmacophore- based virtual screening , molecular docking and bioassay. **Scientific Reports**, [s. l.], n. September, p. 1–21, 2018. Disponível em: <http://dx.doi.org/10.1038/s41598-018-33354-6>

JENNINGS, P. Toxicology in Vitro '" The future of in vitro toxicology "'. **Toxicology in Vitro**, [s. l.], v. 29, p. 1217–1221, 2015.

JOHN, E. M.; SHAIKE, J. M. Chlorpyrifos: pollution and remediation. **Environmental Chemistry Letters**, [s. l.], v. 13, n. 3, p. 269–291, 2015. Disponível em: <http://link.springer.com/10.1007/s10311-015-0513-7>

KHANSARI, N.; SHAKIBA, Y.; MAHMOUDI, M. Chronic inflammation and oxidative stress as a major cause of age-related diseases and cancer. **Recent Patents on Inflammation & Allergy Drug Discovery**, [s. l.], v. 3, n. June 2015, p. 73–80, 2009.

KLIMENT, C. R.; OURY, T. D. Oxidative stress , extracellular matrix targets , and idiopathic pulmonary fibrosis. **Free Radical Biology and Medicine**, [s. l.], v. 49, n. 5, p. 707–717, 2010. Disponível em: <http://dx.doi.org/10.1016/j.freeradbiomed.2010.04.036>

KOELLNER, G. et al. Active-site Gorge and Buried Water Molecules in Crystal Structures of Acetylcholinesterase from Torpedo californica. **J Mol Biol**, [s. l.], v. 296, n. 2, p. 713–735, 2000.

LANCTÔT, K. L.; RAJARAM, R. D.; HERRMANN, N. Therapy for Alzheimer's disease: How effective are current treatments? **Therapeutic Advances in Neurological Disorders**, [s. l.], v. 2, n. 3, p. 163–180, 2009.

LEE, P. W. et al. Nifedipine. In: **Handbook of Metabolic Pathways of Xenobiotics, First Edition**. [s.l: s.n.]. p. 1–4.

LI, H.; HORKE, S.; ULRICH, F. Vascular oxidative stress , nitric oxide and atherosclerosis. [s. l.], v. 237, p. 208–219, 2014.

LIMONCIEL, A. The Past , Present , and Future of Chemical risk assessment. In: **In Vitro Toxicology Systems, Methods in Pharmacology and Toxicology**. [s.l: s.n.]. p. 3–23.

LÓPEZ, M. D.; PASCUAL-VILLALOBOS, M. J. Mode of inhibition of acetylcholinesterase by monoterpenoids and implications for pest control. **Industrial Crops and Products**, [s. l.], v. 31, n. 2, p. 284–288, 2010.

LOVE, S. Oxidative Stress in Brain Ischemia. **Brain Pathology**, [s. l.], v. 131, p. 119–131, 1999.

LU, J. et al. Multi-Target Drugs : The Trend of Drug Research and Development. **PlosOne**, [s. l.], v. 7, n. 6, p. 1–6, 2012.

MAKOLA, M. M. et al. The Effect of Geometrical Isomerism of 3 , 5-Dicaffeoylquinic Acid on Its Binding Affinity to HIV-Integrase Enzyme : A Molecular Docking Study. **Evidence-Based Complementary and Alternative Medicine**, [s. l.], v. 2016, p. 1–10, 2016.

MANDELLI, M.; TOGNONI, G.; GARATTINI, S. Clinical Pharmacokinetics of Diazepam. **Clinical Pharmacokinetics**, [s. l.], v. 3, n. 1, p. 72–91, 1978.

MARITIM, A. C.; SANDERS, R. A.; WATKINS, J. B. I. Diabetes , Oxidative Stress , and Antioxidants : A Review. **J BIOCHEM MOLECULAR TOXICOLOGY**, [s. l.], v. 17, n. 1, p. 24–38, 2003.

MCCORRY, L. K. Physiology of the Autonomic Nervous System. **Acta Anaesthesiologica Scandinavica**, [s. l.], v. 8, n. 4, p. 17–20, 2007.

MEHTA, M.; ADEM, A.; SABBAGH, M. New acetylcholinesterase inhibitors for alzheimer's disease. **International Journal of Alzheimer's Disease**, [s. l.], v. 2012, 2012.

MISRA, M. K. et al. Oxidative stress and ischemic myocardial syndromes. **Med Sci Monit**, [s. l.], v. 15, n. 10, p. 209–219, 2009.

MONTANARI, C. A. **Quimica medicinal: contribuição e pesrspectiva no desenvolvimento da farmacoterapia**, 1995.

MOTTA, V. T. Enzimas. In: **Bioquímica Básica**. São Paulo. p. 1–34.

NACHMANSOHN, D.; ROTHENBERG, M. A. Studies on cholinesterase. **Journal of Biological Chemistry**, [s. l.], n. 158, p. 653–666, 1945.

NADEEM, A. et al. Increased oxidative stress and altered levels of antioxidants in asthma. **Journal of Allergy and Clinical Immunology**, [s. l.], v. 111, n. 1, p. 72–78, 2003.

NELSON, D. L.; COX, M. M. **Principios de Bioquímica de Lehninger**. 6ª ed. Porto Alegre.

NICOLET, Y. et al. Crystal Structure of Human Butyrylcholinesterase and of Its Complexes with Substrate and Products. **Journal of Biological Chemistry**, [s. l.], v. 278, n. 42, p. 41141–41147, 2003.

NOGARA, P. A. et al. Virtual screening of acetylcholinesterase inhibitors using the lipinski's rule of five and ZINC databank. **BioMed Research International**, [s. l.], v. 2015, 2015.

NUÑEZ-FIGUEREDO, Y. et al. Characterization of the anxiolytic and sedative profile of JM-20: a novel benzodiazepine – dihydropyridine hybrid molecule. **Neurological Research**, [s. l.], v. 35, n. 8, p. 804–812, 2013. a.

NUÑEZ-FIGUEREDO, Y. et al. Characterization of the anxiolytic and sedative profile of JM-20: a novel benzodiazepine–dihydropyridine hybrid molecule. **Neurological Research**, [s. l.], v. 35, n. 8, p. 804–812, 2013. b. Disponível em: <https://www.tandfonline.com/doi/full/10.1179/1743132813Y.0000000216>

NUÑEZ-FIGUEREDO, Y. et al. JM-20, a novel benzodiazepine-dihydropyridine hybrid molecule, protects mitochondria and prevents ischemic insult-mediated neural cell death in vitro. **European Journal of Pharmacology**, [s. l.], v. 726, n. 1, p. 57–65, 2014. a. Disponível em: <http://dx.doi.org/10.1016/j.ejphar.2014.01.021>

NUÑEZ-FIGUEREDO, Y. et al. Antioxidant effects of JM-20 on rat brain mitochondria and synaptosomes: Mitoprotection against Ca2+-induced mitochondrial impairment. **Brain Research Bulletin**, [s. l.], v. 109, p. 68–76, 2014. b. Disponível em: <http://dx.doi.org/10.1016/j.pharep.2018.02.013>

NUÑEZ-FIGUEREDO, Y. et al. A novel multi-target ligand (JM-20) protects mitochondrial integrity, inhibits brain excitatory amino acid release and reduces cerebral ischemia injury in vitro and in vivo. **Neuropharmacology**, [s. l.], v. 85, p. 517–527, 2014. c.

NUÑEZ-FIGUEREDO, Y. et al. The effects of JM-20 on the glutamatergic system in synaptic vesicles , synaptosomes and neural cells cultured from rat brain. **Neurochemistry International**, [s. l.], v. 81, p. 41–47, 2015. Disponível em: <http://dx.doi.org/10.1016/j.neuint.2015.01.006>

NUÑEZ-FIGUEREDO, Y. et al. Therapeutic potential of the novel hybrid molecule JM-20 against focal cortical ischemia in rats. **Journal of Pharmacy & Pharmacognosy Research**, [s. l.], v. 4, n. 4, p. 153–158, 2016.

NUÑEZ-FIGUEREDO, Y. et al. Multi-targeting effects of a new synthetic molecule (JM-20) in experimental models of cerebral ischemia. **Pharmacological Reports**, [s. l.], v. 70, n. 4, p. 699–704, 2018. Disponível em: <http://dx.doi.org/10.1016/j.pharep.2018.02.013>

OCHOA, R.; RODRIGUEZ, C. A.; ZULUAGA, A. F. Perspectives for the structure-based design of acetylcholinesterase reactivators. **Journal of Molecular Graphics and Modelling**, [s. l.], v. 68, p. 176–183, 2016. Disponível em: <http://dx.doi.org/10.1016/j.jmgm.2016.07.002>

OMS. World health organization model list of essential medicines. **Mental and Holistic Health: Some International Perspectives**, [s. l.], v. 21, p. 119–134, 2019.

OSSENI, R. A. et al. Tacrine-induced reactive oxygen species in a human liver cell line: The role of anethole dithiolethione as a scavenger. **Toxicology in Vitro**, [s. l.], v. 13, n. 4–5, p. 683–688, 1999.

PETRONILHO, E. da C.; PINTO, A. C.; VILLAR, J. D. F. Acetilcolinesterase: Alzheimer e guerra química. **Revista Militar de Cinência e Tecnologia**, [s. l.], v. XXVIII, p. 3–14, 2011.

PICCIOTTO, M. R.; HIGLEY, M. J.; MINEUR, Y. S. Acetylcholine as a neuromodulator: cholinergic signaling shapes nervous system function and behavior. **Neuron.**, [s. l.], v. 76, n. 1, p. 116–129, 2013.

PIRES, D. E. V; BLUNDELL, T. L.; ASCHER, D. B. pkCSM: Predicting Small-Molecule Pharmacokinetic and Toxicity Properties Using Graph-Based Signatures. **Journal of Medicinal Chemistry**, [s. l.], n. 58, p. 4066–4072, 2015.

PIRES, D. E. V; KAMINSKAS, L. M.; ASCHER, D. B. Prediction and Optimization of Pharmacokinetic and Toxicity Properties of the Ligand. In: **Computational Drug Discovery and Design, Methods in Molecular Biology**. [s.l: s.n.]. v. 1762p. 271–284.

POHANKA, M. Acetylcholinesterase inhibitors: a patent review (2008 – present). **Expert Opinion on Therapeutic Patents**, [s. l.], v. 22, n. 8, p. 871–886, 2012. Disponível em: <http://www.tandfonline.com/doi/full/10.1517/13543776.2012.701620>

POHANKA, M. Alzheimer´s Disease and Oxidative Stress : A Review. **Current Medicinal Chemistry**, [s. l.], v. 21, p. 356–364, 2014.

RACCHI, M. et al. Acetylcholinesterase inhibitors : novel activities of old molecules. [s. l.], v. 50, p. 441–451, 2004.

RAHAL, A. et al. Oxidative Stress, Prooxidants, and Antioxidants: The Interplay. **BioMed Research International**, [s. l.], v. 2014, p. 1–19, 2014.

RAHMAN, I. et al. Systemic and pulmonary oxidative stress in idiopathic pulmonary fibrosis. **Free Radical Biology & Medicine**, [s. l.], v. 27, n. 99, p. 60–68, 1999.

RAMÍREZ-SÁNCHEZ, J. et al. Neuroprotection by JM-20 against oxygen-glucose deprivation in rat hippocampal slices: Involvement of the Akt/GSK-3β pathway. **Neurochemistry International**, [s. l.], v. 90, p. 215–223, 2015.

REPINE, J. E. et al. Oxidative Stress in Chronic Obstructive. **Am J Respir Crit Care Med**, [s. l.], v. 156, n. 10, 1997.

RICHENDRFER, H.; CRETON, R. Chlorpyrifos and malathion have opposite effects on behaviors and brain size that are not correlated to changes in AChE activity. **NeuroToxicology**, [s. l.], v. 49, p. 50–58, 2015. Disponível em: <http://dx.doi.org/10.1016/j.neuro.2015.05.002>

ROBINSON, V. Finding alternatives : an overview of the 3Rs and the use of animals in research. **School Science Review**, [s. l.], v. 87, n. December, p. 1–4, 2005.

ROSENBERRY, T. L. et al. Comparison of the Binding of Reversible Inhibitors to Human Butyrylcholinesterase and Acetylcholinesterase: ACrystallographic, Kinetic and Calorimetric Study. **Molecules**, [s. l.], v. 22, p. 1–21, 2017.

SALDANHA, C. Human Erythrocyte Acetylcholinesterase in Health and Disease. **Molecules**, [s. l.], v. 22, n. 1499, p. 1–10, 2017.

SAMEEM, B. et al. A review on tacrine-based scaffolds as multi-target drugs (MTDLs) for Alzheimer ' s disease. **European Journal of Medicinal Chemistry**, [s. l.], v. 128, p. 332–345, 2017.

SIEGEL, G. et al. **Basic neurochemistry - Molecular, cellular, and medical aspects**. Seventh Ed ed. USA.

SINKO, G. et al. Mechanism of stereoselective interaction between butyrylcholinesterase and ethopropazine enantiomers. **Biochimie**, [s. l.], v. 93, p. 1797–1807, 2011.

SPILOVSKA, K. et al. Multitarget Tacrine Hybrids with Neuroprotective Properties to Confront Alzheimer's Disease. **Current topics in medicinal chemistry**, [s. l.], v. 17, p. 1006–1026, 2017.

UTTARA, B. et al. Oxidative Stress and Neurodegenerative Diseases : A Review of Upstream and Downstream Antioxidant Therapeutic Options. **Current Neuropharmacology**, [s. l.], v. 7, p. 65–74, 2009.

VICTOR, V. M. et al. Oxidative Stress , Endothelial Dysfunction and Atherosclerosis. **Current Pharmaceutical Design**, [s. l.], v. 15, p. 2988–3002, 2009.

WARREN, J. D.; FLETCHER, P. D.; GOLDEN, H. L. The paradox of syndromic diversity in Alzheimer disease. **Nature Reviews Neurology**, [s. l.], v. 8, n. 8, p. 451–464, 2012. Disponível em: <http://dx.doi.org/10.1038/nrneurol.2012.135>

WESSLER, I. et al. The non-neuronal cholinergic system in humans : Expression , function and pathophysiology. [s. l.], v. 72, p. 2055–2061, 2003.

WESSLER, I. K.; KIRKPATRICK, C. J. The Non-neuronal Cholinergic System : an Emerging Drug Target in the Airways. [s. l.], p. 423–434, 2001.

WESSLER, I. K.; KIRKPATRICK, C. J. Detection of Non-neuronal Acetylcholine. In: **Neuromethods**. [s.l: s.n.]. v. 107p. 205–220.

WESSLER, I.; KIRKPATRICK, C. J. Acetylcholine beyond neurons : the non-neuronal cholinergic system in humans. [s. l.], n. January, p. 1558–1571, 2008.

WESSLER, I.; KIRKPATRICK, C. J.; RACK, K. Non-Neuronal Acetylcholine, a Locally Acting Molecule, Widely Distributed in Biological Systems/: Expression and Function in Humans. **Pharmacology & Therapeutics**, [s. l.], v. 77, n. 1, p. 59–79, 1998.

WONG-GUERRA, M. et al. JM-20 protects memory acquisition and consolidation on scopolamine model of cognitive impairment. **Neurological Research**, [s. l.], v. 00, n. 00, p. 1–14, 2019. Disponível em: <https://doi.org/10.1080/01616412.2019.1573285>

WOREK, F. et al. Effect of human plasma on the reactivation of sarin-inhibited human erythrocyte acetylcholinesterase. **Archives of toxicology**, [s. l.], v. 74, n. 1, p. 21–26, 2000.

YAN, J. H. et al. Alzheimer's disease and mild cognitive impairment deteriorate fine movement control. **Journal of Psychiatric Research**, [s. l.], v. 42, n. 14, p. 1203–1212, 2008.

YIANNOPOULOU, K. G.; PAPAGEORGIOU, S. G. Current and future treatments for Alzheimer's disease. **Therapeutic Advances in Neurological Disorders**, [s. l.], v. 6, n. 1, p. 19–33, 2013.

ANEXO A - PARECER DO COMITÊ DE ÉTICA EM PESQUISA COM SERES HUMANOS (CEP)

UNIVERSIDADE FEDERAL DE SANTA MARIA/ PRÓ-REITORIA DE PÓS-GRADUAÇÃO E PESQUISA

PARECER CONSUBSTANCIADO DO CEP

DADOS DO PROJETO DE PESQUISA

Título da Pesquisa: Avaliação da toxicidade do JM-20 e seus derivados na viabilidade de leucócitos humanos.

Pesquisador: João Batista Teixeira da Rocha

Área Temática:

Versão: 2

CAAE: 14656919.4.0000.5346

Instituição Proponente: Universidade Federal de Santa Maria/ Pró-Reitoria de Pós-Graduação e

Patrocinador Principal: MINISTERIO DA CIENCIA, TECNOLOGIA E INOVACAO

DADOS DO PARECER

Número do Parecer: 3.471.823

Apresentação do Projeto:

Projeto vinculado ao PPG de Bioquímica Toxicológica do Centro de Ciências Naturais e Exatas da UFSM.

As amostras serão obtidas de 20 doadores voluntários saudáveis mediante consentimento. Será coletado 10 mL de cada participante em tubo contendo heparina. O tubo com sangue venoso será centrifugado e o plasma obtido será utilizado para o ensaio de viabilidade celular. O plasma obtido será purificado através de sucessivas lavagens com solução de lise de hemácias. Após, os leucócitos serão mantidos em tampão Hank's para manter a viabilidade dos mesmos. Os leucócitos isolados (2 x 106 /mL-1) serão incubados durante três horas com DMSO (0,5%), 1 mM de t-butil hidroperóxido (controle positivo) ou o composto indicado em uma solução de tampão de Hank's. Após o termino do período de incubação será adicionado o azul de Tripan e será realizada uma contagem com auxílio do microscópio ótico dos leucócitos viáveis e não viáveis. Contém critérios de inclusão e exclusão dos sujeitos de pesquisa.

Os dados obtidos serão expressos como média ± erro padrão. A análise estatística dos dados será realizada através de análise de variância (ANOVA) de duas vias, seguida pelo teste de Newman Keuls quando for necessário. Todas as análises serão realizadas utilizando o programa Prism®. Os

Endereço: Av. Roraima, 1000 - prédio da Reitoria - 2º andar
Bairro: Camobi **CEP:** 97.105-970
UF: RS **Município:** SANTA MARIA
Telefone: (55)3220-9362 **E-mail:** cep.ufsm@gmail.com

valores de p <0.05 serão considerados significativos.

Apresenta cronograma de execução.

Objetivo da Pesquisa:
Avaliar o efeito do composto JM-20 e seus derivados na viabilidade celular de leucócitos humanos.

Avaliação dos Riscos e Benefícios:
Considerando-se as características do projeto, a descrição de riscos e benefícios apresentada pode ser considerada suficiente.

Comentários e Considerações sobre a Pesquisa:
.

Considerações sobre os Termos de apresentação obrigatória:
Os termos de apresentação obrigatória podem ser considerados suficientes.

Recomendações:
Veja no site do CEP - http://w3.ufsm.br/nucleodecomites/index.php/cep - na aba "orientações gerais", modelos e orientações para apresentação dos documentos. ACOMPANHE AS ORIENTAÇÕES DISPONÍVEIS, EVITE PENDÊNCIAS E AGILIZE A TRAMITAÇÃO DO SEU PROJETO.

Conclusões ou Pendências e Lista de Inadequações:
.

Considerações Finais a critério do CEP:

Este parecer foi elaborado baseado nos documentos abaixo relacionados:

Tipo Documento	Arquivo	Postagem	Autor	Situação
Informações Básicas do Projeto	PB_INFORMAÇÕES_BÁSICAS_DO_PROJETO_1362786.pdf	01/07/2019 14:47:17		Aceito

UNIVERSIDADE FEDERAL DE SANTA MARIA/ PRÓ-REITORIA DE PÓS-GRADUAÇÃO E PESQUISA

Continuação do Parecer: 3.471.823

Outros	INSTRUMENTOSDECOLETADEDADOS.pdf	01/07/2019 14:46:27	João Batista Teixeira da Rocha	Aceito
Projeto Detalhado / Brochura Investigador	Projetocepjm20.pdf	01/07/2019 14:46:08	João Batista Teixeira da Rocha	Aceito
TCLE / Termos de Assentimento / Justificativa de Ausência	TERMODECONSENTIMENTOLIVREESCLARECIDOcor.pdf	01/07/2019 14:45:46	João Batista Teixeira da Rocha	Aceito
Outros	Pendencias.pdf	28/06/2019 10:19:16	João Batista Teixeira da Rocha	Aceito
Outros	TERMODECONFIDENCIALIDADEcorreto.pdf	28/05/2019 08:14:45	João Batista Teixeira da Rocha	Aceito
Folha de Rosto	JM20folharosto3.pdf	27/05/2019 13:46:51	João Batista Teixeira da Rocha	Aceito
Outros	projeto63983gap.pdf	24/05/2019 15:24:31	João Batista Teixeira da Rocha	Aceito
TCLE / Termos de Assentimento / Justificativa de Ausência	TERMODECONSENTIMENTOLIVREESCLARECIDO.pdf	24/05/2019 15:23:15	João Batista Teixeira da Rocha	Aceito
Declaração de Instituição e Infraestrutura	JM20autorizacao.pdf	22/05/2019 17:29:37	João Batista Teixeira da Rocha	Aceito
Projeto Detalhado / Brochura Investigador	Projetojm20.pdf	22/05/2019 17:29:17	João Batista Teixeira da Rocha	Aceito

Situação do Parecer:
Aprovado

Necessita Apreciação da CONEP:
Não

SANTA MARIA, 26 de Julho de 2019

Assinado por:
CLAUDEMIR DE QUADROS
(Coordenador(a))

Endereço: Av. Roraima, 1000 - prédio da Reitoria - 2º andar
Bairro: Camobi **CEP:** 97.105-970
UF: RS **Município:** SANTA MARIA
Telefone: (55)3220-9362 **E-mail:** cep.ufsm@gmail.com